



Wisconsin Geological and Natural History Survey
3817 Mineral Point Road
Madison, Wisconsin 53705-5100
TEL 608/263.7389 FAX 608/262.8086
<http://www.uwex.edu/wgnhs/>

James M. Robertson, Director and State Geologist

Evaluation of the Solute Transport Model Developed for the Proposed Crandon Mine Tailings Management Area and Reclaim Pond

Madeline B. Gotkowitz, Wisconsin Geological and Natural History Survey
Daniel T. Feinstein, U.S. Geological Survey
Christopher P. Carlson, Wisconsin Department of Natural Resources

2004

Open-File Report 2004-02
1 CD-ROM

Technical Working Group

Kenneth R. Bradbury, Wisconsin Geological and Natural History Survey
Christopher P. Carlson, Wisconsin Department of Natural Resources
Charles P. Dunning, U.S. Geological Survey
Daniel T. Feinstein, U.S. Geological Survey
Madeline B. Gotkowitz, Wisconsin Geological and Natural History Survey
Randall J. Hunt, U.S. Geological Survey
David M. Johnson, Wisconsin Department of Natural Resources
Galen Kenoyer, RMT, Inc.
James T. Krohelski, U.S. Geological Survey

This report represents work performed by the Wisconsin Geological and Natural History Survey and is released to the open files in the interest of making the information readily available. This report has not been edited or reviewed for conformity with Wisconsin Geological and Natural History Survey standards and nomenclature.

TABLE OF CONTENTS

List of Figures	iii
List of Tables	iv
1. Introduction.....	1
1.1 Purpose and scope of the Tailings Management Area / Reclaim Pond model	1
1.2 Purpose and scope of review.....	1
1.3 Review of an uncalibrated solute transport model.....	2
2. Geology.....	3
2.1 Surficial Deposits.....	3
2.2 Bedrock.....	4
3. Groundwater and surface water conditions in vicinity of TMA/RP	4
3.1 Hydrostratigraphic Units.....	5
3.1.1 Upland Lakebed and Wetland Deposits.....	5
3.1.2 Recent Unlithified Deposits	6
3.1.3 Glacial Unlithified Deposits	6
3.1.4 Pre- to Early Wisconsinan Till/Massive Saprolite.....	6
4. Description of applicant's TMA / RP model	6
4.1 Conceptual model of contaminant transport at the TMA / RP	6
4.2 Computer Codes.....	7
4.3 Model structure	8
5. Model Evaluation.....	10
5.1 Conceptual model and translation to numerical model.....	10
5.2 Revisions to the model.....	11
5.2.1 Boundary conditions and hydraulic conductivity	11
5.2.2 Stress periods	12
5.2.3 Exfiltration rates.....	12
5.3 Methods used to evaluate results	12
6. Results from revised model and sensitivity to selected features.....	13
6.1 Numerical solver in MT3D.....	13
6.2 Sensitivity to source area	14
6.3 TMA exfiltration rate.....	15
6.4 Drawdown and recovery of water levels at the model boundary.....	16
6.5 Dispersion	17
6.5.1. Longitudinal dispersivity	17
6.5.2 Transverse dispersivity	17
6.6 Vertical hydraulic conductivity.....	18
6.7 Pumping rate and dispersivity.....	19
6.8 Porosity	20
6.9 Representation of the pinchout zone.....	21
7. Range of results.....	23
7.1 Range of inputs for selected model parameters	23
7.2 Range of mass distribution at key times	24
7.3 Maximum scaled concentrations reaching the TMA DMZ	25
8. Conclusions.....	26
9. References.....	27

Appendix 1	Modifications to the MT3DMS Code.....	76
Appendix 2	Breakthrough curve locations in model domain.....	82

LIST OF FIGURES

- Figure 1. Crandon area base map and Swamp and Pickeral Creek groundwater basins.
- Figure 2. Location of TMA flow and transport model domain.
- Figure 3. Water table map of Crandon area generated from calibrated regional flow model.
- Figure 4. TMA cells, Reclaim Pond and their design management zones (DMZs).
- Figure 5. Maximum concentrations at the TMA DMZ with various numerical solvers.
- Figure 6. Maximum concentrations with various numerical solvers and low vertical dispersivity.
- Figure 7. Maximum concentrations along the TMA DMZ from the TMA source, Reclaim Pond source, and combined sources.
- Figure 8. Maximum concentrations along the Reclaim Pond DMZ from the TMA source, Reclaim Pond source, and combined sources.
- Figure 9. Effect of long-term exfiltration rate on maximum concentrations reaching the TMA DMZ.
- Figure 10. Effect of instantaneous drawdown and recovery compared to stepped drawdown and recovery.
- Figure 11. Maximum concentrations at TMA DMZ with a decrease in longitudinal dispersivity.
- Figure 12. Breakthrough curves along the TMA DMZ.
- Figure 13. Maximum concentrations under varying longitudinal dispersivity at low transverse dispersivities.
- Figure 14. Maximum concentrations with changes in transverse horizontal and vertical dispersivity.
- Figure 15. Breakthrough curve under reduced transverse dispersivities.
- Figure 16. Maximum concentrations with no transverse vertical and no transverse horizontal dispersivity.
- Figure 17. Maximum concentration along the TMA DMZ with a reduction in vertical hydraulic conductivity.
- Figure 18. Breakthrough curves demonstrating effect of reduction in vertical hydraulic conductivity.
- Figure 19. Maximum concentrations with changes in dewatering rate and vertical dispersivity.
- Figure 20. Water table during mine dewatering and after recovery at high, low and proposed maximum pumping rates.
- Figure 21. Breakthrough curves demonstrating effect of mine dewatering rates with no vertical dispersivity.
- Figure 22. Concentrations over model domain at low and high porosity.
- Figure 23. Total mass reaching head-dependent and river boundaries over time, $n = 5, 10$ and 30% .
- Figure 24. Maximum concentrations along the TMA DMZ at early times and over 650 years.
- Figure 25. Applicant's interpretation and one possible alternative interpretation of the pinchout zone.
- Figure 26. Location of hypothetical high-K channel in pinchout zone, layers 2 through 6.
- Figure 27. Water table from first and last stress periods of TMA/RP flow model for pinchout zone configurations.
- Figure 28. Cumulative mass discharge to river cells and head dependent boundary cells.
- Figure 29. Breakthrough curves in three layers downgradient of high -K channel location.
- Figure 30. Contour plots of the plume at 50 and 80 years in pinch out zone simulations.
- Figure 31. Contours of plume concentrations at 25 years time.

Figure 32. Contours of concentrations at 650 years at high long-term exfiltration rates.
Figure 33. Breakthrough curves at cells west and east of model domain.
Figure 34. Range of maximum relative concentrations at the TMA DMZ at early times and entire 650-year simulation.

LIST OF TABLES

Table 1. Model layers in regional model and TMA/RP model.
Table 2. Six model runs that comprise a complete simulation.
Table 3. Parameters assigned in model versions.
Table 4. Numerical solvers used in modeling contaminant transport from the TMA/RP.
Table 5. TMA Cell 1A percolation rates by stress period.
Table 6. TMA Cell 1B percolation rates by stress period.
Table 7. TMA Cell 2 percolation rates by stress period.
Table 8. TMA Cell 3 percolation rates by stress period.
Table 9. Phases of landfill operations with distinct exfiltration rates, in Applicant's model.
Table 10. Simulations testing model sensitivity to dispersivity.
Table 11. Sensitivity to vertical hydraulic conductivity and dispersivity.
Table 12. Maximum concentrations at the TMA DMZ with changes in porosity and vertical dispersivity.
Table 13. Model runs to evaluate effect of pinchout zone.
Table 14. ECURVE results at the TMA DMZ.
Table 15. Exfiltration rates for TMA and RP.
Table 16. Maximum concentrations along the TMA DMZ over 650 and 150 years of the simulation.

1. INTRODUCTION

In May of 1995, the Crandon Mining Company (later changed to Nicolet Minerals Company [NMC]) submitted the initial set of permit applications and supporting documents to the Wisconsin Department of Natural Resources (WDNR) for the proposed Crandon Mine in southern Forest County, Wisconsin (Foth and Van Dyke, 1995a) (Figure 1). Since then, the applicant has revised, updated and provided additional documents through the middle of 2003. An assessment of potential impacts to groundwater from mine waste facilities is required by the WDNR to be included with the submittals.

A technical working group (TWG) consisting of hydrogeologists and hydrologists from WDNR, the Wisconsin Geological and Natural History Survey (WGNHS), the U.S. Geological Survey (USGS), and RMT, Inc., was assembled to assist the WDNR. A major purpose of the group was to review and evaluate groundwater-related data, project submittals, and modeling, and to subsequently develop a final assessment of expected impacts to groundwater quality from the operation of the proposed mine waste facilities for the Environmental Impact Statement (EIS). Major work products of the TWG include evaluation of computer models submitted by the applicant to simulate regional groundwater flow (Krohelski and others, 2004), solute transport for the proposed Tailings Management Area (TMA) and Reclaim Pond (RP) (this report), and a review of the solute transport model for the reflooded mine (Kenoyer, 2004).

1.1 Purpose and scope of the Tailings Management Area / Reclaim Pond model

The applicant and its consultant, HSI GeoTrans, developed the groundwater flow and solute transport model reviewed here as a part of the supporting documentation for the permit application for the proposed mine (HSI GeoTrans, 1995a, 1996, 1998a, 1998b, 1999a, 1999b, 2000). The model simulates the transport of constituents dissolved in groundwater from the TMA and RP (Figure 2). The applicant used the model described in this report to evaluate potential compliance of the TMA and RP with groundwater standards and predict project environmental impacts. The model includes two components; a groundwater flow model that simulates the movement of groundwater in saturated geologic formations underlying the facility, and a solute transport model that uses the solution from the flow model to simulate the movement of solutes dissolved in the groundwater.

1.2 Purpose and scope of review

The purpose of this review was to determine the suitability of the applicant's model for simulating solute transport in groundwater in the vicinity of the proposed TMA and RP, make revisions to the model as deemed necessary and appropriate, and use the revised model to evaluate potential impacts to groundwater. This report documents the review and evaluation, and serves as a reference document to support the EIS (to be written and distributed by the WDNR) and the subsequent permit decisions.

The scope of the review included evaluating the suitability of the applicant's conceptual model for solute transport at the TMA and the subsequent translation of the conceptual model to a numerical model. The sensitivity of the model results to elements of the model design and parameterization was also assessed. We revised limited aspects of the model, such as the numerical approach (solver) used in the computer program. Boundary conditions and parameter

values were also modified as necessary to be consistent with the regional groundwater flow model (Krohelski and others, 2004). We then used the revised TMA model to estimate a range of potential impacts to groundwater from the TMA and RP, based on our estimates of key parameters, such as dispersivity and porosity. Several memos prepared during the course of this review summarize key findings and conclusions that framed the revisions made to the model prior to estimating the range of impacts. These memos addressed the effects of dispersivity and numerical solver on model results (Gotkowitz, 2000a), the impact of the TMA source term (Gotkowitz, 2000b), and a comparison of impacts to groundwater from the TMA and the RP (Gotkowitz, 2000c). Information presented in these memos is included in this report.

This review did not include evaluation of potential chemical constituents from mine waste, their expected concentrations from the source area, or the flux rate of constituents from the TMA and RP to groundwater. These aspects of the project were assessed by others under the direction of the WDNR. Results from their work are referenced where this review makes use of their findings. This review does not include predictions of actual constituent concentrations resulting from these transport and source term reviews. These predictions were conducted separately by the WDNR; this review relies upon scaled values in presentation of model results. The applicant also developed a model to simulate contaminant transport in the vicinity of the reflooded mine, which was reviewed by Kenoyer (2004).

1.3 Review of an uncalibrated solute transport model

Solute transport models used to predict solute concentrations in groundwater at a point in time and space can be calibrated to measurements of a contaminant or tracer plume at the facility being studied. In this way, modelers gain confidence that their simulations of concentrations into the future are based on a model that, at a minimum, does a reasonable job of simulating historical conditions. Calibration targets for a transport model are not available at a proposed facility where there is no historical contamination and where field testing of injected tracers has not been undertaken. In this case, because site-specific parameters cannot be estimated with field data, substantial uncertainty is inherent in the model results (e.g., Mehl and Hill, 2001; Hunt and Zheng, 1999). Where site-specific data are not available for model calibration, an acceptable approach is to assign a range of reasonable parameter values, based on those published in the technical literature for similar geologic and hydrogeologic conditions and based on professional judgment. Using such a range of parameter inputs produces a range of potential results.

The solute transport model reviewed here is an uncalibrated model; it has not been adjusted to match an observed set of site specific solute concentrations. Therefore, the utility of this review is limited to assessing the overall suitability of the model design to simulating conditions similar to what exists on-site, determining the parameters that the model is sensitive to, and assigning a range of reasonable values to these parameters. As such, the results presented here should not be interpreted as a certain prediction of future groundwater concentrations. The range of results does not capture all the uncertainty inherent in the model's representation of the natural system, but we believe that the upper and lower limits of the range provide a reasonable estimate of potential impacts of the TMA on groundwater quality for purposes of regulatory evaluation.

2. GEOLOGY

The geologic setting of the area of the proposed mine is described in detail in Section 3 of the applicant's Environmental Impact Report (EIR; Foth and Van Dyke, 1995a/1998). A portion of that description is summarized here because aspects of the geologic setting, such as the complex geometry of geologic deposits and the spatial variability of geologic parameters effecting solute transport, are critical in the construction of a quantitative solute transport model.

2.1 Surficial Deposits

The bedrock in the area around the Crandon ore body is primarily covered by unlithified deposits of glacial drift (till and associated sand and gravel) with lesser modern deposits of aeolian, alluvial, colluvial, and organic material. The glacial deposits vary from 50 to 350 ft in thickness (Simpkins and others, 1987). Till is typically exposed at the surface in drumlins that are clustered on upland areas. Associated glacial meltwater sands and gravels have filled in low-lying areas in and around the uplands, forming pitted and unpitted outwash plains and aggraded meltwater channels. Locally, the drift is overlain by post-glacial sediments consisting of wind-blown silts and fine sand (loess), organic deposits and alluvium.

During the Pleistocene epoch (2 million to 10,000 years ago), the region was repeatedly covered by glaciers. Deposits from four major glacial advances have been recognized in the vicinity of the Crandon ore body. A majority of the Pleistocene deposits currently found in the area appear to be from the late Wisconsinan glaciation and are about 25,000 to 10,000 years old. In some locations, Pre- to Early- Wisconsinan age sediments lie directly on top of the bedrock.

Southern Forest County is located along the margins of two lobes of the Wisconsinan ice sheet, the Langlade Lobe and the Green Bay Lobe. During Late Wisconsin time, the region was overridden first by the Green Bay Lobe and subsequently by the Langlade Lobe. This has resulted in a complex and diverse near-surface glacial stratigraphy and a varying topography of drumlins and moraines separated by lowlands. With each glacial advance, the then-existing topography controlled deposition of near-continuous outwash in the lowlands and somewhat discontinuous deposition of outwash in the uplands (Dunning and others, 1997). The site of the proposed mine and operations is located largely on a drumlin upland consisting of varying thicknesses of Late Wisconsinan till and outwash underlain by Pre- to Early Wisconsinan till and outwash. The Pre- to Early Wisconsinan till formations generally contain less sand and more silt and clay than the younger, Late Wisconsinan tills. Associated with the tills and outwash in the uplands are some ancient lacustrine deposits. Localized remnant loess deposits are present on hillsides in the drumlin upland. Accumulated sediments in lakes at the site consist of organics, silt, clay and sand. Wetlands at the site are underlain by accumulations of wetland sediments, consisting of organics, silt, and clay. The lowland areas adjacent to the drumlin uplands consist predominantly of alluvial and wetland sediments overlying Early Wisconsinan outwash and Pre- to Early Wisconsinan till.

The footprint of the TMA (Figure 1) is located in an area of drumlin uplands that is adjacent to a lowland area to the east. Upland outwash deposits are likely to be discontinuous with those in the lowlands. Till deposits in the uplands are expected to be continuous with those of the lowlands (Dunning and others, 1997).

2.2 Bedrock

The Crandon ore body is hosted in Early Proterozoic-age (late Precambrian time, between 1.8 and 1.9 billion years ago) bedrock of the Southern Province of the Canadian Shield. The bedrock at the site consists of metamorphosed submarine volcanic and associated marine sedimentary units that have undergone significant deformation. Bedding planes in the ore body are now aligned almost vertically along the east-west axis.

During Late Proterozoic (from deformation/metamorphism to 550 million years ago) and Phanerozoic (from 550 million years ago to the present) time, the bedrock was extensively weathered in the area of the ore body. Variability in bedrock weathering, along with structural trends (faults and fractures) and bedrock drainage patterns, produced the existing, irregular bedrock surface. The degree of bedrock weathering varies, due primarily to varying rock chemistry. Both physical and chemical weathering has resulted in mineral transformation into clays, oxides, enhanced fracturing, and material translocation. Investigations conducted in the 1980s described a layer of low permeability materials, termed the “resistive layer”, lying over the ore body (Rowe, 1984). Additional studies and reinterpretations of earlier data identified this layer as a combination of massive saprolite and Pre- to Early- Wisconsinan till. Massive saprolite is a clay-rich, highly decomposed rock formed in place by chemical weathering of igneous, sedimentary and metamorphic rocks. At the TMA site, the saprolite is directly overlain by the Pre- to Early Wisconsinan till. The layer of massive saprolite and till varies from about 10 to 80 ft in thickness in the TMA area. Below this layer lies structured saprolite, which is rock that has been weathered to mostly clays, iron oxides and quartz, but still retains the original rock structure.

3. GROUNDWATER AND SURFACE WATER CONDITIONS IN VICINITY OF TMA/RP

On a regional scale, the hydrogeologic conditions in the project area consist of unsaturated and saturated unlithified (primarily glacially-derived) material overlying saturated crystalline bedrock. In this area, the major water-bearing units are sands and gravels within the glacial drift. Groundwater flow occurs primarily within the surficial sediments, with the majority of flow focused within the more permeable outwash deposits.

Till deposits at the project site are extensive and contain sediments with a wide range of grain sizes. Each of the units within the glacial deposits are generally highly variable in composition. Till hydraulic conductivity ranges widely from about 0.0001 to 10 ft/day (Foth and Van Dyke, 1995a). Outwash, which was washed and sorted by glacial meltwater, consists of sandy and gravelly deposits with hydraulic conductivity ranging from about 0.01 to 200 ft/day (Foth and Van Dyke, 1995a). In contrast, lenses of lacustrine silts or clays located beneath existing upland lakes and some wetlands, and also scattered within the outwash and till deposits from paleo-lakes, have low hydraulic conductivity that impedes the movement of water. The conductivity of these materials ranges from about 0.00001 to 2 ft/day (Foth and Van Dyke, 1995a). The permeability of the bedrock is expected to be very low except along fractures and in substantially weathered zones. Though some water wells in the area are completed within the bedrock, the

major source of water for most of those wells is probably drainage from the overlying glacial material to fractures in crystalline rock.

The Precambrian bedrock exhibits both primary and secondary porosity/permeability features. The effective porosity of intact metamorphic rock is typically less than two percent, as voids that make up that porosity are generally small and not well interconnected. Therefore, the primary permeability of the bedrock in the study area is assumed to be very small. The ability of the Precambrian bedrock to transmit water is governed by the presence of secondary permeability features. Secondary features, including weathered zones (such as the saprolite) and interconnected fractures, occur largely within the upper portions of the bedrock. In the vicinity of the TMA, vertical hydraulic gradients are expected to be downward from the massive saprolite and glacial materials to the underlying bedrock, based on field data collected along the strike of the ore body (Rowe, 1984 and Foth & VanDyke, 1995c).

In general, high water-table elevations occur within upland areas and around upland lakes and wetlands (as in the vicinity of the proposed TMA), and low water-table elevations occur in lowland areas associated with streams, wetlands or lakes (as in the area of Hemlock Creek) (Figure 3). Groundwater recharge areas are typically associated with upland areas. Groundwater discharge areas are typically restricted to a narrow band along streams and around lowland wetlands and lakes. A regional groundwater high of about 1,640 ft above sea level is located in the vicinity of Lake Lucerne. Groundwater lows of about 1,532 ft above sea level are located near the outlets of Rice Lake and Pickerel Lake. At the proposed TMA, the landfill cells overlie a local groundwater high of about 1594 ft above sea level. The water table decreases in elevation to the northwest, toward Swamp Creek, and to the northeast toward Hemlock Creek.

3.1 Hydrostratigraphic Units

Hydrostratigraphic units are geologic deposits that are significant in characterizing the groundwater flow system of interest. These units may be entire geologic formations or several formations together, or may be specific features within formations. The definition of hydrostratigraphic units in a particular area depends, in part, on the scale at which the groundwater system is being analyzed. In the regional groundwater flow model, hydrostratigraphic units for the site area were identified as 1) the localized upland lakebed and wetland deposits, 2) the Late Wisconsinan to present unlithified glacial or fluvial deposits (the recent unlithified deposits), 3) the Pre- to early Wisconsinan-age till/massive saprolite, and 4) the Precambrian bedrock (HSI GeoTrans, 1995; Krohelski and others, 2004). The bedrock has a much lower hydraulic conductivity than the unlithified deposits. Hydraulic gradients are largely downward from the overlying unlithified deposits to the bedrock in the vicinity of the TMA. For these reasons, the most significant impacts of transport from the TMA are assumed to occur in the uppermost aquifer; therefore, the Precambrian bedrock is not further considered here.

3.1.1 Upland Lakebed and Wetland Deposits

Upland lakebed and wetland deposits are localized hydrostratigraphic units important to the hydrologic behavior of the upland lakes and many of the larger upland wetlands near the project site. These deposits consist of low-permeability silts and clays, which have accumulated in small basins in the upland areas.

3.1.2 Recent Unlithified Deposits

The upper-most unlithified deposits that extend across the site area consist of glacial and post-glacial material. The post-glacial deposits are aeolian-, colluvial-, or alluvial-derived and present only at the land surface. The aeolian deposits consist of loess (fine sand and silt) deposited during the period immediately following the Late-Wisconsinan glaciation. These deposits have subsequently been substantially modified by erosion and slope-processes. The colluvial deposits result from creep on upland slopes that modify the existing sediments. The alluvial deposits, located in the stream valleys, consist mostly of high-permeability stratified sand and gravel. Some overbank silt fines underlie many of the stream-side wetlands.

3.1.3 Glacial Unlithified Deposits

The glacial deposits consist mostly of Late Wisconsinan-age tills and associated outwash. The tills are unstratified to weakly stratified, and are composed of a wide variety of source rock with a wide range of grain sizes, from silt and clay to gravel and boulders. Till hydraulic conductivity varies widely over the site area and is controlled by the local nature of the till deposit. The Late Wisconsinan-age tills are laterally extensive in nature, but their presence at the ground surface is limited primarily to the upland areas, such as at the proposed TMA. Much of the recharge to the groundwater occurs through these upland till units.

The outwash, deposited largely by pro- and sub-glacial meltwater streams, consists of high-permeability sand and gravel. The Late Wisconsinan-age outwash deposits are also extensive, but mostly discontinuous, across the uplands. They are present in the vicinity of the TMA, but are not likely continuous from the uplands area to the lowlands associated with Hemlock and Swamp Creeks (Dunning and others, 1977). Swamp and Hemlock Creeks incise outwash through most of their lengths and receive groundwater discharge as their baseflow.

3.1.4 Pre- to Early Wisconsinan Till/Massive Saprolite

The Pre- to Early Wisconsinan till and massive saprolite are geologic units with substantially different geneses that were grouped as a single hydrostratigraphic unit because of their juxtaposition in the stratigraphy and similar hydrologic characteristics. In the vicinity of the TMA, the Pre- to Early- Wisconsinan-age tills reside stratigraphically on top of the massive saprolite. Together, at the scale of the study area, the massive saprolite and the Pre- to Early-Wisconsinan till act as a single hydrologic unit with a moderate to low permeability. This unit appears to be present throughout the area of interest and lies between the younger unlithified sediments and the bedrock in the groundwater flow system.

4. DESCRIPTION OF APPLICANT'S TMA / RP MODEL

The TMA / RP flow and transport model and subsequent revisions to it are fully documented by the applicant in HSI GeoTrans (1996, 1998a, 1999a, 1999b, 2000). A brief summary is presented here.

4.1 Conceptual model of contaminant transport at the TMA / RP

The applicant's conceptual model of contaminant transport from the TMA / RP specifies several phases of source loading from the TMA and RP. In the latest version of the model (HSI

GeoTrans, 2000), these phases include a loading period for each of the three TMA cells (Figure 4), a two-year period of consolidation and covering, a post-closure period during which leakage occurs through hypothetical imperfections in the composite liner, and a fourth, final phase during which leakage occurs through the degraded composite liner. Source loading from the RP to groundwater is characterized in two additional phases. During the RP operational phase, surface decant water and leachate from the TMA will be discharged to the pond. In the RP post-operational phase, only TMA leachate will be discharged to the pond. (Each of these six periods constitutes a single model run.)

In the model, solutes predicted to exfiltrate through the TMA and RP liners are applied directly to the water table as a concentration associated with a recharge flux (the exfiltration rate from the TMA and RP). Potential effects of transport through the vadose zone (such as sorption onto solids, evaporative concentration, or chemical transformations) are not considered. The conceptual model includes the processes of advection and dispersion within the aquifer. Molecular diffusion, sorption onto aquifer solids (retardation) and chemical reactions within the aquifer are not considered. Geologic characterization of the subsurface materials is used to identify areas of similar hydraulic conductivity. This conceptual model implies that beyond the strength and timing of the source function, dilution and mixing along flow paths are the only processes that affect groundwater concentrations.

Contaminant mass exits the groundwater system at locations of groundwater discharge to surface water bodies. The TMA is within the Swamp Creek / Hemlock Creek groundwater basin, near the groundwater divide with the Pickeral Creek basin (Figures 1 and 3). Groundwater discharge occurs to the northeast at Hemlock Creek, and to the northwest to Swamp Creek. There are no groundwater discharge areas located between the source areas and the design management zones (DMZs) of the TMA and RP. The DMZs are the point of compliance for groundwater standards, and are located 150 ft away from the RP and 1200 ft from the TMA boundaries (Figure 4). (These two DMZs are at different distances because the TMA and the RP fall into different classes of regulated facilities.)

4.2 Computer Codes

A groundwater flow simulation is a necessary component to the simulation of contaminant transport, because the results of the flow simulation provide the advective flow field for the transport simulation. The applicant used MODFLOW (McDonald and Harbaugh, 1988; Harbaugh and McDonald, 1996), a finite difference three-dimensional groundwater flow model code, to simulate groundwater flow over the TMA transport model domain. A version of MODFLOW provided by HSI GeoTrans, corresponding to the MODFLOW96 code distributed by the USGS, was used for this review.

The MT3D computer code (Zheng, 1990) is widely used in the practice of contaminant transport because it offers three-dimensional simulations of aquifer transport and is compatible with MODFLOW. The applicant used MT3D⁹⁶ (Zheng, 1996), which was the current version of the code at the time the model was initially constructed. MT3D is frequently updated as a result of on-going research. During early phases of this review, the latest published version of the program, MT3DMS (Zheng and Wang, 1998) was used. Subsequent improvements to MT3DMS

were made by the developer of the code for the WDNR's use in this review (discussed below), and later portions of the review were conducted with this modified version.

The applicant provided several FORTRAN programs for pre-processing model input and post-processing model results. ACALC was used to create and modify input arrays for hydraulic conductivity and recharge flux. The program SUPERPOS multiplies each of six model runs that comprise a full simulation by the constituent source concentrations and sums these six concentration arrays to generate results for the full simulation. The program ECURVE reads the MT3D output for a single run, or the SUPERPOS output for a full simulation, and writes the maximum concentration occurring along the DMZ and its row, column, layer location, for each model time step. Output from this program is useful in evaluating potential compliance with a numerical standard at the DMZ.

The pre- and post- processor Groundwater Vistas (Rumbaugh and Rumbaugh, 1996) was also used for portions of this review to visualize model input and output, and in some cases to modify model input.

4.3 Model structure

The applicant constructed the TMA model by extracting the portion of the regional groundwater flow model (HSI GeoTrans, 1998b) that encompasses the TMA and RP, and developing it as a sub-model that runs independently of the regional model. The purpose of the sub-model was to refine the discretization of the model domain without exceeding computational capacity, and to permit rotation of the grid to align it with the principal directions of groundwater flow in the vicinity of the TMA. The applicant assessed the MODFLOW groundwater flow portion of the transport model by checking the similarity of the resulting flow field to that produced by the regional model in the vicinity of the TMA and by comparing modeled particle travel times to travel times calculated from groundwater chlorofluorocarbon (CFC) data collected at the project site (Saad, 1996).

The applicant's TMA sub-model has 76 rows, 73 columns, and 7 layers, with a row, column spacing of 100 ft by 100 ft. The grid was rotated 35 degrees west of north (HSI GeoTrans, 1998a) so that the primary direction of flow from the TMA to Hemlock Creek is along the x-axis of the model grid (Figure 2). Layer thickness is variable across the domain. Layer 1 of the TMA sub-model is the equivalent of regional flow model layer 1; layer 2 of the regional model was divided to form layers 2, 3, and 4 of the TMA sub-model; regional model layer 3 became TMA model layers 5 and 6; and regional model layer 4 is the equivalent of TMA model layer 7 (Table 1). Dividing of layers in this fashion was done to increase resolution of the model in the outwash (the higher conductivity units). Because the layering is not done strictly along hydrostratigraphic contacts, the applicant developed a FORTRAN computer code (called ACALC) that uses an averaging method to calculate the hydraulic conductivity of each model cell based on the proportion of each material present in that cell.

Boundary conditions in the TMA sub-model include a no-flow boundary at the base of the model; the model does not simulate flow or transport between the base of the Pre- to Early-Wisconsinan till/massive saprolite layer and deeper bedrock formations (the massive saprolite is considered hydrogeologically similar to the overlying Pre- to Early- Wisconsinan till). The

northeastern boundary of the sub-model is set at Hemlock Creek, which is represented with the MODFLOW River package. The creek is modeled as a fully-penetrating boundary in the glacial aquifer by designating all model cells northeast of the creek inactive. This imposes a condition of no flow or transport across or under the creek. The general head boundary condition is used along the northwestern, southwestern and southeastern edges of the sub-model. Heads were extracted from the regional model at cells that fall on the corner boundaries of the sub-model domain. Using a FORTRAN utility developed by HSI GeoTrans, these values of head were interpolated to derive the head values along the horizontal boundaries of the sub-model. This distribution of head along the boundaries is used in each model layer, so that the boundary condition does not impose a vertical gradient. The heads at the sub-model boundaries change at year 32 of the transport simulation, reflecting in an approximate way the change in the regional flow field after dewatering of the mine ceases.

In the applicant's sub-model, recharge is applied to the model domain outside of the TMA and RP footprints at a rate of 9.7 inches per year, which is the recharge rate used in the applicant's regional flow model. Areas receiving recharge rates other than background include surface water runoff basins, discharge wetlands, and seepage wetlands (seepage wetlands were represented with MODFLOW river cells) (HSI GeoTrans, 1998a).

Recharge rates representing exfiltration from the TMA (Appendix A of HSI GeoTrans, 1998a,) were calculated with the HELP model (Schroeder and others, 1994). Recharge rates representing exfiltration rates from the RP were calculated with an analytical model that accounts for diffusion and leakage through the pond's composite liner (Attachment 4 of HSI GeoTrans, 1998a). In the solute transport model, flow within the three TMA cells and the RP is not simulated. Mass loading to the groundwater flow system from the TMA cells and the RP is represented by a concentration associated with exfiltration (recharge) water applied to the top of the water table (the water table is below the base of the TMA and RP liners).

In the applicant's transport model, the MT3D simulation covers 650 years, divided into 22 model stress periods of various lengths of time. TMA and RP exfiltration rates are assumed to be constant within a stress period and to vary between stress periods to simulate changing flux rates from the source areas. Changes in the exfiltration rate coincide with various phases of the facility development. For example, the exfiltration rate is greater when a TMA cell is open and accepting waste and decreases after the cap has been installed, because process water is not being discharged to the cell and the cap reduces the amount of precipitation that enters the cell. Over the course of several revisions of their model, this scheme was refined so that in the final version (HSI GeoTrans, 2000) a complete transport model simulation includes the results of six 650-year simulations added together, or "superposed", in order to accommodate changes in the source term concentration over time and differences between TMA and RP source terms (Table 2).

In each of the six simulations, recharge water from the TMA (runs 1 through 4) or RP (runs 5 and 6) is assigned a unit concentration value during the model stress periods representing the appropriate phase of the simulation. Recharge water applied to model cells outside of the active source area in that run is assigned a concentration of zero. After the six runs are complete, the six resulting concentration arrays are multiplied by a user-specified source concentration for each run for a particular constituent, and the six arrays are then summed to generate the concentration

of a constituent over the complete transport simulation. For example, sulfate may be expected to have a source concentration of 2,000 ppm during TMA loading, 1,500 ppm during consolidation, 300 ppm under capped conditions, and 2,000 ppm after liner breakdown. Each of these values would be multiplied by the concentrations from runs 1 through 4, respectively. The sulfate concentrations expected in exfiltration from the RP during operation and post operation would be multiplied by the results of runs 5 and 6, respectively. These six concentration arrays would then be summed to arrive at a concentration array for sulfate over the 650 year simulated period. This design allows for multiple contaminants to be evaluated using the output from a single set of model runs. The applicant developed a FORTRAN program named SUPERPOS to calculate this superposition of results.

The applicant presents two complete simulations: the best engineering judgment for transport (BEJT) parameter set and the practical worst case for transport (PWCT) parameter set. These runs differ in that PWCT uses lower values of dispersion and lower values of vertical hydraulic conductivity in all model layers (Table 3). Both the BEJT and PWCT scenarios use the same set of exfiltration rates from the TMA and RP.

5. MODEL EVALUATION

5.1 Conceptual model and translation to numerical model

The Applicant's conceptual model of contaminant transport from the TMA and RP described in the preceding section is considered adequate for the purposes of evaluating the impacts to groundwater quality for solutes that are expected to be non-reactive and non-sorbative, such as sulfate. The assumption of no retardation or decay in the unsaturated or saturated zones is appropriate for these solutes, which will undergo little to no chemical degradation or transformation in the subsurface.

This conceptual model, by ignoring processes of sorption and transformation, is likely to over-predict concentrations of some constituents arriving at the DMZ. Metals and metalloids, such as arsenic and copper, have an affinity for some solid or colloidal material in the aquifer matrix, such as iron and manganese hydroxides. Sorption would tend to retard the contaminant plume, leading to later arrival times, and potentially lower maximum concentrations if the sorption capacity of the aquifer solids is high. These same constituents might also undergo a decrease in concentration along a flow path due to precipitation of mineral solids. Both sorption and mineral precipitation are reversible reactions, and if geochemical or biogeochemical conditions change, sorbed or precipitated constituents can act as a secondary source of contaminants in the aquifer. Therefore, these processes could conceivably lower early-time concentrations but become a longer-term, low-concentration source of constituents to groundwater if geochemical chemical conditions change over time.

However, disregarding the effects of sorption and transformation is expected to lead to an over-prediction of maximum concentrations for most solutes of interest, and is therefore considered a conservative assumption for evaluating compliance with numerical water quality standards. Under the assumption that all constituents are treated as conservative (i.e., no sorption and no

transformations), the methods of scaling and superposition of results can be applied to the simulations so that one set of model runs suffices for all constituents of interest.

Solute fate and transport in the unsaturated zone is not considered in the TMA model. Contaminants are assumed to arrive instantaneously at the water table without undergoing degradation, sorption or dispersion within the vadose zone. This approach is conservative, in that neglecting vadose zone processes will yield conservatively high estimates of concentrations reaching the water table at shorter times from the source areas.

In reality, the majority of advective transport will remain within the unlithified formations because these deposits are much more transmissive to both water and contaminants than the less porous, underlying bedrock. In the model, contaminants remain in the unlithified deposits because a no-flow boundary is used at the base of the model. The assumption that any contaminant flux to the bedrock is negligible may produce a conservatively high estimate of concentrations within the glacial deposits.

5.2 Revisions to the model

During the course of this review, we made limited revisions to the model submitted by the applicant. These revisions were made so that the TMA model would be consistent with revisions made to the regional groundwater flow model by the TWG (Krohelski and others, 2004), and to correct some of the concerns noted during the sensitivity analyses described below.

5.2.1 Boundary conditions and hydraulic conductivity

The values assigned to the general head boundary conditions were changed from those used by the applicant. The values assigned were extracted from the regional model simulations at various mine-inflow extraction rates (the High End rate of 1250 gpm; the applicant's proposed limit of 602 gpm; and the Low End rate of 285 gpm)¹. This process included running the regional flow model with a particular pumping rate and then interpolating the simulated heads horizontally, along the rows of cells constituting the boundaries of the TMA model.

Changes to the background recharge rate, hydraulic conductivity values, and updates to the configuration of the river cells and wetlands were incorporated for use in the revised TMA model so that it was consistent with changes made to the equivalent area in the regional model. The background recharge rate was increased slightly from the applicant's model, by a factor of 1.02299 for the Low End and proposed limit runs and 1.02247 for the High End run. Hydraulic conductivities and vertical conductance values were reduced slightly from the applicant's values by a factor of 0.96516 for the Low End and proposed limit cases and a value of 0.93252 for the high end case. Seepage wetlands were removed from the River package, and instead were simulated as areas receiving the dryland recharge rate applied to the model. This change removed the seepage wetlands as areas of focused groundwater recharge and was made to make the TMA model consistent with the TWG regional flow model. This change did not have a

¹ These regional flow model simulations are referred to in Krohelski and others (2004) as follows: the High End run is HHCUIB and incorporates High End inputs with extensive grouting for the copper phase of the mining. The proposed limiting rate run is ZINC1A, which incorporates Low End inputs with limited grouting for the zinc phase of mining. The Low End run is called LLZN1B: it incorporates Low End inputs with extensive grouting for the zinc phase of mining.

significant effect on the flow field of the TMA model. The River package was also altered to include simulation of Creek 33-8 in the southeast portion of the TMA model domain.

5.2.2 Stress periods

Although the total amount of time of the simulations was kept constant (650 years), the time was divided into more transport stress periods than the 20 or 22 stress periods in the versions of the TMA model submitted by the applicant. Thirty-four stress periods were ultimately used in the revised model to provide more flexibility in testing model boundary conditions and source area exfiltration rates.

5.2.3 Exfiltration rates

The WDNR arrived at final estimates of exfiltration rates from the TMA and RP based on various scenarios of facility design (Benson and Grefe, 2002). The revised model was run with these exfiltration rates (described in Section 7.1) to arrive at a range of predictions from the TMA and RP. Prior to these final simulations, the model was run with various estimates to evaluate the importance of exfiltration rates in the model results (Section 6.3). Exfiltration is applied as a recharge flux to the model, as described in Section 4.3.

5.3 Methods used to evaluate results

Results from model simulations were evaluated in several ways. In one approach, groundwater concentrations at the point of standards enforcement (that is, anywhere along the DMZ) are compared for two or more simulations. The ECURVE utility program, which is a post-processing FORTRAN code for MT3D output developed by the applicant, identifies the maximum concentration anywhere along the DMZ at each time step that output is saved over the period of model simulation. This method emphasizes evaluation of the model in terms of compliance at the point of standards enforcement (the DMZ). It does not yield reliable insight into the morphology of the simulated plume because the point at which concentrations are reported change from time step to time step. Additionally, the locations of the maximum concentration are not necessarily equivalent between simulations displayed on these graphs. The method simply identifies the maximum concentration that arrives anywhere along the DMZ at each time step for each run.

Traditional breakthrough curves, presenting the concentration over time at a particular location, are also used in this report to illustrate model results. These curves allow the reader to understand the evolution of the plume over time at a particular point in space, and to compare that evolution at that point for several simulations.

Results are also evaluated by comparing changes in overall plume development, such as the rate, magnitude and direction of solute migration away from the source areas. This is accomplished by comparing plan view maps of concentrations over time. Where plan view maps are generated from within a single model layer, or where they are generated from concentrations at a particular model elevation, are noted in the figure caption. In some figures, in order to present three-dimensional results in plan view, results are sometimes presented by summing the mass at a model cell over the seven model layers and contouring this planar array. The concentration (assuming a unit source of 1 mg/L) is converted to an equivalent mass by multiplying it by the

saturated thickness of each cell and the porosity, yielding units of mg/square foot. Although uncommon units, this method has the advantage of showing both the lateral distribution of mass and the total mass in the system.

Many of the figures presented in this report contain graphical output of model results. The reader is reminded that although simulations using different exfiltration rates are never compared directly in these figures, portions of the review were completed with different exfiltration rates for the TMA and RP. Therefore, the magnitude of results displayed in a graph should not be compared to the magnitude of results in another graph, unless the same model run number is indicated. Vertical scales were selected so that the result illustrated by each graph is adequately displayed.

6. RESULTS FROM REVISED MODEL AND SENSITIVITY TO SELECTED FEATURES

6.1 Numerical solver in MT3D

At the time that the applicant's TMA model was initially developed, the version of the code publicly available, MT3D96 (Zheng, 1996), offered an explicit finite-difference solution method using upstream weighting. This solver has the advantage of achieving an acceptable contaminant mass balance and shorter model run times, and was used by the applicant for all model runs. However, the finite difference method can introduce numerical dispersion into the model results, causing earlier first arrival times and lower maximum concentrations. The effect of numerical dispersion on model results is not distinguishable from the effect of the physical dispersion that is explicitly specified by the modeler. The other solution method available in the MT3D96 code, the method-of-characteristics (MOC), is a particle-based tracking method. While the MOC method does not introduce numerical dispersion, it may not achieve an acceptable mass balance under all flow conditions. Although these complications of the numerical methods are widely acknowledged in the scientific literature (e.g., Zheng and Bennett, 1995), there is no practical way to identify the exact magnitude of the error in results introduced by either numerical dispersion or mass balance problems.

The latest published version of the program, MT3DMS (Zheng and Wang, 1998) offers additional improvements in the numerical methods available for solving the advection-dispersion equation. Options include a generalized conjugate gradient (GCG) method, which is an implicit finite difference method, applied to the non-advection terms. An implicit finite-difference solver, with centered-in-space or upstream weighting, and a third-order total-variation-diminishing (TVD) method are available for the advection term, in addition to the explicit finite-difference and MOC methods. The TVD solver is preferred because it is mass conservative, minimizes numerical dispersion, and incorporates procedures that limit numerical oscillation (Zheng and Wang, 1998). The implicit finite-difference method with centered-in-space weighting may introduce numerical oscillation but, unlike the explicit finite difference method, is not susceptible to numerical dispersion. Additionally, each method may not converge to a solution under all conditions. For example, a particular method may be sensitive to factors such as irregular thickness of model layers or irregular cell dimensions in the x, y plane.

The new solvers available in MT3DMS were tested on the applicant's June 1999 version of the TMA/RP model. The various combinations of MT3DMS solvers used with the TMA/RP model and the associated complications with each are presented in Table 4. Not all solution methods worked under the scenarios tested. The particle tracking method (the MOC solver) introduced a significant amount of mass balance error in the TMA/RP model. A 9% mass balance error occurs with the BEJT parameter values, and increases to up to 30% when dispersion is reduced from the BEJT values. On the basis of these results, the MOC method did not appear to offer a reasonable solution for this model, and was not considered further in this review.

The implicit finite-difference method with upstream weighting yielded similar results to the explicit finite-difference solution used by the applicant. The implicit method limits numerical oscillation but can introduce significant numerical dispersion due to truncation error (Zheng and Wang, 1998). Results from these simulations are not considered further due to this concern.

Similar maximum concentrations arrive at the TMA DMZ in simulations using the implicit finite-difference method with centered-in-space weighting and using the TVD method, when the model was run with the BEJT dispersion values (Figure 5). However, the simulated maximum concentrations do not show good agreement with lower values of dispersion (Figure 6). Although the centered-in-space technique eliminates numerical dispersion, it appears to cause numerical oscillation in its application to the TMA/RP model.

The TVD solver used with BEJT dispersivity values resulted in a maximum concentration at the TMA DMZ that is 22% greater than the maximum concentration with the explicit finite-difference method (Figure 5). The sensitivity of the model to the numerical solver increases with smaller values of vertical dispersivity. With a vertical dispersivity of 0.5 ft, the maximum concentration at the DMZ with the TVD solver was 36% greater than with the explicit finite-difference method (Figure 6).

The version of the TVD solver in the publicly available MT3DMS code that was used during early portions of this review led to numerical instability in the TMA model at simulation times exceeding 150 years. At the request of the WDNR, the author of the MT3D code improved upon the TVD solver so that the limitations of this method for this model were eventually overcome. These changes are described in a document included as Appendix 1 to this report. Final runs presented here were completed with the revised TVD solver.

6.2 Sensitivity to source area

The purpose of this analysis was to assess the impact of contaminant mass input at the TMA compared to that input at the RP. The results show that with the applicant's estimate of exfiltration in the June 1999 report, the RP is the source of the maximum concentrations that arrive at the RP DMZ and at the TMA DMZ.

The method followed in this sensitivity analysis was to run the model with the BEJT parameters twice, varying the source from the TMA and the RP. In the first run, the concentration associated with recharge from the TMA cells is set to zero and the RP is the only source of contaminant mass to the model. In the second run, the concentration associated with recharge from the RP is set to zero and the TMA is the only source of solute mass to the model. This sensitivity analysis

consisted of only the first of the three model runs that were ultimately superposed to constitute a complete simulation with the June 1999 model. This was a reasonable approach to this analysis because in this version of the model, the RP was operational for the first 31 years of the simulation and was not a contaminant source in the second and third model runs.

Results from these two simulations (Figures 7 and 8) show that the RP is the predominant source of the maximum concentrations reaching the TMA DMZ and the RP DMZ. These simulations also indicate that with either the TMA or the RP as the contaminant source, higher maximum concentrations reach the RP DMZ than reach the TMA DMZ. This is because the plume from the TMA flows west, encountering the RP DMZ prior to reaching the TMA DMZ (Figure 4). The version of the model submitted by the applicant in 2000 (HSI GeoTrans, 2000) addressed these issues by separating out the RP source from the TMA source so that mass input to the groundwater system from the RP is simulated independently of mass input from the TMA. This permits the model to be used to evaluate changes in design of the TMA and RP that affect exfiltration rates. The applicant subsequently revised the design of the RP, reducing the magnitude of the source term from the RP used in subsequent evaluation of the model (Section 7.1).

6.3 TMA exfiltration rate

The purpose of this analysis was to assess model sensitivity to the source function used at the three TMA cells. This was assessed by varying the exfiltration rate from the facility and comparing maximum concentrations arriving at the DMZ over time. The exfiltration rates used in the analysis were provided by Professor Craig Benson, based on a literature review of leakage rates from composite liners (C. Benson, WDNR consultant, February 2000, verbal comm.). Model results indicate that simulated constituent concentrations reaching the DMZ increase significantly during the post-closure period if exfiltration rates estimated from the scientific literature are used rather than rates predicted by the applicant's HELP model simulations of the TMA (Attachment 2 to HSI GeoTrans, 1998a).

The applicant used the same set of exfiltration rates from the facility in their BEJT and PWCT simulations; these rates were based on output from the HELP model. These exfiltration rates, applied at each of the three TMA cells (1 A and B, 2 and 3), are presented in Tables 5 through 8, respectively. The exfiltration rate from each TMA cell varies over time in discrete phases of the landfill operations, such as pre-construction, operations, consolidation, and with the landfill cap in place (Table 9). The exfiltration rate generally decreases as operations cease and the cell caps are constructed and maintained.

The exfiltration rates used in this sensitivity analysis for each TMA cell are also presented in Tables 5 through 8. These rates were based on the literature review of leakage rates from composite liners conducted by Benson. He suggested that a reasonably conservative assumption is a liner leakage rate of 0.65 L/ha-d (2.08×10^{-7} ft/d) for operational TMA phases. Based on a long-term study of a similarly constructed cap in a similar climate, Benson suggested that a conservative estimate of a post-capping liner leakage rate is 1 mm/yr (8.99×10^{-6} ft/d). The leakage rate increases over time because the pre-closure, operational rate is a result of liner leakage with a leachate collection system in operation. The post-closure rate is a result of

assuming that long-term leakage through the liner with the leachate collection system no longer in operation is equal to the long-term leakage rate through the TMA cap.

These exfiltration rates were applied in this sensitivity analysis considering an estimate by the applicant that each TMA cell will drain to field capacity at about 115 years after the cap is installed. Once field capacity is reached, exfiltration from the facility is expected to equal infiltration through the cap. In model run “1mmperc”, the applicant’s BEJT model parameters were used with the exception of the exfiltration rate. The HELP model results presented by the applicant were used during all operational and 115-year post-capping phases where the HELP model results exceeded the 2.08×10^{-7} ft/d leakage rate estimated by Benson; 2.08×10^{-7} ft/d was used during phases where it exceeded the HELP model results. For all times after 115 years post-capping, the cap infiltration rate of 8.99×10^{-6} ft/d was used as the TMA exfiltration rate. These rates were applied to the base of each TMA cell; rates from the lower and upper side slopes of the TMA cells were not changed from the applicant’s values (Tables 5 through 8).

Model results from the sensitivity run “1mmperc” are presented along with results from the BEJT and PWCT runs in Figure 9. (Each of these three sets of results are the composites of the three model runs, t09c1, t09c2 and t07c3, that constitute a complete, 650-year simulation in the June 1999 version of the model.) Relative to the slight increase in maximum concentrations resulting from the PWCT over the BEJT parameters, increasing the long-term exfiltration rate to 1 mm/yr (8.99×10^{-6} ft/d) with the BEJT parameter set causes a substantial increase in the maximum concentrations arriving at the TMA DMZ. By comparing the results in this Figure to the exfiltration rates in effect during each stress period (Tables 5 through 8), it is apparent that changes to the long-term exfiltration rate cause the rise in concentrations at later times in the “1mmperc” sensitivity run. Because the results presented here are based on a relative unit concentration value, the difference between the simulations may be more pronounced if the source concentrations are greater during the later years of the simulation.

6.4 Drawdown and recovery of water levels at the model boundary

The applicant’s model simulates successive steady-state conditions, meaning that although transient effects are not simulated, boundary conditions change during the simulation from one steady-state condition to another. During the first 32 years of the 650-year simulation (the period of mine operations), heads at the boundaries are lower, reflecting pumping for mine dewatering. Water levels increase by the full amount of water level recovery in one step, simulating an instantaneous recovery of the system after cessation of pumping.

The effect of simulating more detail in the drawdown and recovery of water levels was tested by inserting more steps in the change in water levels at the boundaries of the TMA model. In this simulation, 60% of the total drawdown from pre-mining water levels is simulated from the beginning of the simulation to year two, 80% occurs after two years of mine operations, and 100% of the drawdown is simulated after six years of operation. 60% of water level recovery following the cessation of dewatering is simulated to occur at the end of mining operations (32 years), 80% of recovery at 34 years, and 100% of recovery at 38 years. Although this pattern of drawdown and recovery was somewhat arbitrary, it was thought to be sufficient to test the sensitivity of the model to the assumption of instantaneous drawdown and recovery.

Results from this simulation are similar to those from where drawdown and recovery are assumed to be instantaneous (Figure 10). The maximum concentrations reaching the TMA DMZ are not significantly affected by this change in boundary conditions.

6.5 Dispersion

Dispersion is specified in the model to account for the effect of small-scale heterogeneities that are not incorporated in the deterministic array of hydraulic conductivity values assigned to the model grid. The dispersion parameter has a similar effect on model results to that of numerical dispersion, generally decreasing simulated concentrations due to increased mixing and spreading of contaminant mass along flow paths. Model sensitivity to dispersion was evaluated with various combinations of longitudinal, transverse horizontal and transverse vertical dispersivity values (Table 10). These simulations were compared to the applicant's BEJT run, in which longitudinal, transverse horizontal and vertical dispersivity values were set at 50, 5 and 5 ft, respectively.

6.5.1. Longitudinal dispersivity

Maximum concentrations arriving at the TMA DMZ over time are similar in run disp03, in which longitudinal dispersivity was decreased by an order of magnitude (to 5 ft) while transverse horizontal and vertical dispersivities were held at 5 ft, as in the applicant's BEJT case (Figure 11). The similarity in the results is also illustrated by breakthrough curves from layers 7 and 4 at a cell along the TMA DMZ (Figures 12a and b). The breakthrough curves demonstrate that concentrations over time at that location are similar in shallow and deep layers, indicating that the vertical distribution of mass over time is not affected by changes to the longitudinal dispersivity.

The sensitivity of the model to longitudinal dispersivity was also evaluated using lower values of horizontal and vertical transverse dispersivities. Both transverse dispersivities were decreased to 0.5 ft and longitudinal dispersivity was varied from 50 to 0.5 ft (Table 10, runs disp04, disp05 and disp06). Maximum concentrations arriving at the TMA DMZ over time are essentially identical in these three runs, supporting the conclusion that concentrations at the point of compliance are insensitive to changes in longitudinal dispersivity (Figure 13).

6.5.2 Transverse dispersivity

The TMA/RP model was run with various combinations of values for transverse horizontal (α_{TH}) and transverse vertical (α_{TV}) dispersivity to test the sensitivity of the model to these parameters. As discussed in Section 7.1 of this report, vertical transverse dispersivity is commonly assigned a value that is one to two orders of magnitude smaller than horizontal transverse dispersivity, based upon an analysis of field data presented by Gelhar and others (1992). Results comparing various values of α_{TH} and α_{TV} to the BEJT case are presented in Figure 14. Run disp07, in which only α_{TV} is reduced, results in a maximum concentration that is about 3.5 % lower than run disp06, in which both α_{TH} and α_{TV} are reduced, indicating that the change in transverse vertical dispersivity accounts for much of the change in results. Both runs exceed (by about 24% for disp06 and 28 % for disp07) the maximum concentration that arrives at the DMZ in the BEJT case.

The effect of the higher vertical transverse dispersivity used in the applicant's BEJT model is to drive contamination into lower layers in the model at earlier times, which leads to more spreading of mass throughout the layers and lower concentrations ultimately reaching the TMA DMZ. This is illustrated by two presentations of the model results. Figure 14 shows that with the higher vertical dispersivity of the BEJT simulation, the maximum concentration reaching the DMZ is lower than under low vertical dispersivity (model runs disp07 and disp06), and that the maximum concentration in the BEJT simulation occurs in a deeper model layer (model layer 7 rather than model layer 4). A breakthrough curve located along the western boundary of the TMA DMZ (Figure 15) also illustrates differences in the vertical distribution of mass through the aquifer thickness under different vertical dispersivity. Under the BEJT condition of vertical dispersivity of 5 ft, mass arrives earlier in this deep layer than with a vertical dispersivity of 0.5 ft. The earlier, deeper spreading of the plume with higher vertical dispersivity causes more mixing of the mass at earlier times in the simulation, ultimately lowering the maximum concentrations reaching the DMZ (Figure 14).

Results from a simulation with no transverse vertical dispersivity and a simulation with no transverse horizontal dispersivity confirm that the model is sensitive to changes in transverse vertical rather than transverse horizontal dispersivity (Figure 16). These results indicate that while eliminating horizontal transverse dispersivity induces little change from the BEJT case, eliminating vertical dispersivity substantially increases (by more than two times) the maximum concentrations arriving at the TMA DMZ.

6.6 Vertical hydraulic conductivity

In the applicant's PWCT run, values assigned to both dispersion and vertical hydraulic conductivity parameters are reduced (Table 11). In order to evaluate the effect of a decrease in vertical conductivity independently of changes to dispersion, we used the applicant's June 1999 PWCT model (here, vertical hydraulic conductivity is reduced by an order of magnitude from the BEJT case) and increased the dispersion terms to the BEJT values of 50, 5 and 5 ft.

A reduction in vertical conductivity, the "lowkv" run, has little effect on the model results. Similar but slightly lower maximum concentrations reach the TMA DMZ than in the BEJT case (Figure 17). This suggests that the model is relatively insensitive to changes in vertical conductivity, and supports the conclusion that dispersion is the parameter that promotes significant mixing (and therefore, lowering of concentrations) along groundwater flowpaths.

The lack of model sensitivity to K_v is also demonstrated in contaminant breakthrough curves from a model cell west of the TMA (Figure 18). When both vertical dispersivity and K_v are decreased in the PWCT parameter set, higher concentrations arrive in layer 4 (higher in the model) and lower concentrations arrive in layer 7 (the bottom layer). However, when only K_v is lowered, the breakthrough curves are very similar to those under higher K_v and vertical dispersivity (the BEJT case). Of these three simulations, the PWCT run results in the highest concentrations at the TMA DMZ, which is attributable to less dispersion and therefore less mixing of the plume. A decrease in K_v without a decrease in vertical dispersivity does not reduce mixing of the contaminant mass, and concentrations are approximately the same as the BEJT case. The implication is that the mixing of the plume that leads to lower concentrations in the

BEJT case is controlled largely by the dispersion term; increases in K_v do not significantly contribute to mixing of the plume and lowering predicted concentrations.

6.7 Pumping rate and dispersivity

The model sensitivity to the pumping rate used in mine dewatering was evaluated by running the transport model with the flow fields resulting from boundary conditions generated by the regional model under three pumping rates. The pumping rates selected were those determined to be the High End (1177 gpm), Low End (285 gpm) and the applicant's proposed maximum (602 gpm) from the regional flow model. (The High End rate was subsequently refined to 1250 gpm, {Krohelski and others, 2004}; but because 1250 gpm is not substantially higher than 1177 gpm, runs performed for this analysis were not repeated with 1250 gpm. The higher pumping rate is used in subsequent portions of this review; see section "Range of inputs for selected model parameters".)

In terms of maximum concentrations reaching the TMA DMZ, the model is more sensitive to pumping rates at lower values of vertical dispersivity (Figure 19). The model results, evaluated in the terms of maximum concentration at the TMA DMZ, are relatively insensitive to changes in mine dewatering rate at a vertical dispersivity of 0.5 ft because at higher values of dispersivity, dispersive mixing (and therefore dilution, or overall lowering of concentrations) overwhelms the differences in concentration caused by changes in the advective flow field induced by different pumping rates. As shown in Figure 19c, under zero vertical dispersivity conditions, higher pumping rates result in substantially higher concentrations at the TMA DMZ.

In the absence of vertical mixing caused by dispersion, the plume is more strongly controlled by the advective flow field. This is demonstrated in Figures 19b and 19c, which show that at values of 0.05 ft and no vertical dispersivity, the maximum concentrations that arrive at the TMA DMZ are sensitive to the mine dewatering rate. The advective flow field resulting from various pumping rates is shown through illustrations of the water table (Figure 20). During the period of mine operation, the high pumping rate results in a steeper gradient to the west (Figure 20c). This results in faster transport of the contaminant plume towards the DMZ and the western model boundary, as demonstrated by a breakthrough curve at the western TMA DMZ (Figure 21a). More mass exits the model domain at earlier times under the high pumping rate scenario due to the increase in advective velocity. The higher pumping rate also causes a shift in the groundwater divide towards the east (Figure 20c), causing a greater amount of the source area (the TMA cells) to fall west of the divide. This also drives more mass to the western boundary than under the lower pumping rates. Under the lower and proposed maximum pumping rates, more of the source mass remains in the model domain over a longer period. This is evidenced by higher concentrations in breakthrough curves to the east and north (Figure 21b and 21c) at later times, compared to that of the high pumping rate.

The distribution of mass over time within the model domain and the timing and distribution of contaminant arrival at model boundaries are affected by mine dewatering rate. At high pumping rates and very low vertical dispersivity, higher concentrations reach the TMA DMZ. However, at higher values of vertical dispersivity, dispersive mixing offsets the effect of enhanced advective transport under higher pumping rates.

6.8 Porosity

Porosity affects model results in two ways. An increase in porosity allows the equivalent source mass to mix in a larger pore volume in each cell, resulting in a decrease in cell-by-cell concentrations. The value assigned to porosity also affects the seepage velocity of constituents through the flow field. An increase in porosity decreases the velocity, effectively slowing the arrival time:

$$Velocity = \frac{k}{n_e} \frac{dh}{dl}$$

where k is hydraulic conductivity; n_e is effective porosity; and dh/dl is the hydraulic gradient.

In this sense, lower values of effective porosity may be used as a proxy for high-conductivity pathways in sediments, because the lower effective porosity results in more rapid transport as would occur along preferential pathways in aquifer sediments.

The total porosity of sediments is a relatively easy value to measure in the laboratory. However, the effective porosity (n_e), called for in the implementation of the governing equations in MT3D, cannot be readily measured in the field or laboratory. Effective porosity is smaller than the total porosity, reflecting that some pore space may be poorly connected and contains groundwater that is essentially immobile. Because this parameter is difficult to measure, it is typically considered a lumped parameter that is adjusted during model calibration to yield a good match to observed plume movement and solute accumulation (Zheng and Bennet, 1995; Zheng and Wang, 1998). This approach is difficult to implement in studies such as this one, which involves simulations of a site with no historic contamination to provide model calibration targets. Therefore, the impact of porosity on results was evaluated through a sensitivity analysis.

Although the model includes representation of several types of till and outwash deposits and these materials are assigned various values of hydraulic conductivity, the applicant assigned a single value of porosity to the entire model domain. The applicant used an averaging method to assign a hydraulic conductivity value to each cell, based on the percentages of materials (e.g., coarse versus fine outwash) within a cell. In the course of this review, estimating an average porosity for a cell on the basis of the mix of geologic materials within the cell was considered as an alternative approach to assigning a single value to the entire domain. However, this was deemed too arbitrary because there is no basis for calibration of the resulting simulated plume. We continued to assign a single value of effective porosity to the entire model domain, but varied between simulations within the range of 0.05 to 0.3.

As expected, lower values of porosity result in higher concentrations throughout the domain (Figure 22), because less dilution of the total source mass occurs with lower porosity. The increased seepage velocity related to lower porosity also results in significant changes in the plume. At early times, higher concentrations from the western TMA cells have migrated further towards the western boundary with lower porosity (Figure 22A1). At later times, high concentrations arrive earlier at the eastern TMA DMZ with lower porosity (Figure 22A2). With higher porosity, mass remains closer to the source, resulting in a more compact solute plume (Figures 22B1 and B2).

Faster migration of the plume at lower values of porosity is also illustrated in Figure 23. Here, the cumulative mass reaching head-dependent and river boundaries over time is greater at earlier times with lower values of porosity. Even at 650 years, less mass has exited the system under the high porosity than the low porosity values. Since the amount of mass entering the system is identical for these simulations (all simulate the first phase of TMA loading), it follows that at all times there is more mass remaining within the domain under the high-porosity simulation. Nevertheless, concentrations are lower with higher porosity because the mass is more dilute due to the larger volume of pore space. The similarity in total mass reaching these boundaries under porosity values of 5 and 10% (Figure 23) suggests that the rate of plume migration (that is, the effect of porosity on seepage velocity) is less sensitive to porosity at very low values of porosity.

If evaluated in terms of maximum concentration to reach the DMZ, the model results are sensitive to changes in porosity (Figure 24), with lower porosities resulting in higher concentrations.

Sensitivity to porosity and vertical dispersivity was also evaluated by comparing the maximum concentration observed at the TMA DMZ at porosity values of 0.1 and 0.3 at vertical dispersivities of 0.5 and 0.05 ft. Higher concentrations are observed at lower porosity and lower vertical dispersivity, as expected (Table 12). However, the ratios between the maximum concentrations resulting from different porosities and a given value of vertical dispersivity are similar. This indicates that model sensitivity to porosity is relatively constant with a change in vertical dispersivity.

6.9 Representation of the pinchout zone

The purpose of this set of simulations was to evaluate the effect of changes to the representation of an area with low hydraulic conductivity in the eastern portion of the TMA/RP model, referred to as the “discontinuity” in outwash deposits (Dunning and others, 1997) or the “pinchout zone” (Krohelski and others, 2004). The applicant initially constructed the regional flow model assuming that the glacial outwash unit was continuous across the landscape, making the outwash in the uplands directly connected to the outwash in the lowlands. The applicant had included a zone of reduced hydraulic conductivity in the outwash beneath the eastern portion of the TMA in their 1996 transport model (HSI GeoTrans, 1996). Following additional review of the area and the data, the Technical Working Group (TWG) concluded that a more reasonable interpretation would be to assume continuity of glacial till units across the landscape, rather than continuity of the outwash (Dunning and others, 1997). In the TMA/RP model, the result of this change in the geologic interpretation was that the sand and gravel outwash deposits of the uplands should be separated from those of the lowlands by one or more lower-hydraulic conductivity (K) units. The applicant subsequently incorporated this geologic feature into the groundwater flow and transport models for the TMA/RP, beginning with the 1998 version of the model (HSI GeoTrans, 1998a), by assigning lower hydraulic conductivity values to a series of cells in model layers 2 through 6. Hydraulic conductivities assigned to layers 1 and 7 were not changed (Table 13).

The evaluation presented here was completed to assess the effect of the lateral extent of this low-K zone as placed in the applicant’s 1998 model. Specifically, the zone of discontinuity in the outwash deposits may be a narrower feature in the landscape than is depicted by the pinchout zone in the applicant’s model. Figure 25 shows the applicant’s current interpretation and one

possible alternative interpretation (referred to here as the TWG interpretation) that was evaluated during this review.

The first step in testing the effect of the width of the pinchout zone was to incorporate the TWG interpretation into the TWG regional flow model (Appendix V of Krohelski and others, 2004). The Low End Case, Zinc Phase, Version 1 of the regional model was used for this purpose. The K value assigned to the fine outwash deposits in the pinchout zone was revised from 6 to 3 ft/d (which is within the range of till conductivities in the regional model), in order to maintain model calibration using the narrower pinchout zone. Boundary conditions for the TMA/RP model were extracted from this version of the regional flow model. The revised pinchout zone configuration, boundary conditions and K-values were then incorporated into the TMA/RP flow and transport models. As an additional test, the effect of a hypothetical high-K channel through the narrow pinchout zone was simulated by assigning the coarse outwash K value to a series of contiguous cells in the pinchout zone along an eastern area near the TMA DMZ (Figure 26). Three model runs were compared to evaluate the effect of this narrower pinchout zone and the high-K channel in this narrower zone (Table 13). These simulations were run with lower vertical dispersivity than the applicant's BEJT case because it was clear from previous work that model results are sensitive to this parameter.

The effect of the revised geology on the simulated water table is illustrated in Figure 27. The TWG (narrower and lower-K) pinchout zone causes a steeper hydraulic gradient at the eastern edge of the TMA DMZ, generally parallel to Hemlock Creek. The water table elevation is also increased to the north in the model domain. The TWG interpretation with a high-K channel has additional effects on the flow field; the gradient flattens in the vicinity of the channel and flow converges on the feature. In both cases, the water table divide is further west than in the applicant's depiction.

The total source mass entering the groundwater system from the facility is within 0.1% in the three simulations (this slight deviation from exactly equal loading is attributed to numerical error in MT3D). Differences in the configuration of the water table and gradient in relation to the solute source area result in changes to the flux of mass away from the TMA over time. This is demonstrated by information on cumulative flux to model boundaries (Figure 28). The cumulative contaminant flux to river cells (along the eastern model boundary) is greater than the contaminant flux to head dependent boundary cells (along the western and northern model boundaries) in simulations with the TWG pinchout zone interpretation. The proportion of mass transported to the east and discharging to river cells is greater with both the narrower pinchout zone and the narrower pinchout zone with high-K channel. In the applicant's interpretation, contaminant flux is more evenly distributed to the west and to the east. These results are consistent with the shift in the groundwater divide to the west with the WDNR's interpretation of the pinchout zone.

Differences in the simulations are also illustrated by breakthrough curves of concentration over time in model layers 3, 4 and 6 at a location 100 ft (one cell) east of the high-K channel (Figure 29). Elevated concentrations arrive earlier in time and at a more shallow depth with the narrower pinchout zone run with high-K channel (run 29_1). Without the high-K channel, the narrower pinchout zone (run 28_1) delays the peak concentration, which also arrives in a deeper layer. The

applicant's interpretation of the pinchout zone (run 25_1) also results in a maximum concentration arriving at this observation point later in time and in a deeper model layer.

Contour plots of the plume at selected times (Figure 30) also demonstrate that the effect of the high K channel is to focus transport through the channel. Note that the center of the eastern portion of the plume in run 25_1 is more southern than the plume in runs 28_1 and 29_1. This is why run 25_1 concentrations are extremely low in the breakthrough curves (Figure 29). The observation point for the breakthrough curve was selected to illustrate the behavior of the center of the plume in run 29_1.

Both narrowing the pinchout zone and simulating a high-K channel within it have a negligible effect on the maximum concentration that arrives at the TMA DMZ throughout a 650-year simulation (Table 14). This is because, in both cases, the maximum concentration occurs at the western edge of the model in early times, at about year 30 of the simulations, consistent with the result using the applicant's interpretation of the pinchout zone. Although more total mass is directed toward the high-K channel over time, the changes in the flow field that move mass in this direction do not concentrate that mass to any significant extent. If the model is evaluated on the basis of highest concentration to reach the TMA DMZ, the narrower pinchout zone and the narrower pinchout zone with a high-K channel yield similar results to the applicant's interpretation.

In conclusion, the TWG interpretation of the pinchout zone, which is narrower and lower K than the applicant's interpretation, affects the distribution of mass as it moves away from the TMA source areas, resulting in a redistribution of mass to Ground Hemlock Creek. Simulating a high-K channel in the narrower pinchout zone causes higher concentrations to arrive earlier at the east end of the channel. Although the mass in the model is redistributed by the change in geologic representation, either as a result of changes in gradient and advective flow rates or due to additional mixing that may occur at some locations, the change in the geologic interpretation does not have a significant effect on the maximum concentrations predicted to reach the TMA DMZ.

7. RANGE OF RESULTS

7.1 Range of inputs for selected model parameters

In order to arrive at a final set of reasonable estimates of the impact of the TMA and RP on groundwater quality, the revised model was run with a range of values for porosity, vertical dispersivity, mine dewatering rate, and source area exfiltration rates. These four inputs were varied because the results of the sensitivity analysis showed that model output is sensitive to each of these inputs.

Effective porosity was varied from 0.1 (10%) to 0.3 (30%), reflecting a reasonable range of uncertainty given the type of materials present in the glacial aquifer. Published values of total porosity of unlithified sediments are consistently broad in the range of values cited. Total porosity of sand and gravel is within 15 to 53%, while silt and clay range from about 34 to 60% (Zheng and Bennet 1995, deMarsily 1986). These values suggest that pore volume of the

materials may be relatively high, leading to high amounts of dilution within the aquifer sediments. However, effective porosity must be assigned in the transport model to appropriately account for advective flux of solutes. A narrower range of effective porosity values are found for un lithified sediments, on the order of 10 to 30% (deMarsily 1986). Specific yield of aquifer sediments, determined through analysis of an aquifer pumping test conducted near the proposed site of the TMA, may also serve as a proxy for effective porosity (deMarsily, 1986). A value of 0.1 was determined for the glacial aquifer (Krohelski and others, 2004), which supports the use of 0.1 to 0.3 for the area of the TMA site.

Vertical dispersivity was varied from 0.05 to 0.5 ft. This is based on a discussion of dispersion presented in Gelhar and others (1992), in which field data of high reliability showed horizontal transverse dispersivity at least one order of magnitude smaller than longitudinal dispersivity, and vertical transverse dispersivity one to two orders of magnitude smaller than horizontal transverse dispersivity. Longitudinal dispersivity is considered scale dependent, increasing with the scale of transport considered. On this basis, the value of 50 ft for longitudinal dispersivity used in the applicant's model is appropriate for the TMA/RP model. Given the ratios presented by Gelhar and others (1992), it is reasonable to assume a horizontal transverse dispersivity of 5 ft, and a vertical transverse dispersivity ranging from 0.05 to 0.5 ft.

Boundary conditions for the revised TMA/RP model were generated from three regional model simulations. These differed only in the mine dewatering rate, which was varied from the TWG Low End value (285 gpm), the applicant's proposed limit (602 gpm), and the TWG High End value (1250 gpm).

The model was run with four sets of TMA exfiltration rates developed by Benson and Grefe (2002) (Table 15). Three of these were determined using the HELP model results for operational periods and analytical methods for post-closure. Scenario HELPA represents a long-term landfill cap infiltration rate of 1 mm/yr (8.99×10^{-6} ft/d) after 116 years post closure. Alternative HELPB is based on the long-term expected performance of a single composite cover, and alternative HELPC is based on the long-term expected performance of a double composite cover. Both the HELPB and HELPC scenarios were derived from the applicant's TMA Cover Contingency Plan (Foth and Van Dyke, 2001). These three scenarios have similar exfiltration rates during operational phases but differ greatly in exfiltration rate applied after landfill closure (Table 15).

The RP exfiltration rate was maintained at the "reduced performance" estimate for pond liner performance from Benson and Grefe (2002) because varying the pond exfiltration rate within the parameters for the updated pond design (Foth & Van Dyke, 2001) did not have a significant effect on the overall solute plume. (Foth & Van Dyke {2001} present a re-designed RP that followed in response to the findings of the sensitivity analysis to the source term described in section 6.2 of this report.) In this version of the model, which incorporates the updated pond design, the solute plume is dominated by transport from the TMA rather than from the RP. Pond exfiltration rates are presented in Table 15.

7.2 Range of mass distribution at key times

Although overall patterns of solute migration are similar, the range of parameters used in these simulations results in substantial differences in the magnitude of solute concentrations across the

model domain at early times (Figure 31). At low values of porosity and vertical dispersivity and a higher pumping rate (Figure 31a,c and e), plume migration to the west is more extensive and concentrations are higher (by at least 100 times) in the deeper model layers (lower elevations). The plume remains more compact and dilute, and focused in upper model layers (higher elevations), in simulations with higher porosity and dispersivity (Figure 31b, d and f).

At later times in the simulation under the HELPA exfiltration scenario (in which the long-term exfiltration rate greatly exceeds the short term rate), overall differences among the contour plots are not as pronounced (Figure 32). Here, the system has reached steady-state concentrations due to the long-term exfiltration rate, which dominates the results. Differences in plume migration patterns are better illustrated by breakthrough curves (Figure 33). Lower porosity and vertical dispersivity with a higher pumping rate result in higher early-time breakthrough to the west, while higher porosity and vertical dispersivity and a lower pumping rate result in later arrival times at this location. Concentrations to the east are dominated by a higher long-term exfiltration rate under both scenarios, as would be predicted by the shift in the water table divide after water levels recover from dewatering (Figure 20).

7.3 Maximum scaled concentrations reaching the TMA DMZ

The final suite of model results, in terms of maximum concentrations arriving at the TMA DMZ, using the range of model inputs presented above, are summarized in Table 16. These results are predicated on the same unit source concentration for a hypothetical constituent over all six simulated source phases (Table 2). Therefore, if some constituents have a much higher concentration during some of the six phases than in others, differences between maximum concentrations simulated for late and early times may become more dramatic when scaled by absolute source concentrations.

Simulations using the HELPA exfiltration rate are dominated by concentrations that arrive after 150 years, as the impact of the much higher exfiltration rate travels through the groundwater system. Concentrations arriving at less than 150 years are very similar, regardless of the exfiltration scenario. This is largely because the exfiltration rates are very similar for early times in the simulation (Table 15). For this reason, not all combinations of the range of values were simulated with the HELPB and HELP C exfiltration rates.

As shown in Table 16, the combination of low vertical dispersivity, low porosity and low mine dewatering rate yield the highest concentrations at the TMA DMZ over the full 650-year simulation. This is because higher concentrations result from simulations in which mixing and dilution are minimized. Under a low vertical dispersivity, model sensitivity to mine dewatering rate is increased, and higher mine dewatering rate results in the highest short-term (under 150 years) concentrations to occur at the TMA DMZ (run 47). At longer model run times, higher concentrations arrive at the TMA DMZ under a lower dewatering rate (run 48). Under a higher vertical dispersivity, simulations in which only the dewatering rate is varied yield similar results (for example, simulations 58, 51 and 57).

Overall, the range of maximum concentrations reaching the TMA DMZ under the scenario of high long-term cap leakage (HELPA exfiltration rate) is from 18 to 27 times the concentrations simulated in the applicant's BEJT model. If the long-term performance of the cap is improved,

the maximum concentrations arrive at the TMA DMZ early in the simulations, and the range of maximum concentrations reaching the DMZ is reduced to 0.2 to 1.6 times the concentrations simulated in the applicant's model. Figure 34 illustrates that at model times under 150 years, the maximum concentration arriving along the TMA DMZ is controlled by model sensitivity to porosity, dispersivity and dewatering rate. Under the scenario of high long-term cap leakage (HELPA exfiltration rate), differences in output attributable to these variables are overwhelmed by the effect of the magnitude of the source function at later times.

8. CONCLUSIONS

The revised model presented in this review is suitable for simulating the flow and transport of solutes from the proposed TMA and RP, though there are limitations to its use. Because there is uncertainty in model input parameters and the transport model is not calibrated, a single value cannot be ascribed to certain model parameters with a reasonable degree of confidence. Therefore, a range of reasonable values must be used, resulting in a range of results. However, this range does not encompass all of the uncertainty in the model design and input parameters, nor the associated results. For example, during this review one particular scenario of potential differences between the actual geologic conditions and those modeled was evaluated (the effect of a narrower pinchout zone). This particular scenario proved to be insignificant in terms of its effect on the maximum solute concentrations to reach the DMZ; however other potential differences between actual and modeled conditions may exist. Actual patterns of contaminant migration at the site could result in solute concentrations lower or higher than the presented range.

Nonetheless, testing model sensitivity to various parameters demonstrates significant sensitivity to porosity, mine dewatering rate and the vertical dispersivity. The model results are most sensitive to the TMA exfiltration rate, which controls the total solute mass input to the model. Estimates of the long-term exfiltration rate vary widely, and result in a very wide range of results. Reasonable ranges have been assigned to model parameters and to the exfiltration rates. Results range from about 0.3 to 27 times the applicant's BEJT case.

The model has been used to evaluate the effect of design changes to the facility. The benefit of lining the RP, adding a double composite cap to the TMA, and the ultimate value in maintaining the integrity of the cap, are clearly demonstrated with the model. The utility of the model to simulate compliance with groundwater standards at the point of compliance is less clear, necessitating the use of a range of expected results.

9. REFERENCES

- Benson, C.H. and R.P. Grefe, 2002. Estimates of leakage rates for the Tailings Management Area and RP liners: proposed Crandon Mine, Forest County, Wisconsin, report to Wisconsin WDNR, December 6, 68p.
- de Marsily, Ghislain, 1986. *Quantitative Hydrogeology: Groundwater Hydrology for Engineers*. Academic Press: San Diego, 440 pp.
- Dunning, C.P., and Johnson, D.M., and Batten, W.G., 1997. Review of the Stratigraphy of Glacial Sediments in the Vicinity of the Proposed Crandon Mine: Memorandum to Chris Carlson, WDNR, June 30, 1997.
- Foth & Van Dyke, 1995a. Environmental Impact Report - prepared for Crandon Mining Company.
- , 1995b. Investigation and evaluation: Saprolite at the Crandon Site: Foth & Van Dyke, February 1995, Environmental Impact Report - prepared for Crandon Mining Company.
- , 1995c. Bedrock hydrogeology at the Crandon site. Foth & Van Dyke, February 1995.
- , 1997. Crandon Project – Response to WDNR Groundwater Model Review Comments, Foth and Van Dyke Memorandum, September 10, 1997.
- , 1998a. Environmental Impact Report - prepared for Crandon Mining Company.
- , 1998b. Crandon Project – Updated lake effect surface water hydrology evaluation revised TMA and plat site configurations: Foth & Van Dyke Technical Memorandum, December 4, 1998 and EIR Appendix 4.2-4.
- , 1998c. Water regulatory permit application for the proposed Crandon project mine site, originally issued June 1996 and updated December 1998. Submitted to the WDNR.
- , 2001. Crandon Project – Verification/Contingency plan for long-term performance of TMA cap, Technical Memorandum from N. Paruakat, D. Rozenowski, and J.P. Giroud, dated November 27, 2001.
- Gelhar, L.W., C. Welty and K.R. Rehfeldt, 1992. A critical review of data on field-scale dispersion in aquifers, *Water Resour. Res.*, vol. 28, no. 7, pp. 1955-1974.
- Gotkowitz, M.B., 2000a. Tailings Management Rea (TMA) model review. Memorandum from Wisconsin Geological and Natural History Survey to Chris Carlson, WDNR, July 12, 2000.

- Gotkowitz, M.B., 2000b. Crandon Mine TMA model: percolation rate. Memorandum from Wisconsin Geological and Natural History Survey to Chris Carlson, WDNR, April 26, 2000.
- Gotkowitz, M.B., 2000c. Crandon Mine TMA model: source from TMA vs. reclaim pond. Memorandum from Wisconsin Geological and Natural History Survey to Chris Carlson, WDNR, April 26, 2000.
- Harbaugh, A.W., and McDonald, M.G., 1996, User's documentation for MODFLOW-96, an update to the U.S. Geological Survey Modular Finite-Difference Groundwater Flow Model: U.S. Geological Survey Open-File Report 96-485, 56 p.
- HSI GeoTrans, 1995a. Numerical simulation of the effect on groundwater and surface water of the proposed zinc and copper mine near Crandon, Wisconsin. Originally submitted as part of the Environmental Impact Report and later replaced by HSI GeoTrans, 1996.
- , 1996. Numerical Simulation of Potential Solute Transport at the Proposed Zinc and Copper Mine Near Crandon, Wisconsin. In Foth and Van Dyke (1995-98) Environmental Impact Report for the Crandon Project, Appendix 4.2-10
- , 1998a. Update to: Numerical Simulation of Potential Solute Transport at the Proposed Zinc and Copper Mine Near Crandon, Wisconsin (April 1998). In Foth and Van Dyke (1995-98) Environmental Impact Report for the Crandon Project, Appendix 4.2-10, pp.124-291.
- , 1998b. Addendum No. 2 to the numerical simulation of the effect on groundwater and surface water of the proposed zinc and copper mine near Crandon, Wisconsin. In Foth and Van Dyke (1995-98) Environmental Impact Report for the Crandon Project, Appendix 4.2-3, pp. 1466-1888 (April, 1998).
- , 1999a. Update No.2 to: Numerical Simulation of Potential Solute Transport at the Proposed Zinc and Copper Mine Near Crandon, Wisconsin (January 1999). In Foth and Van Dyke (1995-98) Environmental Impact Report for the Crandon Project, Appendix 4.2-10, pp.292 - 389.
- , 1999b. Addendum No.1 to: Update No.2 to: Numerical Simulation of Potential Solute Transport at the Proposed Zinc and Copper Mine Near Crandon, Wisconsin (June 1999). In Foth and Van Dyke (1995-98) Environmental Impact Report for the Crandon Project, Appendix 4.2-10, pp.390 - 449.
- , 2000. Update No. 3 to: Numerical Simulation of Potential Solute Transport at the Proposed Zinc and Copper Mine Near Crandon, Wisconsin (March, 2000). In Foth and Van Dyke (1995-98) Environmental Impact Report for the Crandon Project, Appendix 4.2-10, pp.451 - 520.
- Hunt, R. and C. Zheng, 1999. Debating complexity in modeling. *EOS*, Vol. 80, No.3. pg. 29.

- Kenoyer, G. 2004. Evaluation of the solute transport model developed for the reflooded mine at the proposed Crandon Mine. Wisconsin Geological and Natural History Open File Report 2004-XX.
- Krohelski, J.T., editor, 2004. Evaluation of groundwater flow models used to simulate the effects of proposed mining on the groundwater-surface water systems in the vicinity of Crandon, Forest County, Wisconsin. Wisconsin Geological and Natural History Open File Report 2004-XX.
- Mehl, S. and M.C. Hill, 2001. A comparison of solute-transport solution techniques and their effect on sensitivity analysis and inverse modeling results, *Ground Water*, Vol.39 No2, p.300-307.
- McDonald, M.D. and A.W. Harbaugh, 1988. *A modular three-dimensional finite-difference flow model*. Techniques of Water Resources Investigations of the U.S. Geological Survey, Book 6, 586 pp.
- Rowe, R., 1984. Bedrock permeability – Crandon Deposit: Exxon Minerals Company, Crandon Project CMC-NOI-39.
- Rumbaugh, J.O., and Rumbaugh, D.B., 1996. Groundwater Vistas: Environmental Simulations Inc., 2997 Emerald Chase Drive, Suite 100, Hendron, VA, 22071
- Saad, D., 1996. Using chlorofluorocarbons to date ground water and determine hydrologic properties of sediments near the proposed Crandon mine near Crandon, Wisconsin. Memorandum from U.S. Geological Survey to Chris Carlson, WDNR, June 10, 1996.
- Schroeder, P., T. Dozier, P. Zappi, B. McEnroe, J. Sjostrom, R.L. Peyton, 1994. Hydrologic evaluation of landfill performance (HELP); Engineering Documentation for Version 3. U.S. Environmental Protection Agency document EPA/600/R94/168B.
- Simpkins, W.W., McCartney, M.C. and, Mickelson, D.M., 1987. Pleistocene geology of Forest County, Wisconsin: Wisconsin Geological and Natural History Survey Information Circular 61, 22p.
- Zheng, C., 1990. *MT3D, A modular Three-dimensional Transport Model for Simulation of Advection, Dispersion and Chemical Reactions of Contaminants in Groundwater Systems*, Report to the U.S. Environmental Protection Agency Robert S. Kerr Environmental Research Laboratory, Ada, Oklahoma.
- Zheng, C., 1996. MT3D96, Modular three-dimensional transport model.
- Zheng, C. and G.D. Bennett, 1995. *Applied Contaminant Transport Modeling: Theory and Practice*. Van Nostrand Reinhold: New York, 440 pp.

Zheng, C. and P. Patrick Wang, June 1998. *MT3DMS Documentation and Users' Guide, Release DoD_3.00.A*. Technical Report. University of Alabama, Tuscaloosa Alabama.

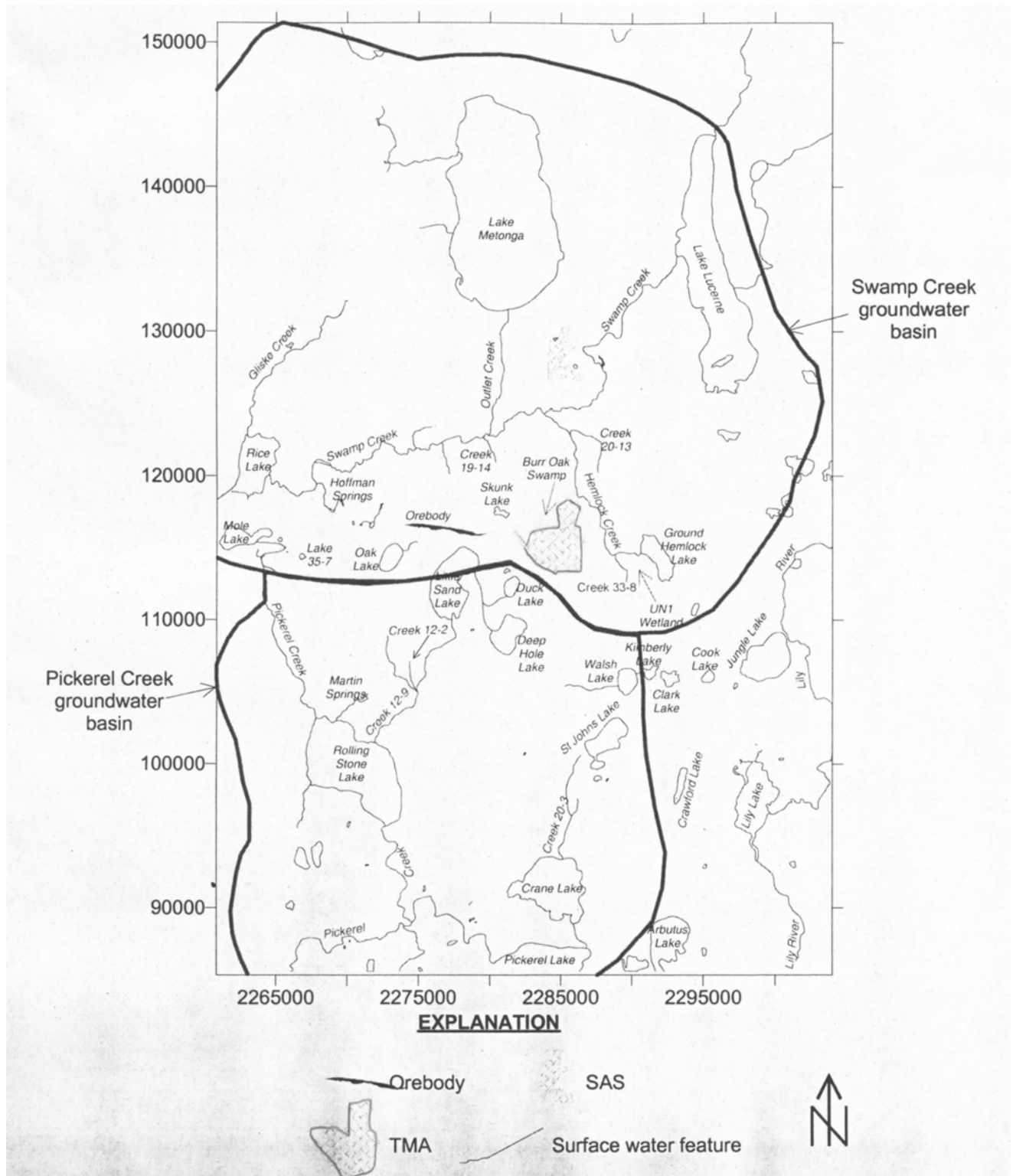


Figure 1. Crandon area base map and Swamp and Pickerel Creek groundwater basins. Map Coordinates in State Plane North, in feet (modified from Foth and VanDyke, EIR, 1995 and Krohelski and others, 2004). Basin delineation described in Krohelski and others (2004).

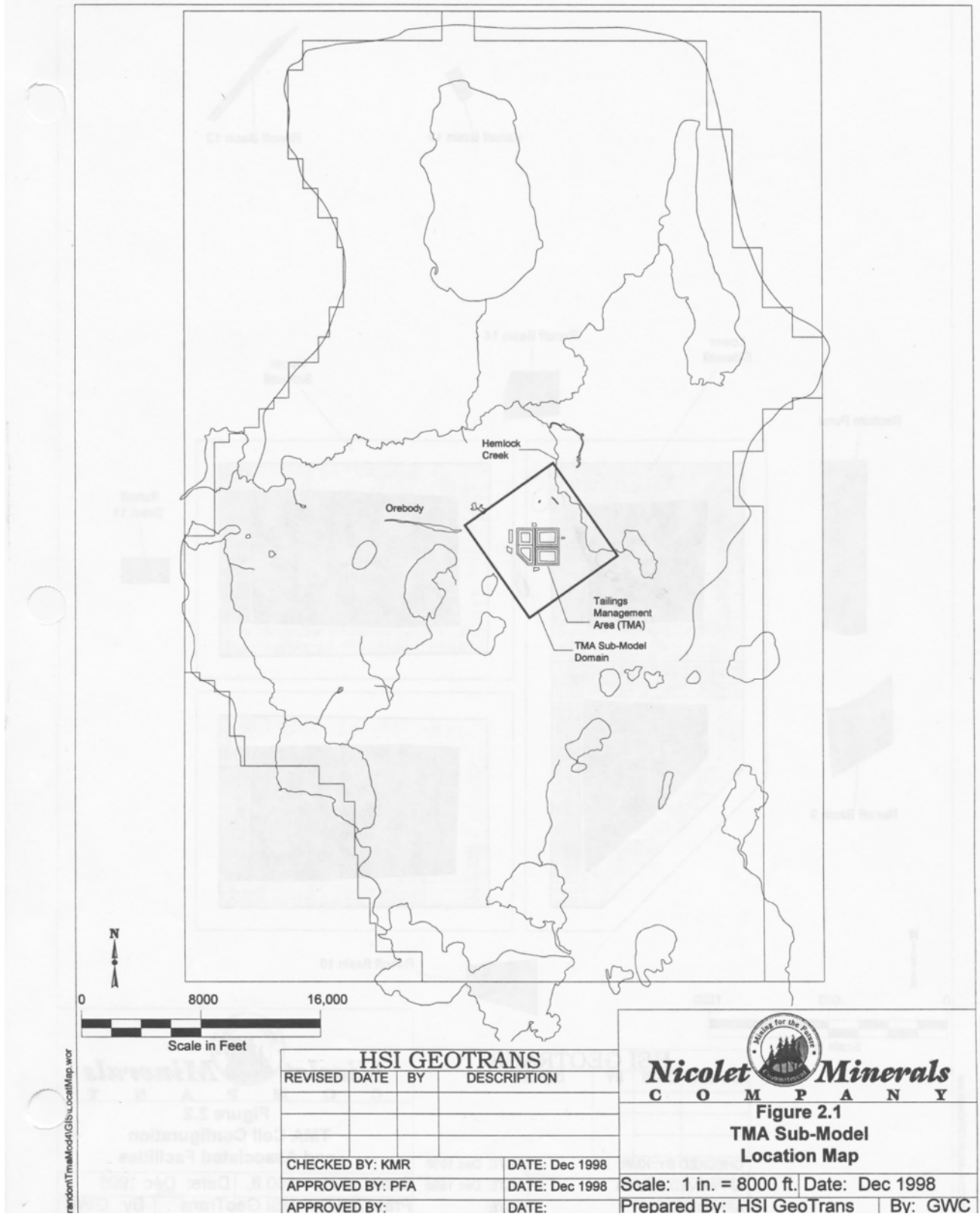


Figure 2. Location of TMA flow and transport model domain (from HSI Geotrans, 1999).

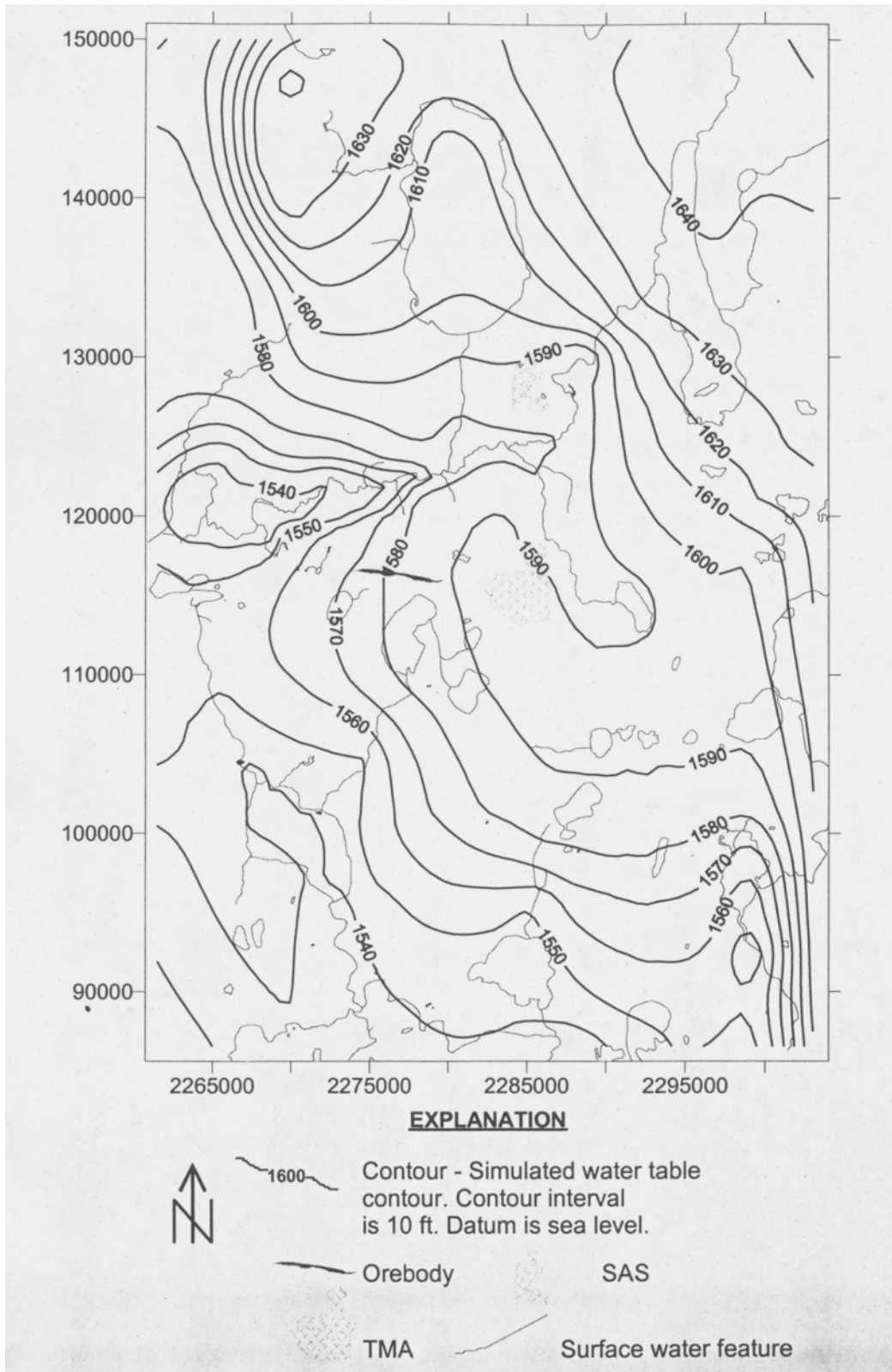


Figure 3. Water table map of Crandon area generated from calibrated regional flow model (Krohelski and others, 2004). Map coordinates are in State Plane North, in feet. SAS is the Soil Absorption Site.

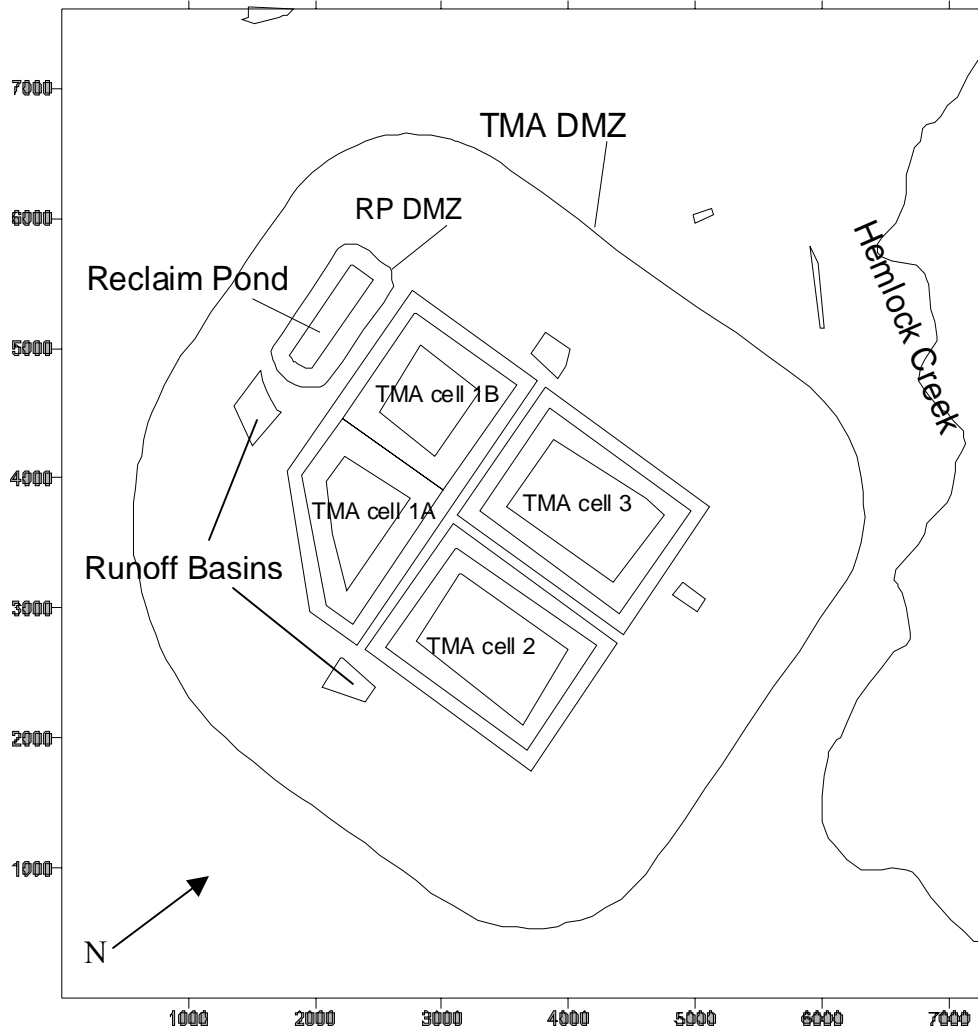


Figure 4. TMA cells, Reclaim Pond and their design management zones (DMZs). Coordinates refer to model grid spacing and are in feet.

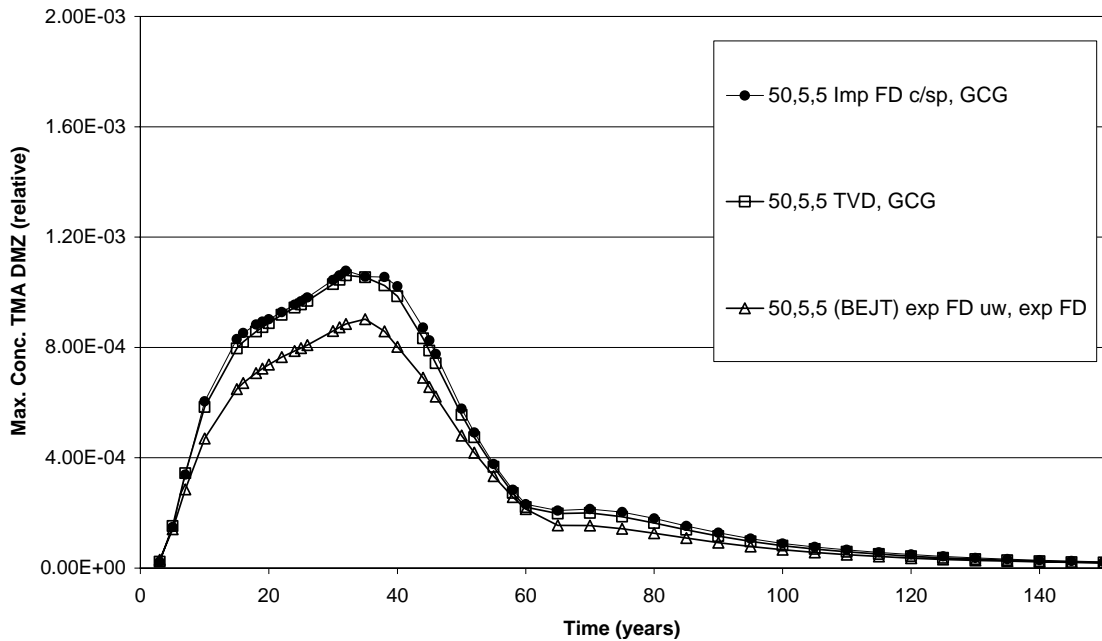


Figure 5. Maximum concentrations at the TMA DMZ with various numerical solvers. All runs were completed with the best engineering judgment for transport (BEJT) dispersivities. Solvers include implicit finite-difference with centered-in-space weighting (Imp FD c/sp) and generalized conjugate gradient (GCG); the total-variation-diminishing (TVD) solver with GCG, and explicit finite-difference with upstream weighting (exp FD uw) used by the applicant.

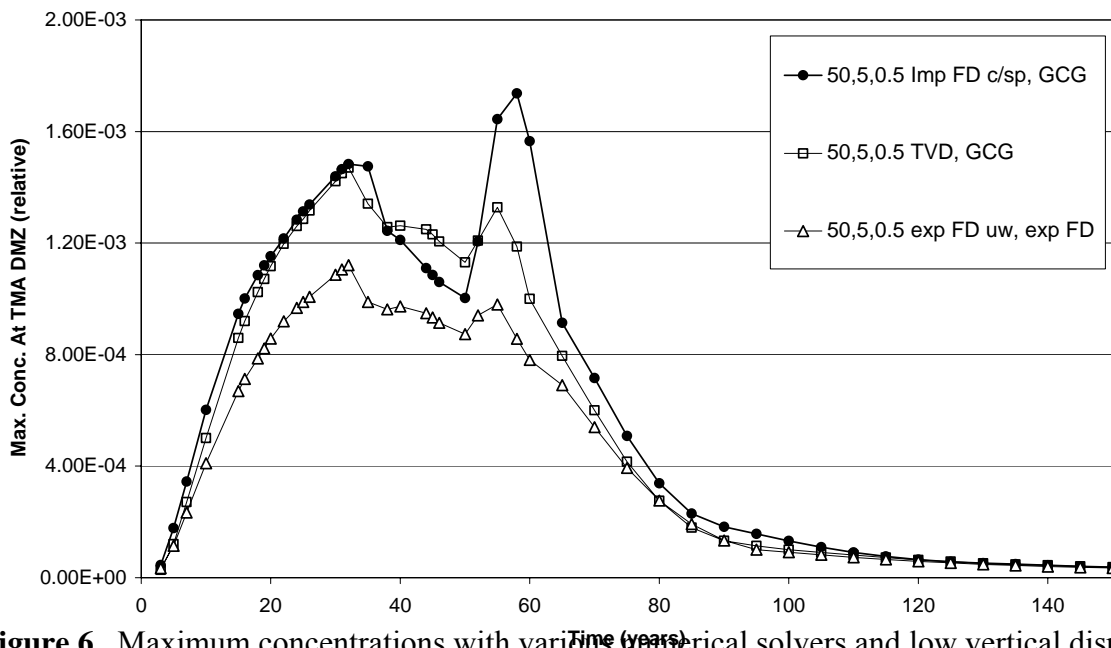


Figure 6. Maximum concentrations with various numerical solvers and low vertical dispersivity. All runs were completed with vertical dispersivity of 0.5 ft. Solvers include implicit finite-difference with centered-in-space weighting (Imp FD c/sp) and generalized conjugate gradient (GCG); the total-variation-diminishing (TVD) solver with GCG, and explicit finite-difference with upstream weighting (exp FD uw) used by the applicant.

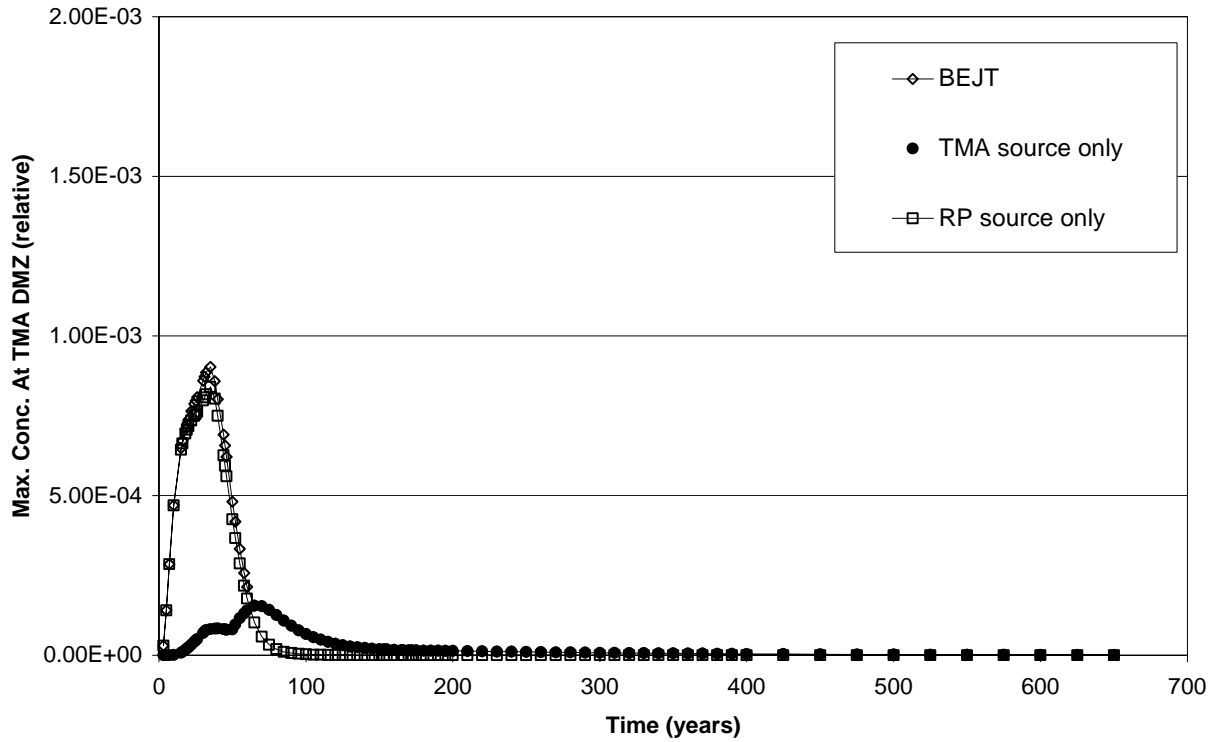


Figure 7. Maximum concentrations along the TMA DMZ from the TMA source, RP source, and combined sources (best engineering judgment for transport, BEJT, case)

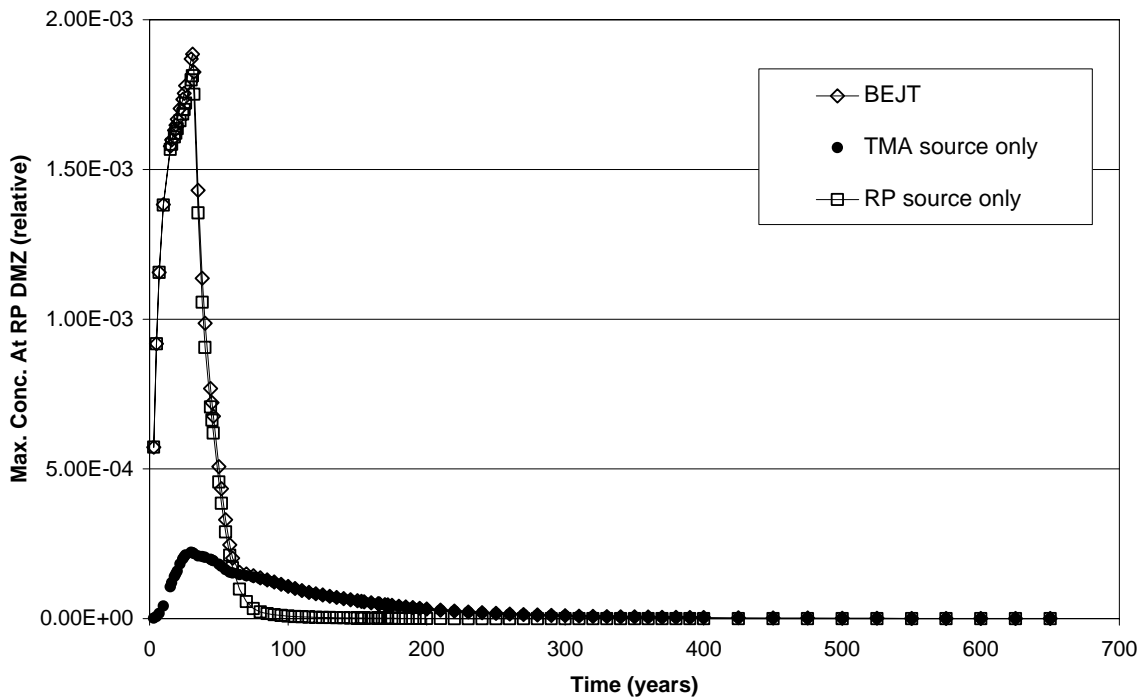


Figure 8. Maximum concentrations along the Reclaim Pond (RP) DMZ from the TMA source, RP source, and combined sources (best engineering judgment for transport, BEJT, case).

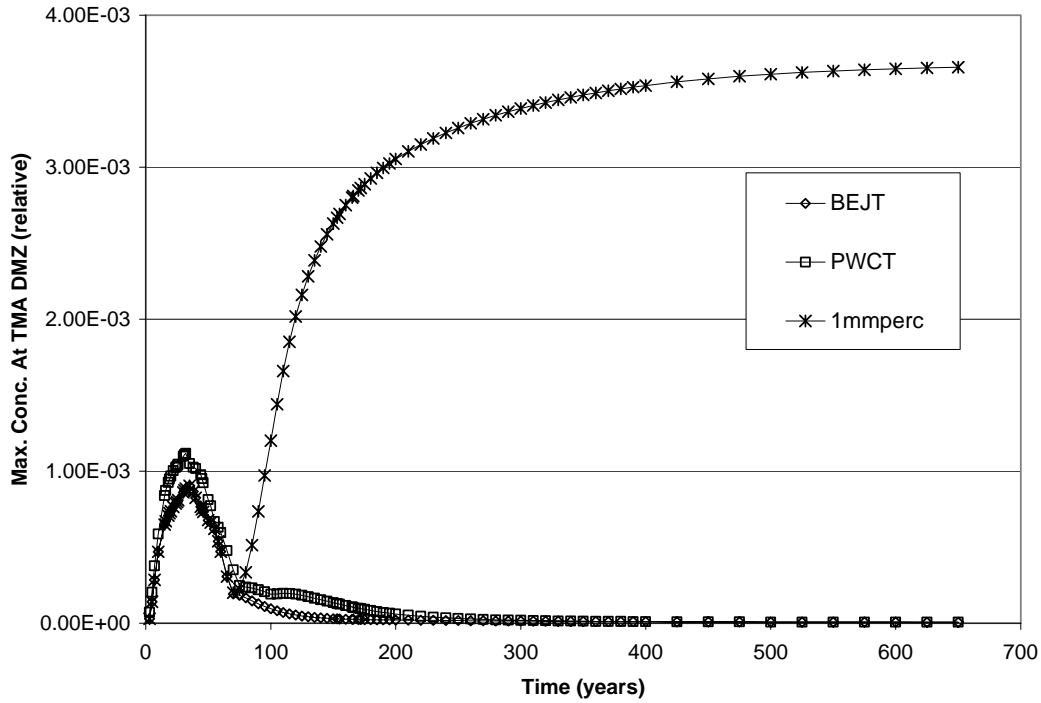


Figure 9. Effect of long-term exfiltration rate on maximum concentrations reaching the TMA DMZ. Runs shown include the applicant's BEJT (best engineering judgment for transport) and PWCT (practical worst case for transport) parameter sets, and the BEJT case with a post-capping liner leakage rate of 1 millimeter per year (labeled in graph as 1 mmperc) (8.99×10^{-6} ft/d).

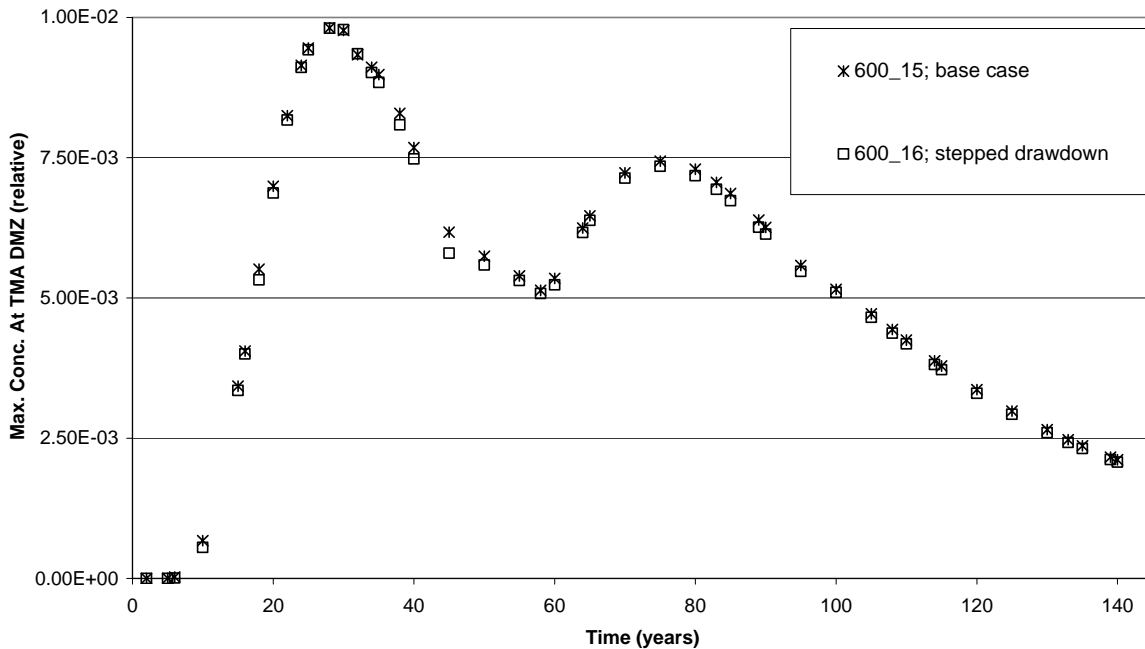


Figure 10. Effect of instantaneous drawdown and recovery compared to stepped drawdown and recovery. Maximum concentrations at the TMA DMZ are shown under base case of instantaneous change and a stepped change in drawdown, or head, at the boundary.

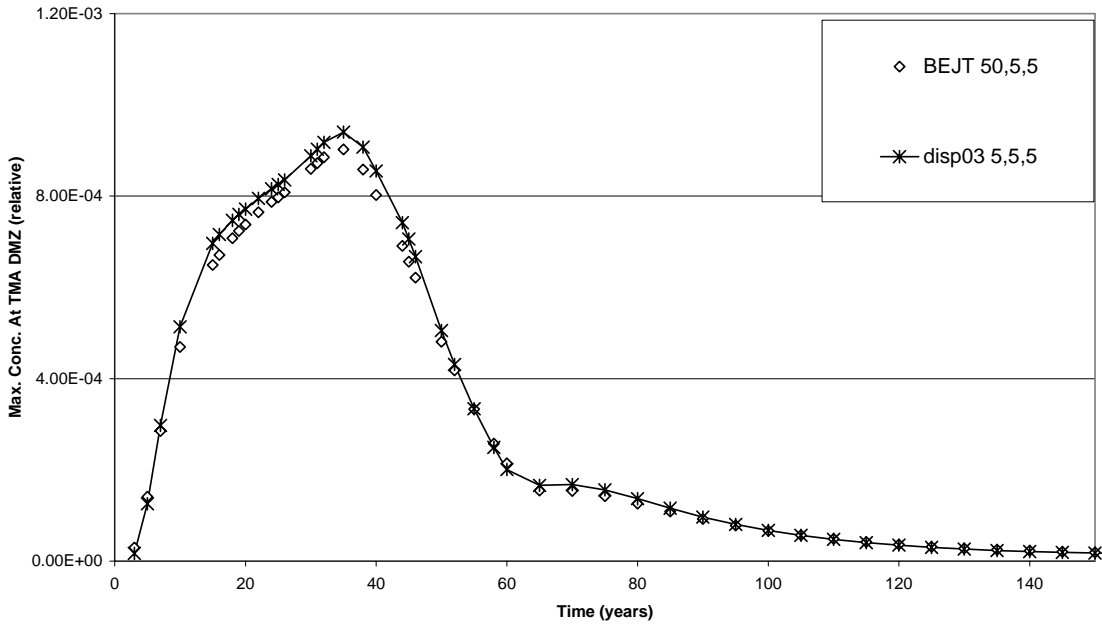


Figure 11. Maximum concentrations at TMA DMZ with a decrease in longitudinal dispersivity. Runs shown are for the applicant’s BEJT (best engineering judgment for transport) longitudinal, horizontal and vertical dispersivities of 50, 5 and 5 ft, respectively, and for the case of longitudinal dispersivity reduced to 5 ft run disp03).

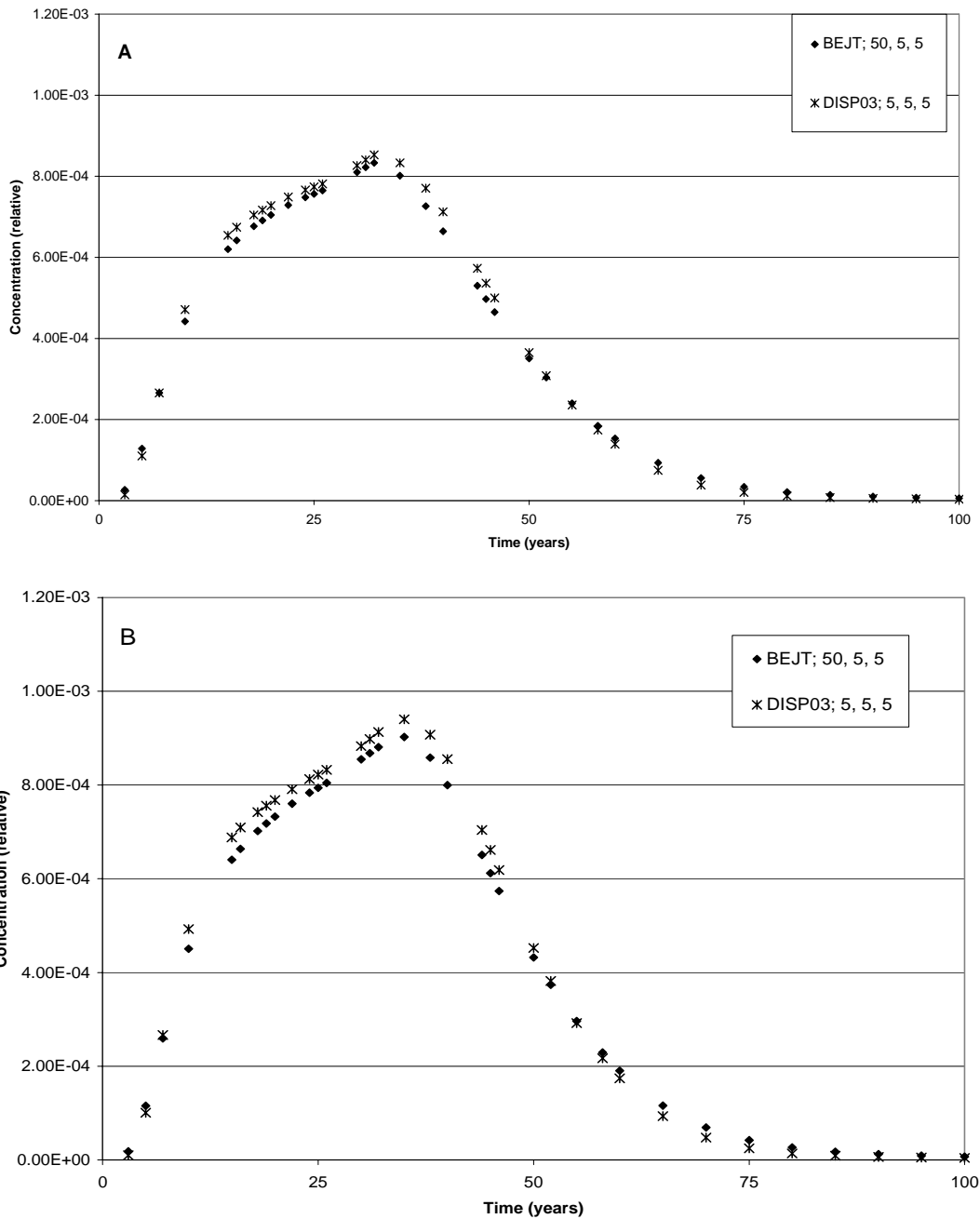


Figure 12. Breakthrough curves along the TMA DMZ. Location of figure A is layer 4, row 22, column 14, and figure B is layer 7, row 22, column 14. Runs shown are for the applicant’s BEJT (best engineering judgment for transport) longitudinal, horizontal and vertical dispersivities of 50, 5 and 5 ft, respectively, and for the case of longitudinal dispersivity reduced to 5 ft (run disp03). See Appendix 2 for locations of breakthrough curves.

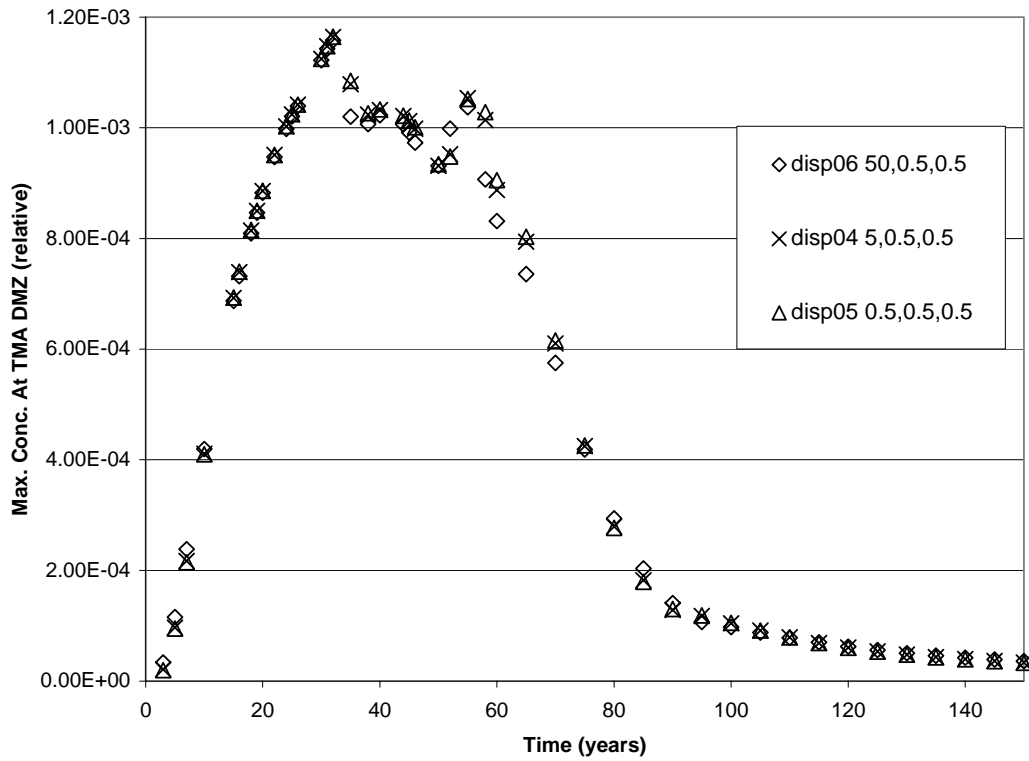


Figure 13. Maximum concentrations under varying longitudinal dispersivity at low transverse dispersivities. Transverse horizontal and vertical dispersivities are set at 0.5 ft. Longitudinal dispersivities vary: 50 ft (run disp06), 5 ft (run disp04), and 0.5 ft (run disp05).

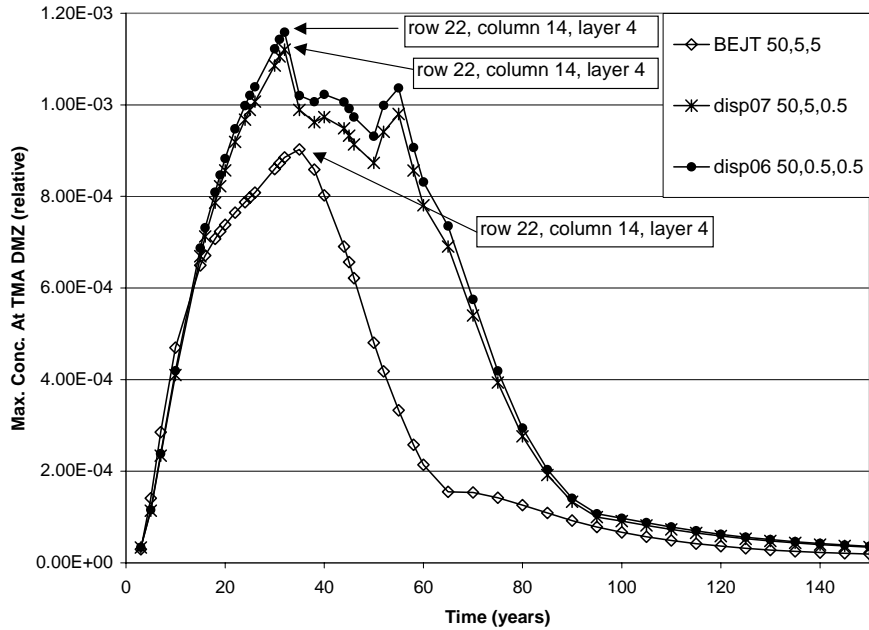


Figure 14. Maximum concentrations with changes in transverse horizontal and vertical dispersivity. The applicant's BEJT case (best engineering judgment for transport, transverse horizontal and vertical dispersivity = 5.0 ft) is compared to a decrease in vertical dispersivity (run disp07, vertical dispersivity = 0.5 ft), and to a decrease in both transverse horizontal and vertical dispersivity (run disp06, transverse horizontal and vertical dispersivity = 0.5 ft). Row, column and layer number identify the model cell located along the DMZ where this maximum concentration occurs in each of the simulations.

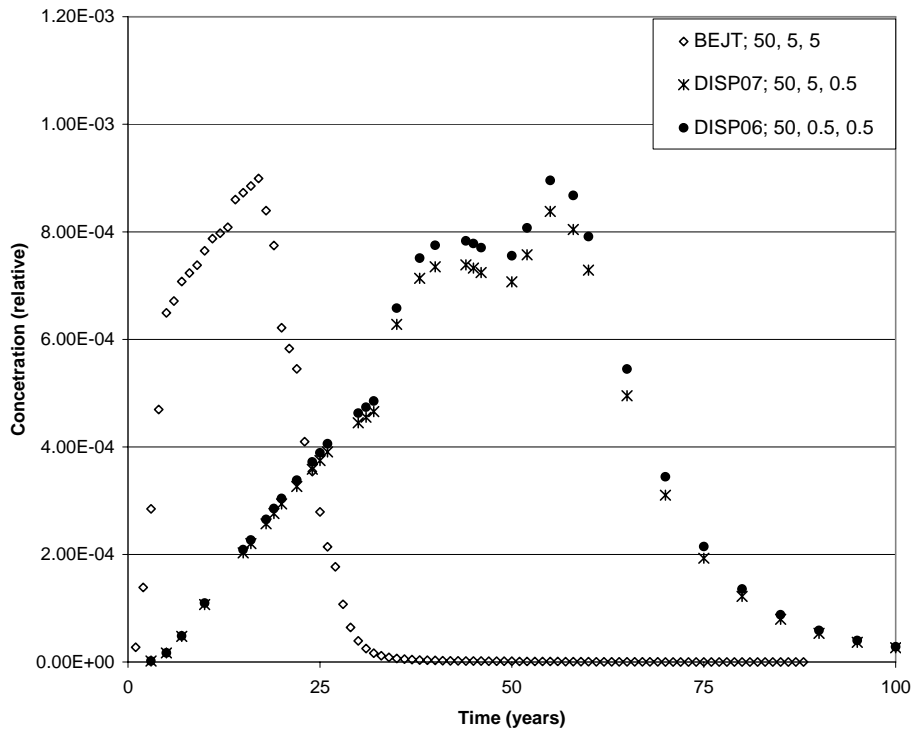


Figure 15. Breakthrough curve under reduced transverse dispersivities. Increased vertical dispersivity drives mass deeper earlier, resulting in more mixing of plume and lower overall concentrations. Model runs are as described in Figure 14 caption. Location is at row 22, column 14, layer 6 (see Appendix 2).

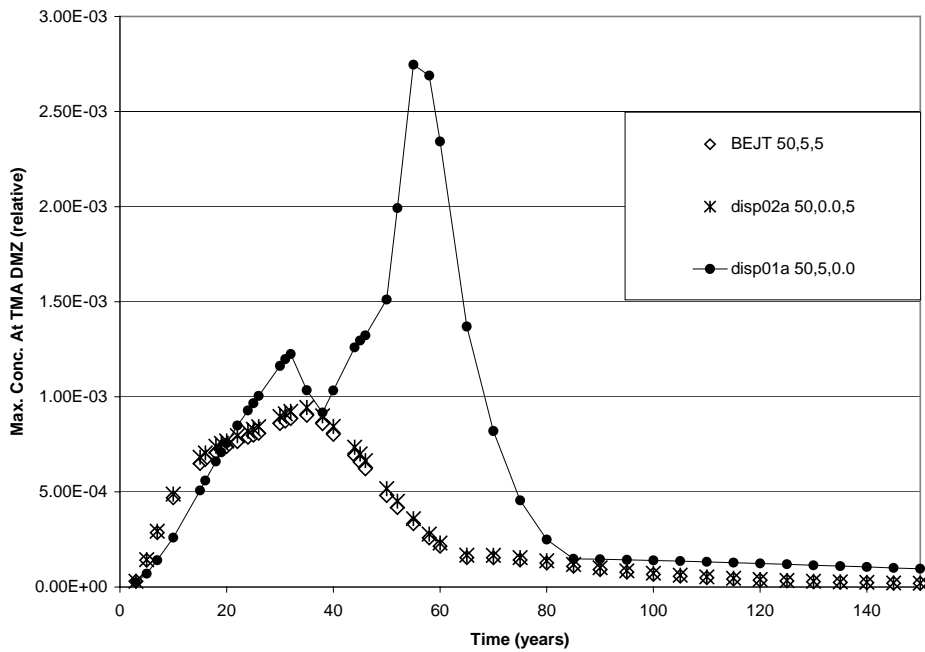


Figure 16. Maximum concentrations with no transverse vertical and no transverse horizontal dispersivity. The applicant’s BEJT (best engineering judgment for transport) case, in which transverse horizontal dispersivity is eliminated (run disp02a), is compared to the case where transverse vertical dispersivity is eliminated (run disp01a).

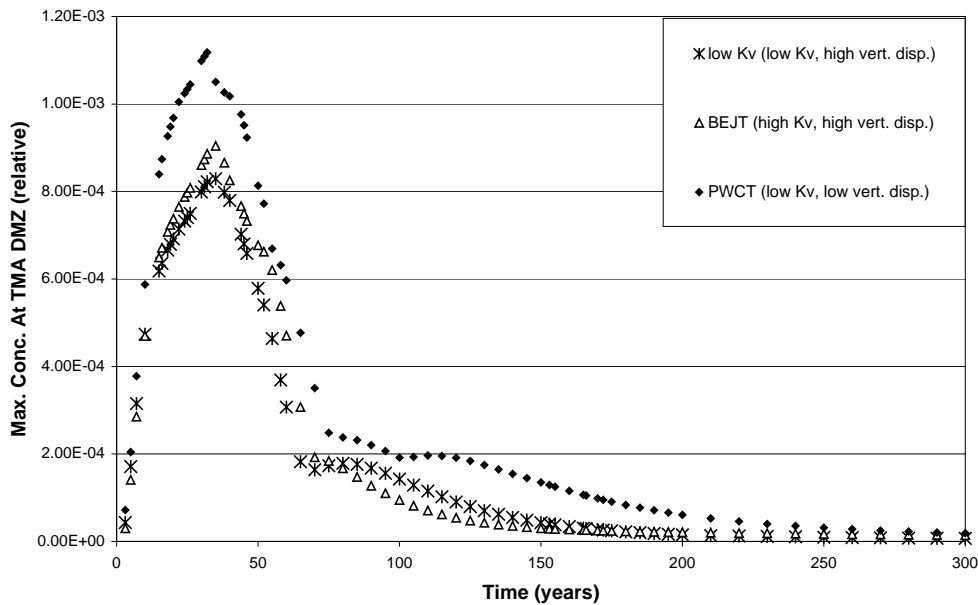


Figure 17. Maximum concentration along the TMA DMZ with a reduction in vertical hydraulic conductivity. Runs shown are for the applicant’s BEJT (best engineering judgment for transport) and PWCT (practical worst case for transport) parameter sets, and for the BEJT case with a lower vertical hydraulic conductivity.

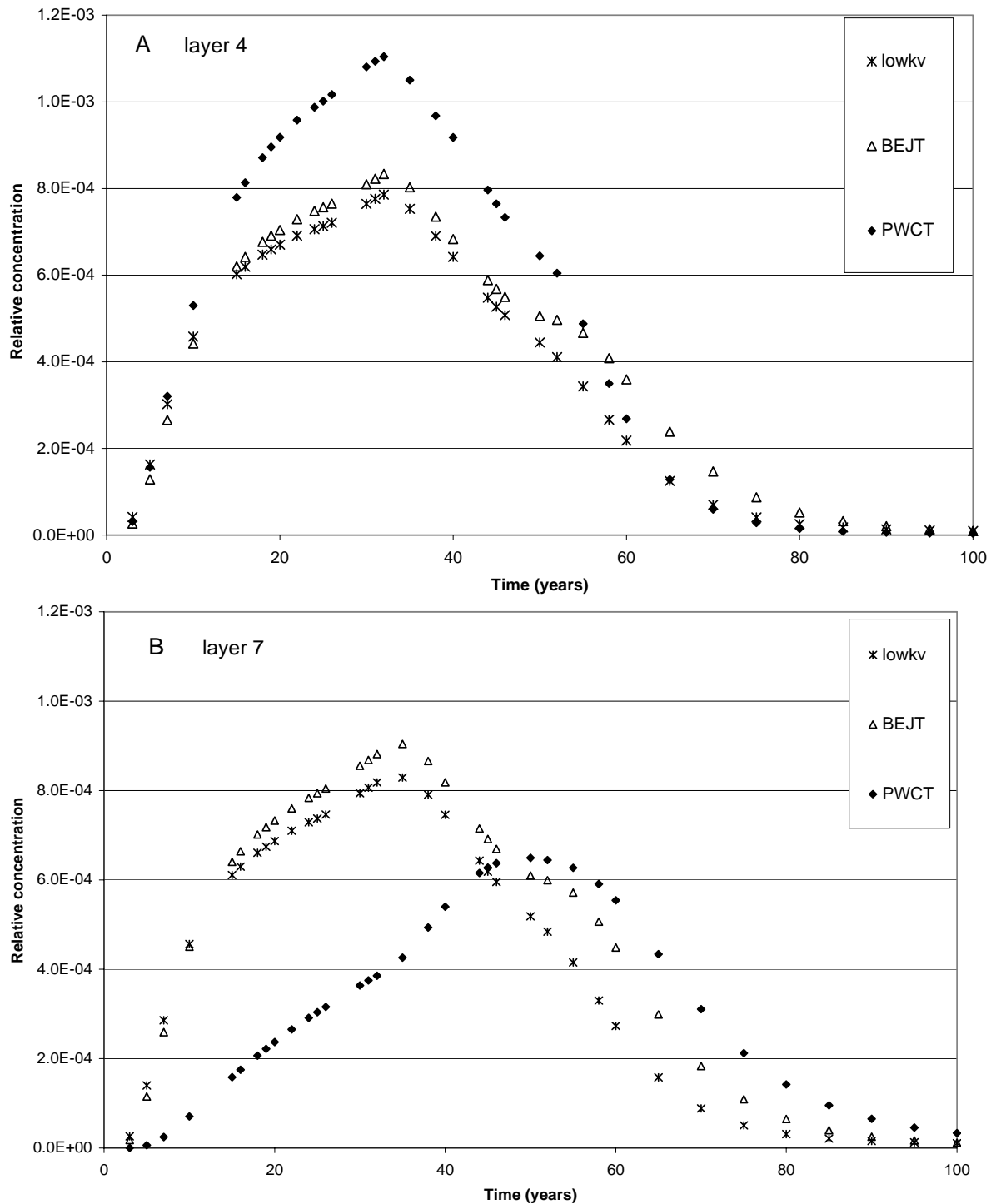


Figure 18. Breakthrough curves demonstrating effect of reduction in vertical hydraulic conductivity (K_v). Simulations are as described in Figure 17 caption. Diagram A (top) shows breakthrough at layer 4, row 22, column 14. Diagram B (bottom) shows breakthrough at layer 7, row 22, column 14. A reduction in K_v results in breakthrough similar to the BEJT (best engineering judgment for transport) case. However, a delay and decrease in concentrations reaching deeper model layers occurs with PWCT (practical worst case for transport) parameters, where both vertical dispersivity and K_v are reduced.

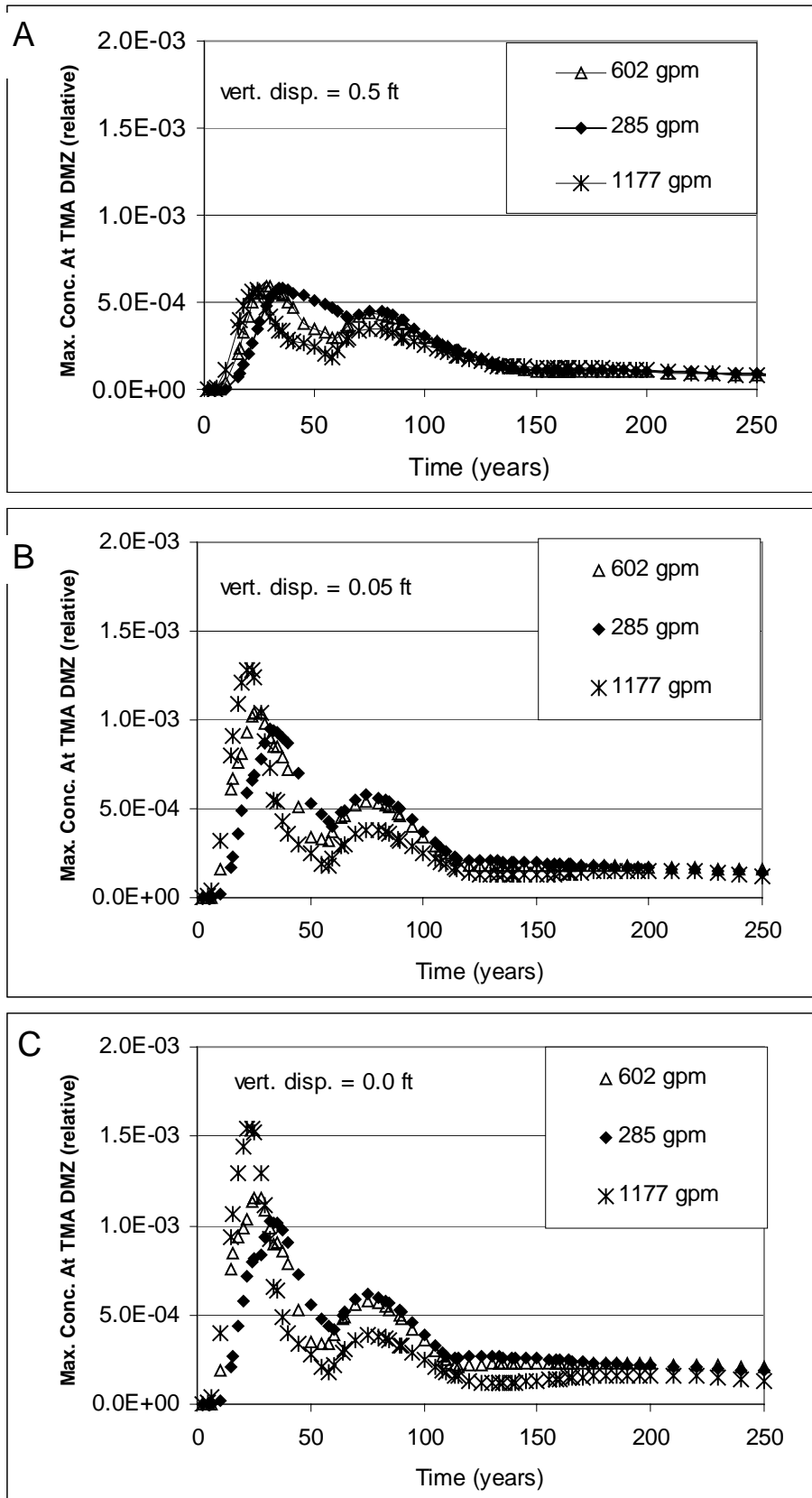


Figure 19. Maximum concentrations with changes in dewatering rate and vertical dispersivity. Results using vertical dispersivity (vert. disp.) of 0.5 ft, 0.05 ft., and 0.0 ft are shown in A, B and C, respectively.

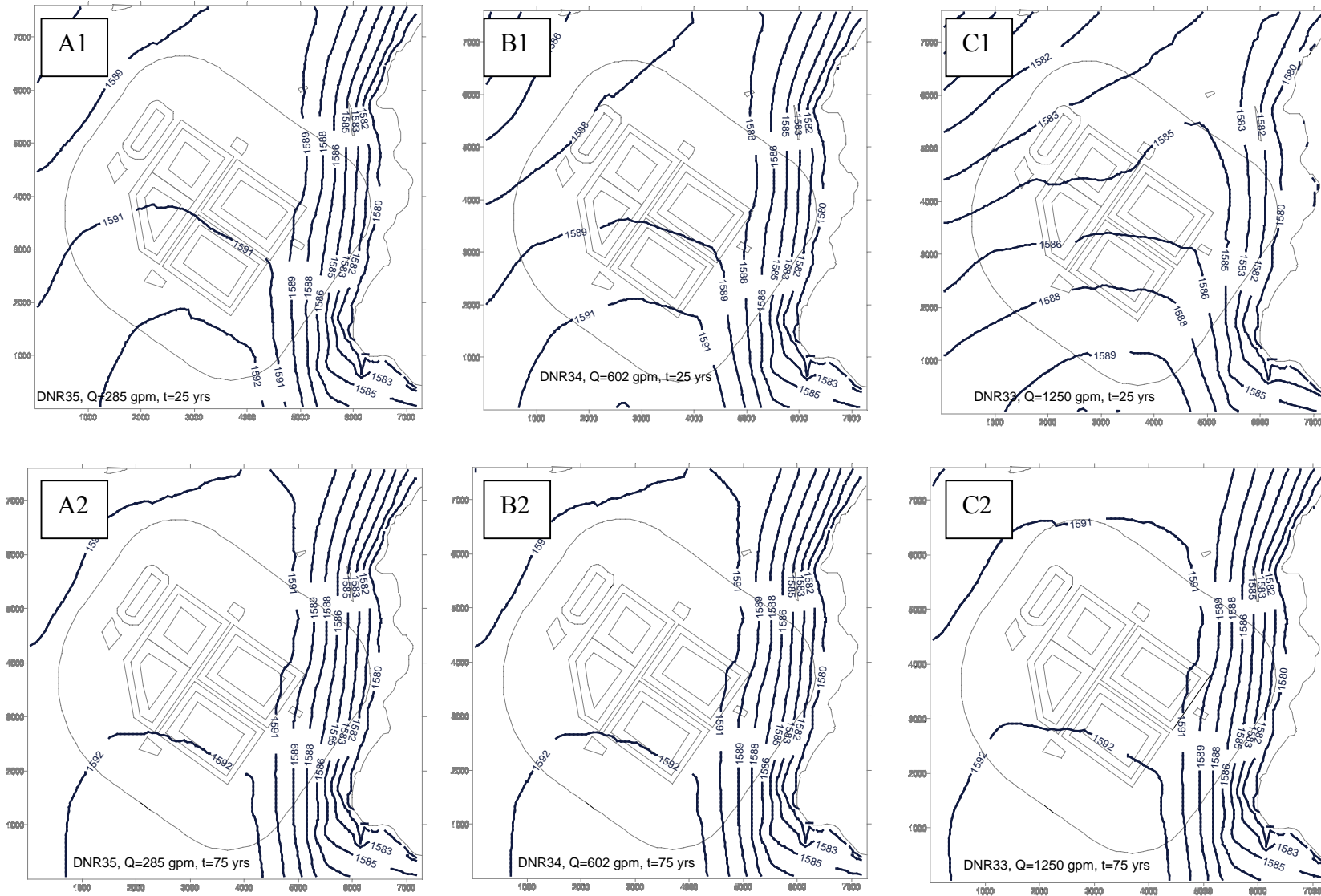


Figure 20. Water table during mine dewatering and after recovery at low, proposed maximum, and high pumping rates (A, B, and C, respectively). Note the shift in the water table divide under the high pumping rate. Times shown are for 25 years and 75 years (1 and 2, respectively). Q = pumping rate in gallons per minute (gpm), t = time in model years.

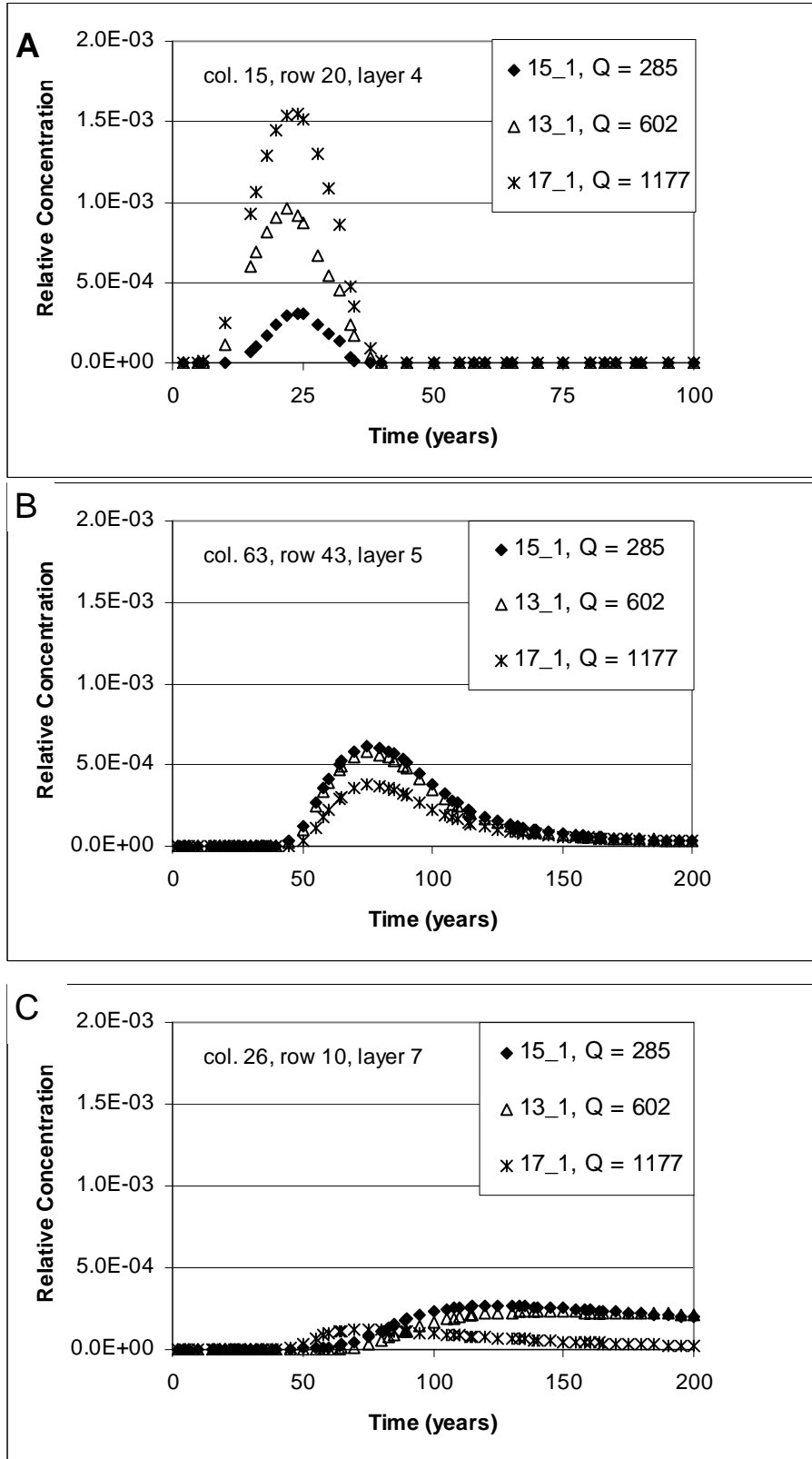


Figure 21. Breakthrough curves demonstrating effect of mine dewatering rates with no vertical dispersivity. Q = pumping rate in gallons per minute. Locations of breakthrough curves column 15,

row 20, layer 4 (A), column 63, row 43, layer 5 (B), and column 26, row 10, layer 7 (C). See Appendix 2 for locations.

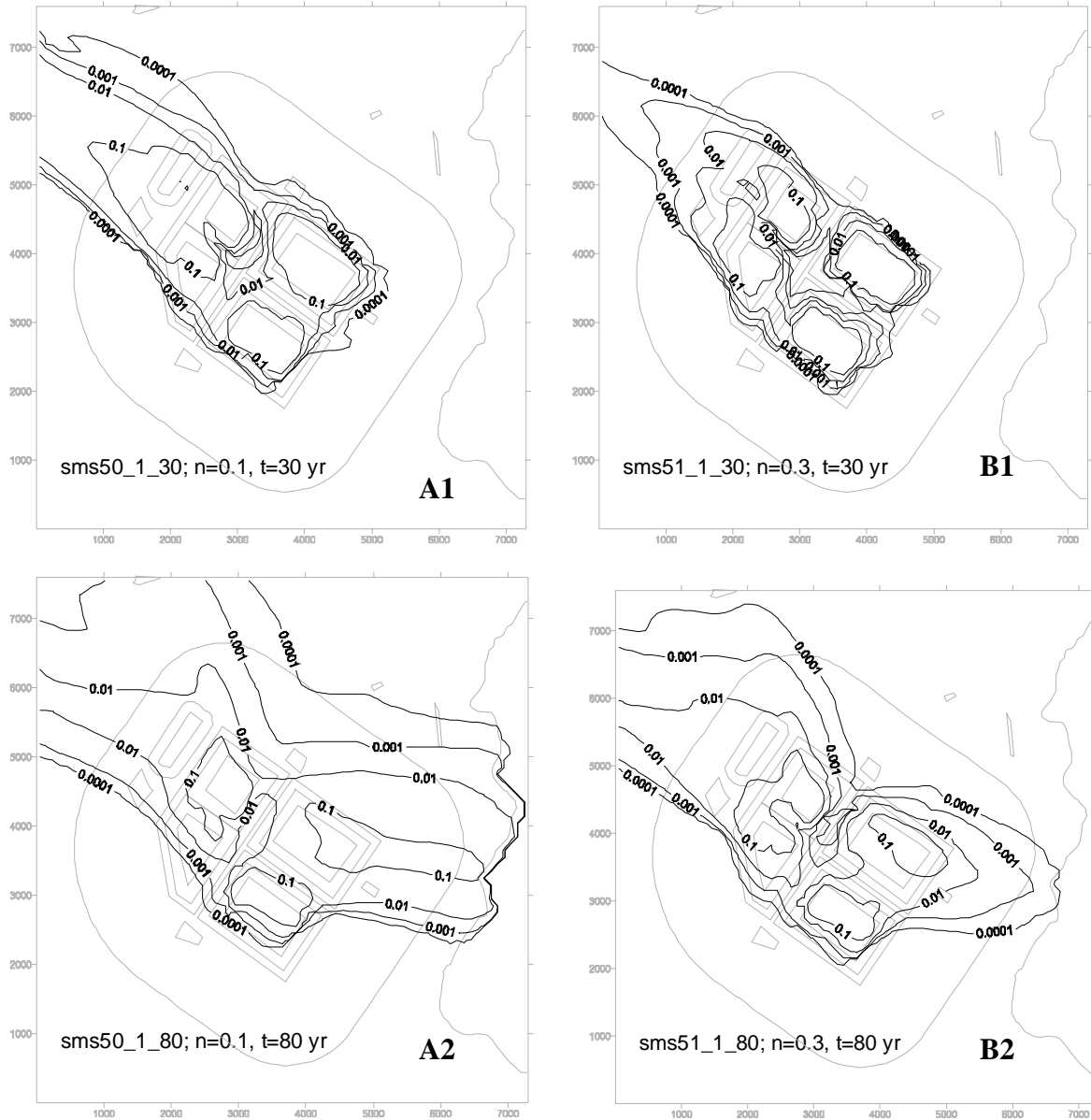


Figure 22. Concentrations over model domain at low and high porosity. Porosity of 10% (A1 and A2) results in higher concentrations. N = porosity, t = time in model years. Porosity of 30% results in lower concentrations at the western TMA DMZ at early times (B1), and lower concentration at the eastern TMA DMZ at later times (B2). Times shown are for 30 years (A1 and B1) and 80 years (A2 and B2).

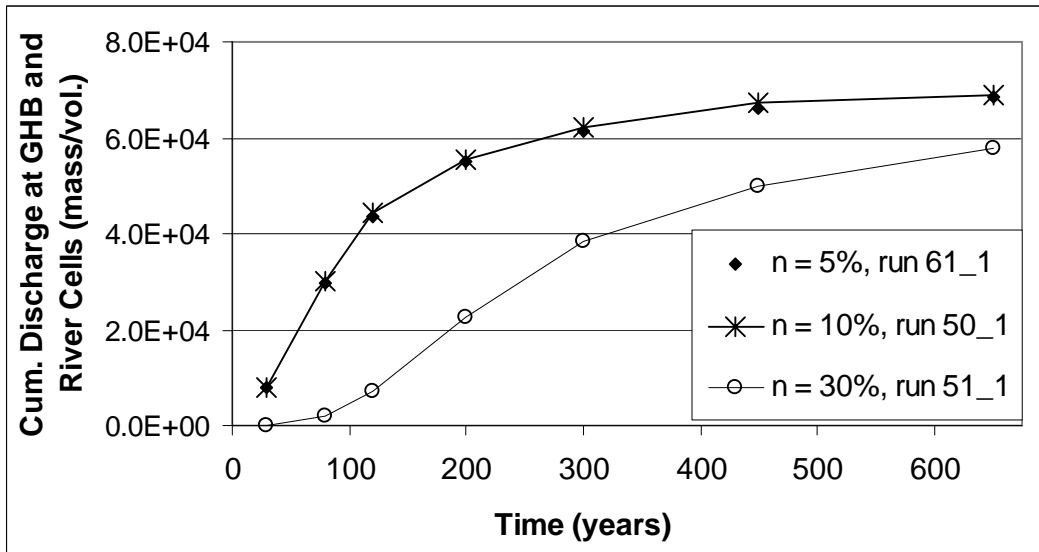


Figure 23. Total mass reaching head-dependent and river boundaries over time, n (porosity) = 5, 10 and 30%. In simulations with lower porosity, increased advective velocity results in more mass reaching model boundaries sooner.

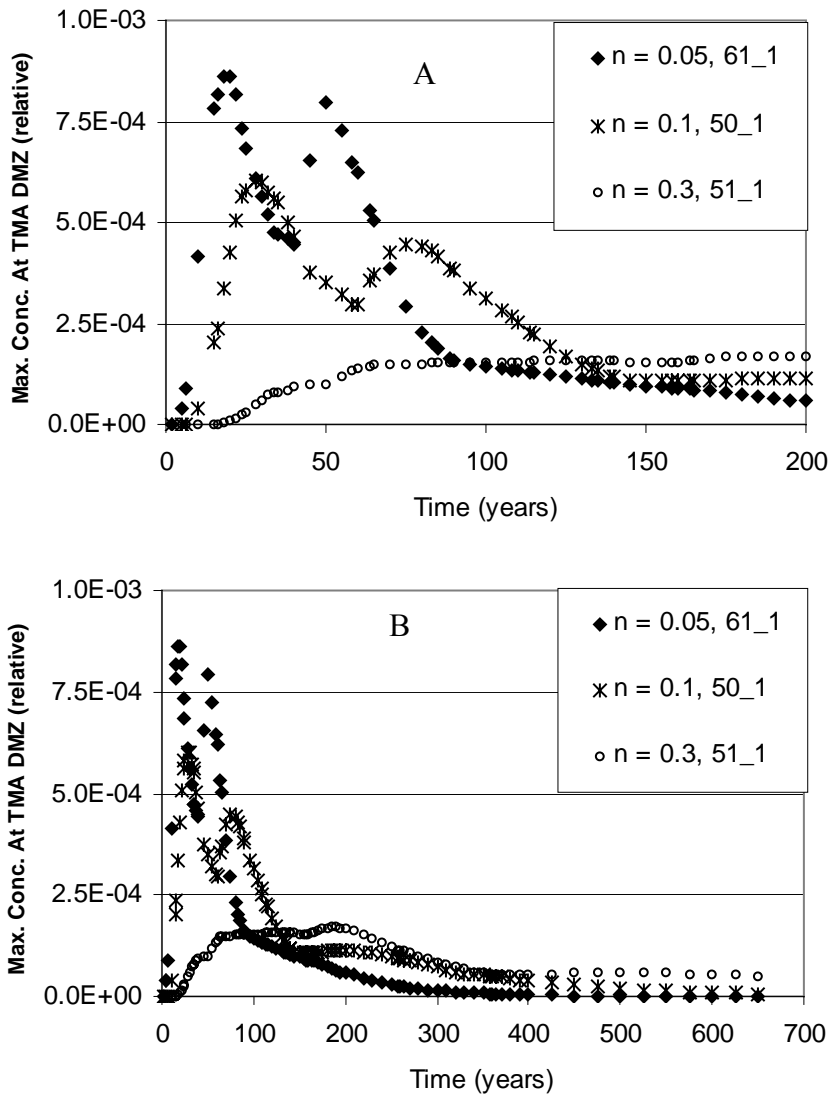


Figure 24. Maximum concentrations along the TMA DMZ at early times (A) and over 650 years (B). The first peak in a curve is the maximum occurrence to west; the second peak marks the arrival of the plume at the eastern TMA DMZ. N = porosity.

Pinchout Zone

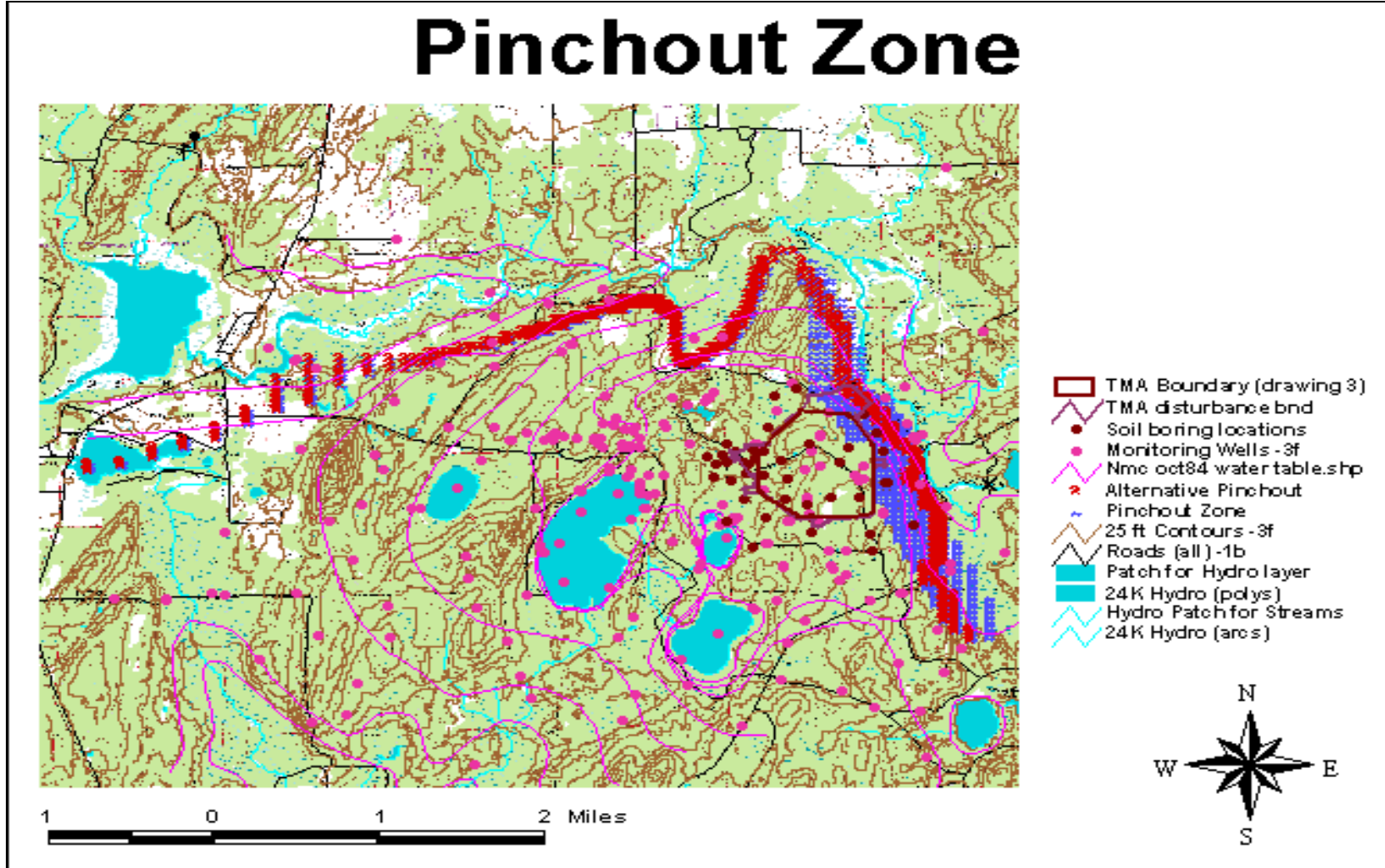


Figure 25. Applicant's interpretation and one possible alternative interpretation of the pinchout zone.

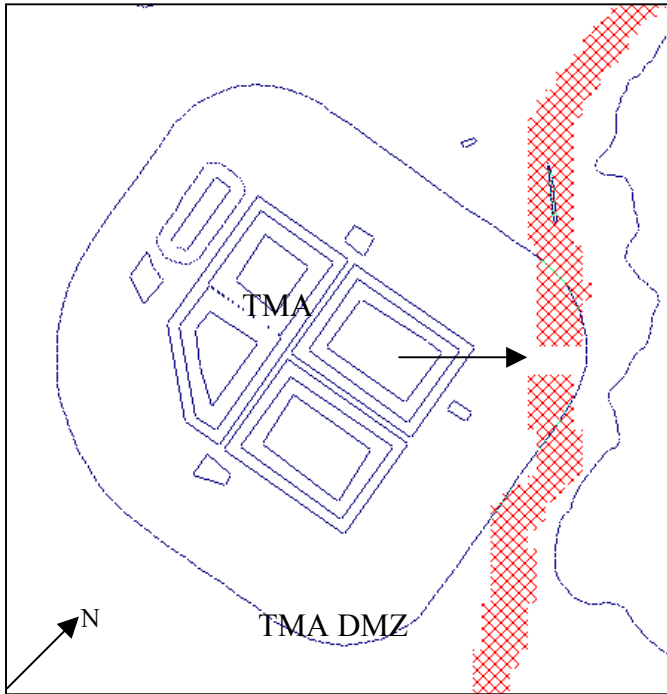


Figure 26. Location of hypothetical high-K (hydraulic conductivity) channel in pinchout zone, layers 2 through 6. Pinchout zone is shown as cross-hatched area. Hemlock Creek is shown to the northeast of the pinchout zone.

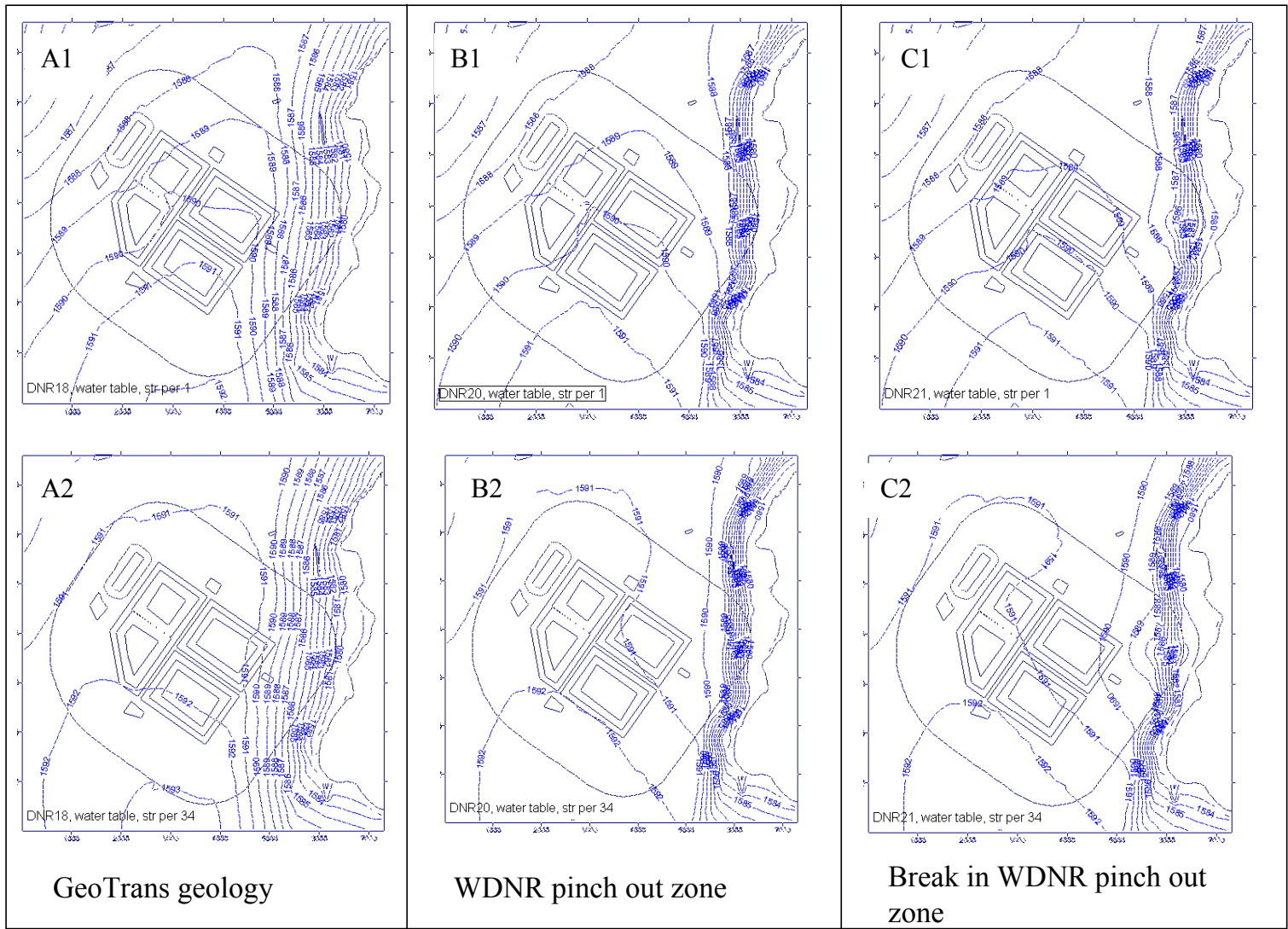


Figure 27. Water table from first (A1, B1 and C1) and last (A2, B2 and C2) stress periods of TMA/RP flow model for pinchout zone configurations (A, applicant's configuration; B, WDNR's configuration; C, WDNR configuration with break).

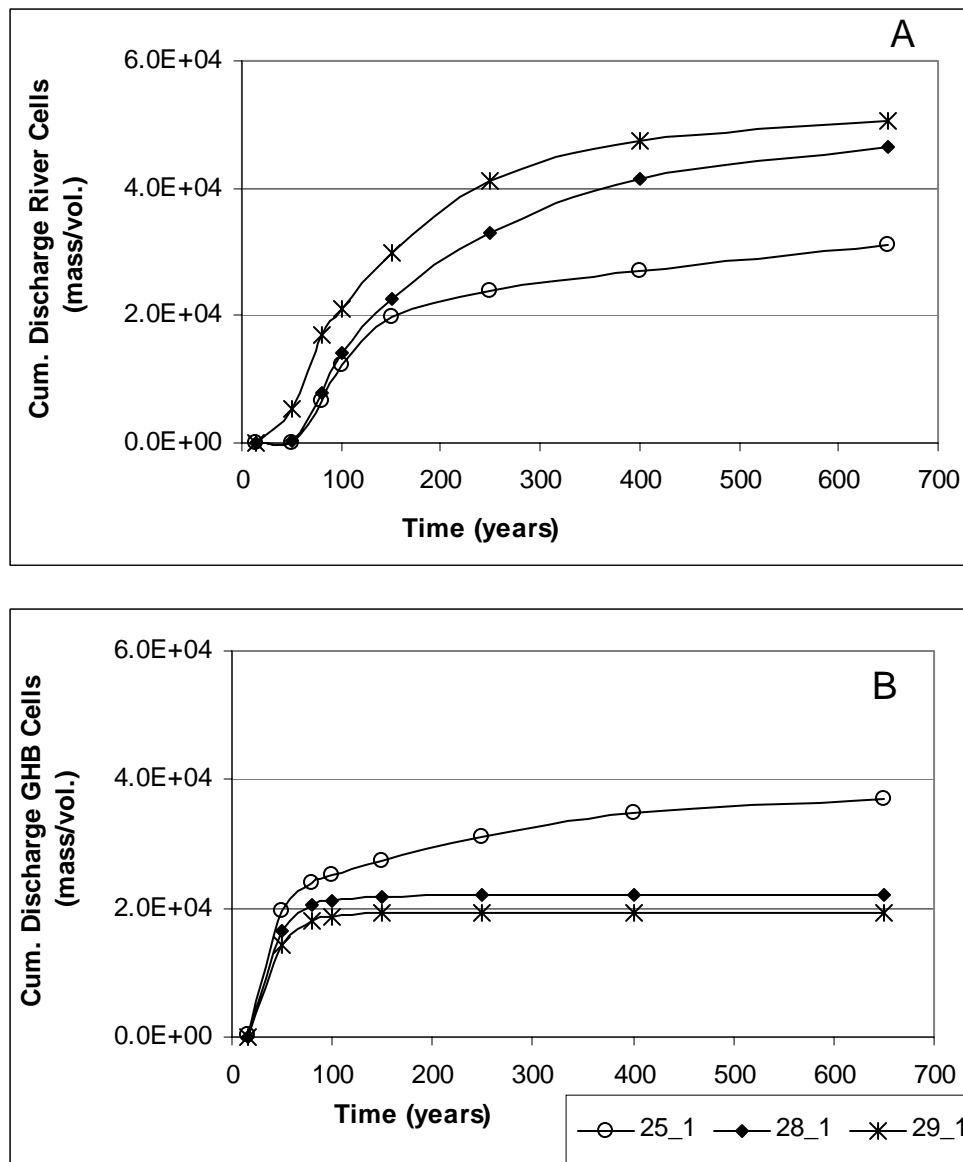


Figure 28. Cumulative mass discharge to river cells (A) and head dependent boundary cells (B). In these pinchout zone runs, the increase in hydraulic gradient in runs with a narrow and lower hydraulic conductivity zone (runs 28_1 and 29_1) towards Hemlock Creek increases contaminant flux in that direction, and flux across other model boundaries decreases. Effect of high-hydraulic conductivity channel (run 29_1) is to accentuate this difference. Less mass flows to the east and the river cells under the applicant's interpretation (run 25_1).

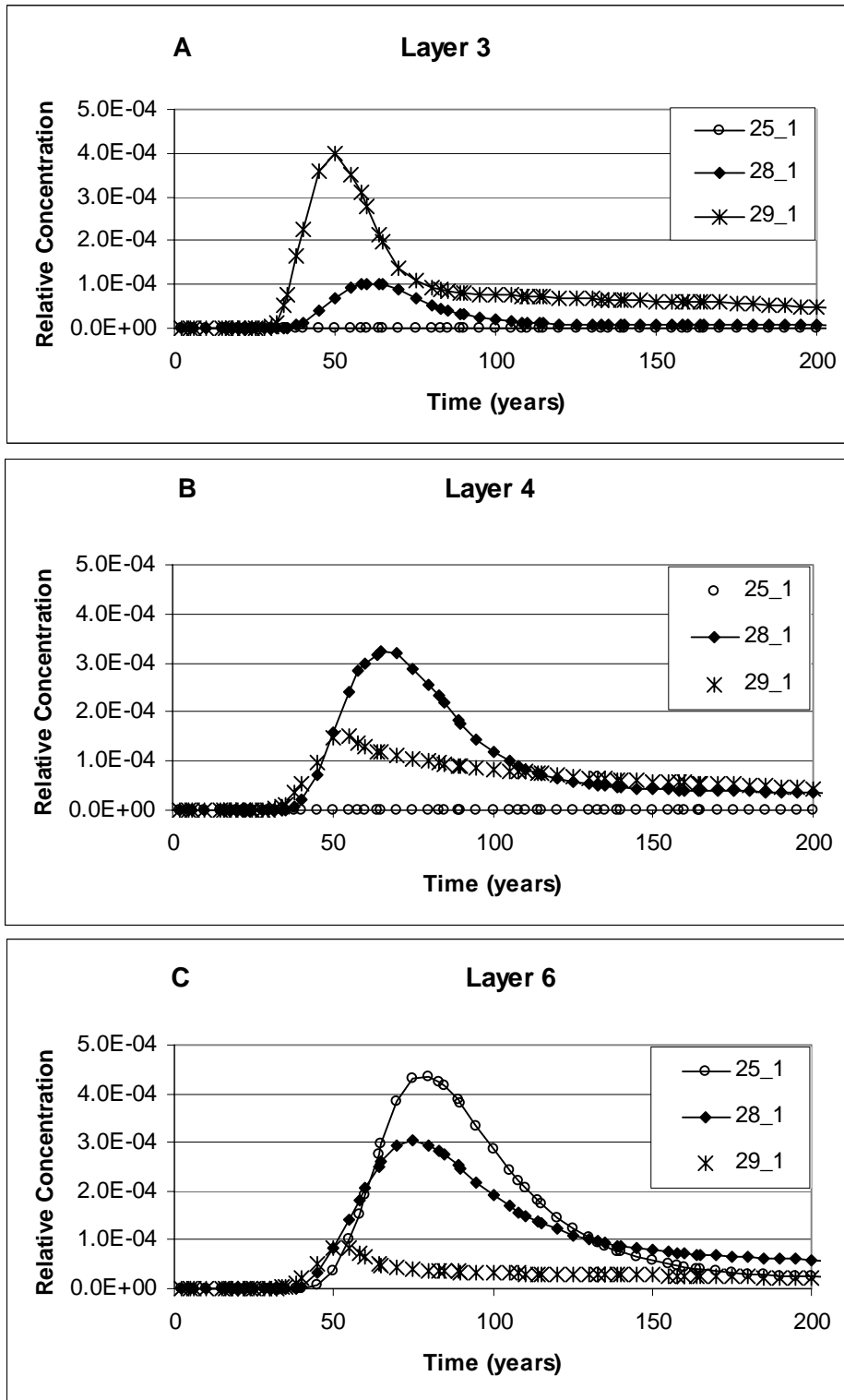


Figure 29. Breakthrough curves in three layers down gradient of high-hydraulic conductivity channel location. Location (row 40, column 63) shown in Appendix 2, A - layer 3; B - layer 4; C - layer 6. Run 25_1 is the applicant's interpretation of the geology, run 28_1 is the WDNR interpretation, and run 29_1 is the WDNR interpretation with a break.

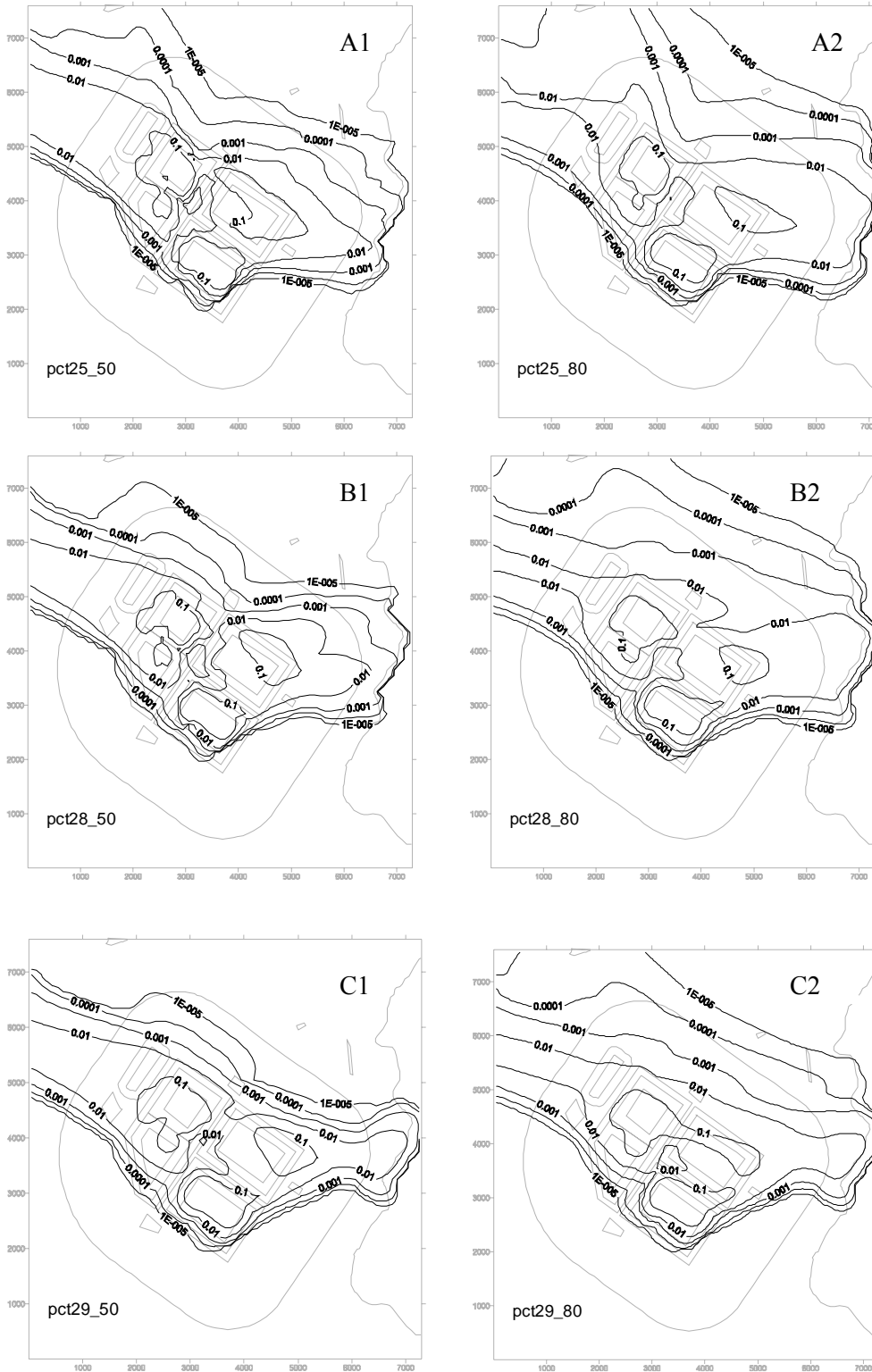


Figure 30. Contour plots of the plume at 50 and 80 years in pinch out zone simulations. Run 25 is the applicant's interpretation of the geology (A), run 28 is the WDNR interpretation (B), and run 29 is the WDNR interpretation with a break (C). Figures A1, B1 and C1 are at 50 years, figures A2, B2 and C2 are at 80 years.

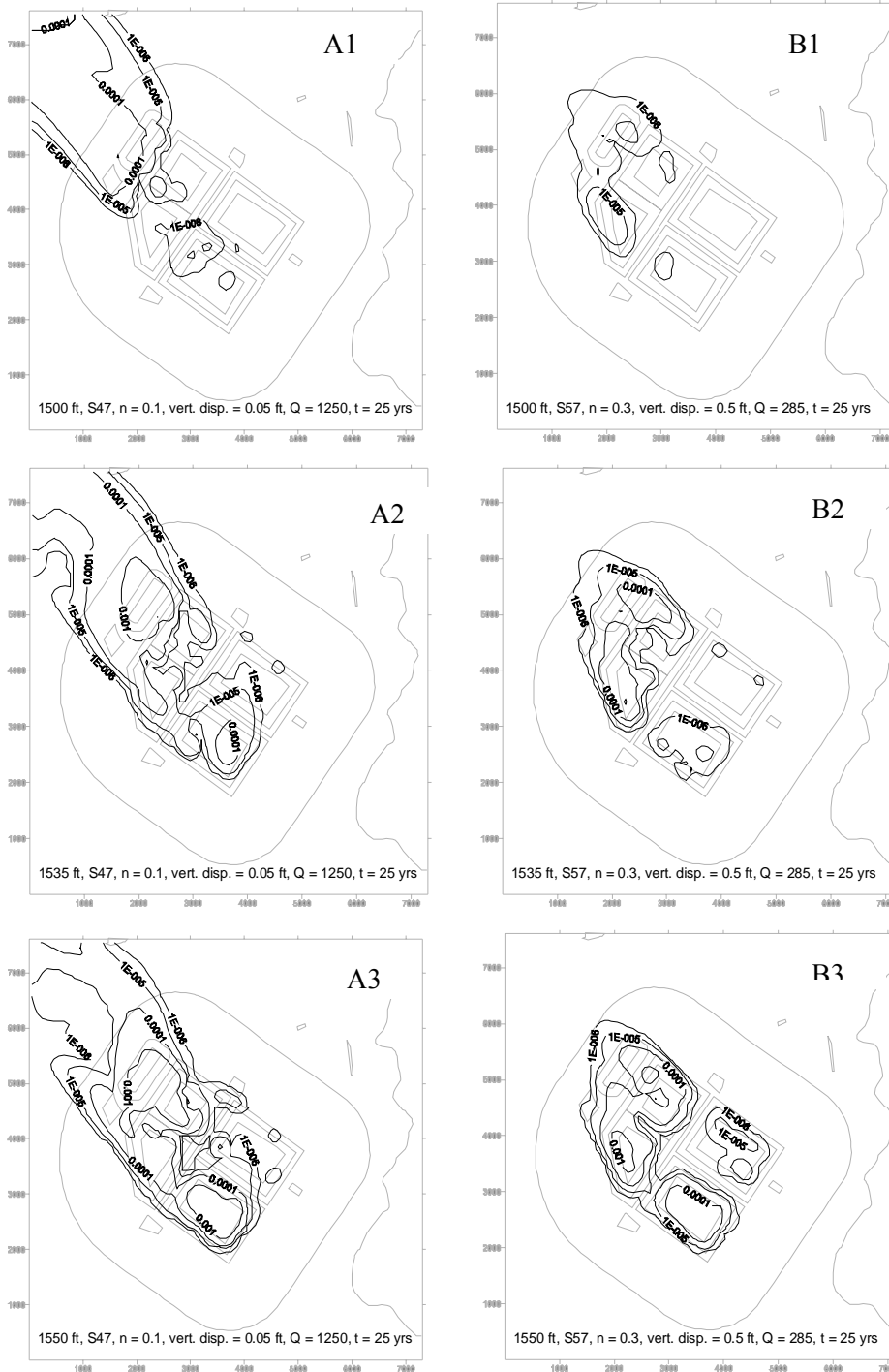


Figure 31. Contours of plume concentrations at 25 years time. Higher concentrations result from lower porosity and dispersivity and higher pumping rate. Figures A1-A3 are low vertical dispersivity and high pumping rate; B1-B3 are at higher vertical dispersivity and lower pumping rate. The elevation of the model at which concentrations are contoured increases from Figures 1 – 3, as labeled on each figure (in ft above sea level).

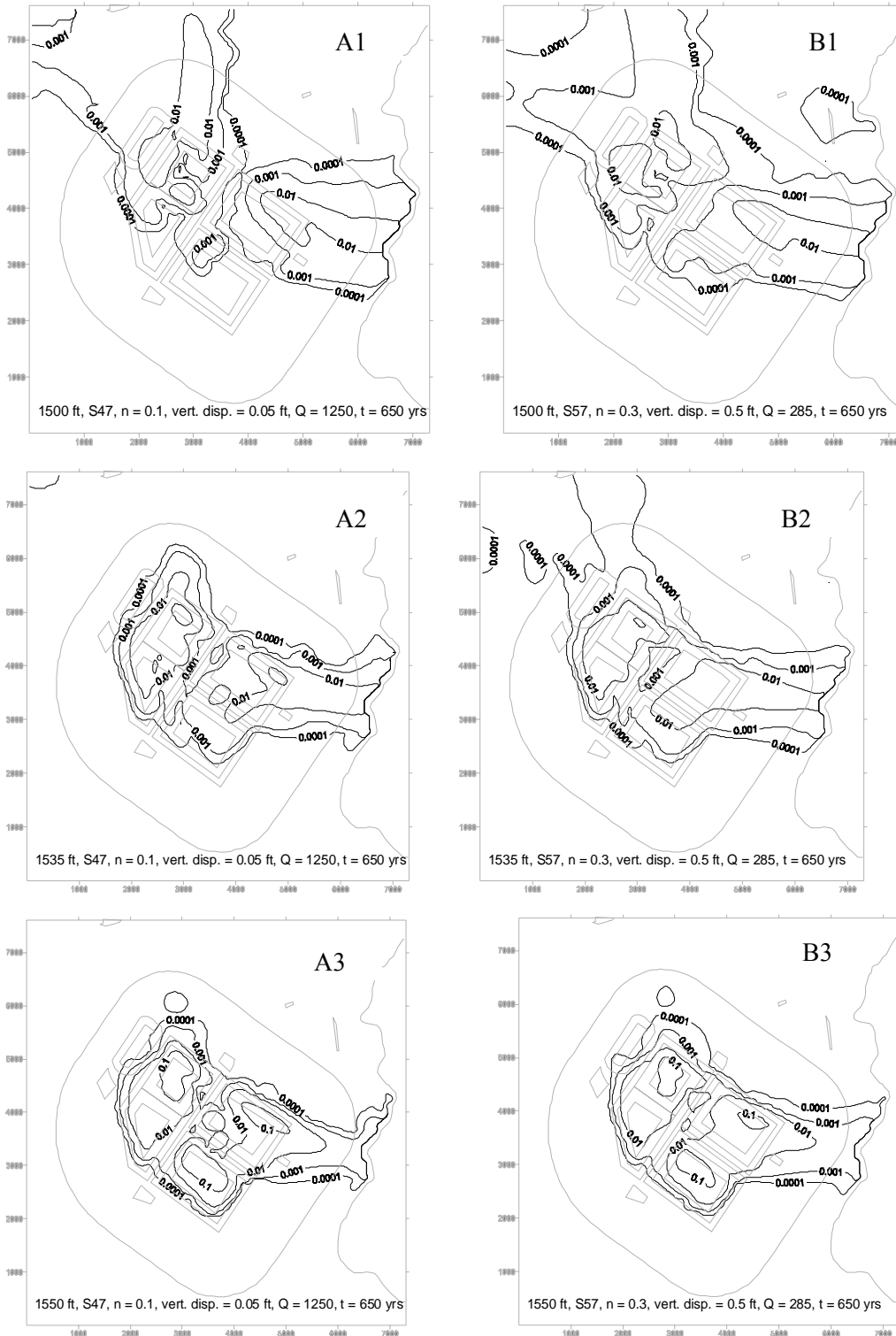


Figure 32. Contours of concentrations at 650 years at high long-term exfiltration rates. N = porosity, vert disp = vertical dispersivity, Q = pumping rate in gallons per minute, t = model time in years. The elevation of each contour plot is indicated. Vertical dispersivity is higher and pumping rate lower in B1-B3. The elevation of the model at which concentrations are contoured increases from figures 1 – 3, as labeled on each figure (in ft above sea level).

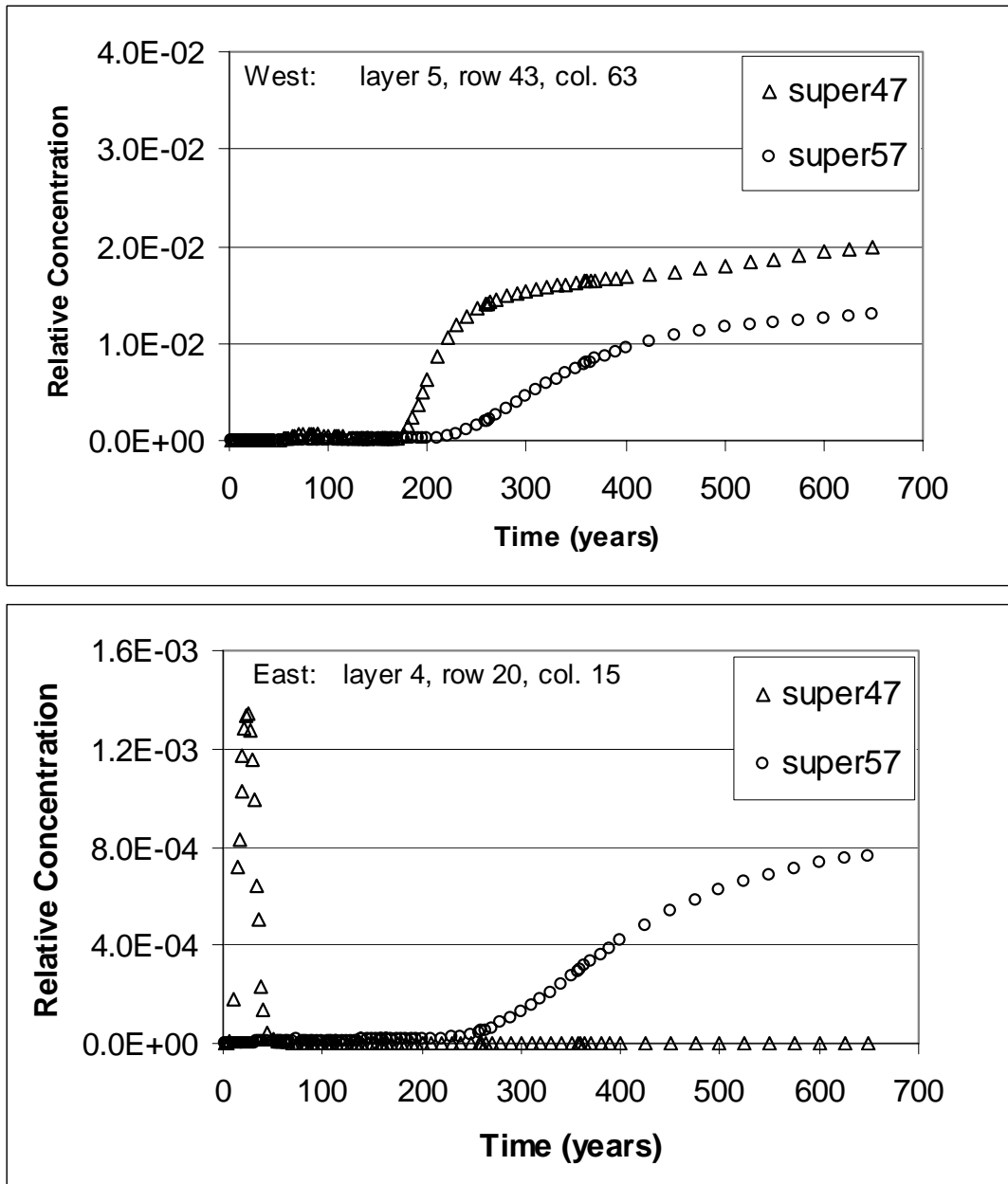


Figure 33. Breakthrough curves at cells west and east of model domain. Note different vertical scales on graphs. Lower porosity and vertical dispersivity values (run 47) result in higher breakthrough to the west (top graph) at early times than with higher porosity and vertical dispersivity (run 57). Concentrations to the east (bottom graph) are affected by the high long-term exfiltration rate in both model runs. The prefix “super” is used with the run name in the legend because the results shown are the superposition of a complete set of six simulations for each model run.

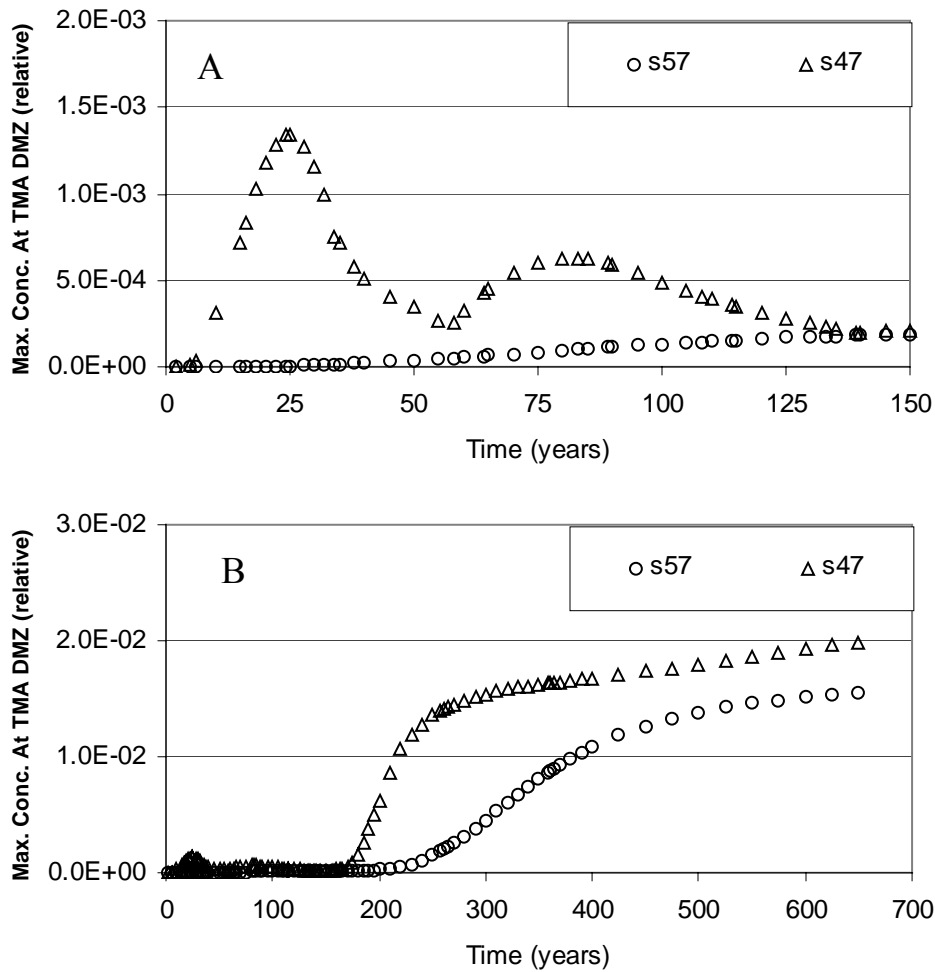


Figure 34. Range of maximum relative concentrations at the TMA DMZ at early times (A) and entire 650-year simulation (B). Range of maximum relative concentrations at the TMA DMZ at early times (A) and overall (B). Simulation S57, with a higher vertical dispersivity of 0.5 ft., higher porosity of 0.3, and lower mine dewatering rate of 285 gpm, results in lower early-time concentrations along the DMZ. At simulation times exceeding 150 years, run 47, with vertical dispersivity of 0.05 ft., porosity of 0.1 and dewatering rate of 1250 gpm, shows similar results to s57 because both simulations are dominated by the large magnitude of the long-term cap leakage rate. Results shown are the superposition of a complete set of six simulations for each model run.

Table 1. Model layers in regional model and TMA/RP model.

Regional Model Layer	Geologic Unit	TMA/RP Model Layers
1	Late Wisconsin Till	1
2	Coarse and Fine Outwash	2, 3 and 4
3	Coarse and Fine Outwash	5 and 6
4	Pre to Early-Wisconsinan Till & Massive Saprolite	7
5	Strongly Weathered Bedrock	not modeled
6	Moderately Weathered Bedrock	not modeled
7	Weakly Weathered Bedrock	not modeled

Table 2. Six model runs that comprise a complete simulation.

Model Run	Source Area	Phase of Facility Operations
1	landfill	operational
2	landfill	consolidation
3	landfill	post-capping
4	landfill	liner breakdown
5	reclaim pond	operational
6	reclaim pond	post-capping

Table 3. Parameters assigned in model versions.

Geologic Unit or Boundary	Parameter	BEJT ¹ Value	PWCT ¹ Value
All Geologic Units	Effective Porosity	0.10	0.10
	Longitudinal Dispersivity	50.0 ft	25.0 ft
	Horizontal Transverse Dispersivity	5.0 ft	2.5 ft
	Vertical Dispersivity	5.0 ft	0.5 ft
Late Wisconsinan Till	Horizontal Conductivity	0.80 ft/d ²	0.80 ft/d
	Vertical Conductivity	0.40 ft/d	0.04 ft/d
Coarse Outwash	Horizontal Conductivity	80.0 ft/d	80.0 ft/d
	Vertical Conductivity	8.0 ft/d	0.8 ft/d
	Pinchout Zone Horizontal Conductivity	6.0 ft/d	6.0 ft/d
	Pinchout Zone Vertical Conductivity	0.6 ft/d	0.06 ft/d
Fine Outwash	Horizontal Conductivity	20.0 ft/d	20.0 ft/d
	Vertical Conductivity	2.0 ft/d	0.2 ft/d
	Pinchout Zone Horizontal Conductivity	6.0 ft/d	6.0 ft/d
	Pinchout Zone Vertical Conductivity	0.6 ft/d	0.06 ft/d
Pre-to Early-Wisconsinan Till and Massive Saprolite	Horizontal Conductivity	2.00 ft/d	2.00 ft/d
	Vertical Conductivity	0.075 ft/d	0.0075 ft/d
Ancient Lacustrine	Horizontal Conductivity	2.00 ft/d	2.00 ft/d
	Vertical Conductivity	0.075 ft/d	0.0075 ft/d
Hemlock Creek	Width	14.0 ft	14.0 ft
	Creekbed Vertical Conductivity	1.0 ft/d	1.0 ft/d
	Creekbed Sediment Thickness	1.0 ft	1.0 ft
	Water Depth	1.0 ft	1.0 ft
Seepage Wetlands	Bottom Sediment Vertical Conductivity	0.003 ft/d	0.003 ft/d
	Bottom Sediment Thickness	5.0 ft	5.0 ft
	Water Depth	2.0 ft	2.0 ft

1) BEJT = best engineering judgment for transport; PWCT= practical worst case for transport

2) ft/d = feet per day

Table 4. Numerical solvers used in modeling contaminant transport from the TMA/RP.

Solver - Advection	Solver – dispersion & sink/source	Concerns
Explicit FD ¹ , upstream weighting ²	Explicit FD	Unacceptable numerical dispersion
MOC ^{3,4}	GCG ⁶ (implicit FD)	Unacceptable mass balance
MOC	Explicit FD	Unacceptable mass balance
Implicit FD, central-in-space weighting	GCG (implicit FD)	artificial oscillation in results
TVD ⁵	Explicit FD	does not reach solution for full 650-year run
TVD	GCG (implicit FD)	does not reach solution with low dispersivities for full 650-year run

Notes:

¹ FD = finite difference

² Explicit FD, upstream weighting was used by NMC in the BEJT and PWCT runs.

³ All other solvers shown in Table 4 were tested as part of this review of applicant's model.

⁴ MOC = method of characteristics

⁵ TVD = total variation diminishing

⁶ GCG = generalized conjugate gradient

Table 5. TMA Cell 1A percolation rates by stress period.

Stress Period	Phase ⁴	Percolation (Exfiltration) Rate (ft/day) ²			Percolation Rate ³ Sensitivity Run ft/day)
		Base	Lower Sideslope	Upper Sideslope	Base
1	A	1.47E-06	5.71E-11	2.21E-03 ¹	1.47E-6
2	A	1.47E-06	5.71E-11	2.21E-03 ¹	1.47E-6
3	B	1.93E-06	5.71E-11	2.34E-10	1.93E-6
4	B	1.93E-06	5.71E-11	2.34E-10	1.93E-6
5	C	8.86E-06	2.28E-10	457E-10	8.86E-6
6	D	7.45E-07	2.28E-10	5.71E-11	7.45E-7
7	D	7.45E-07	2.28E-10	5.71E-11	7.45E-7
8	D	7.45E-07	2.28E-10	5.71E-11	7.45E-7
9	D	7.45E-07	2.28E-10	5.71E-11	7.45E-7
10	E	9.47E-08	5.71E-11	5.71E-11	2.08E-7
11	E	9.47E-08	5.71E-11	5.71E-11	2.08E-7
12	E	9.47E-08	5.71E-11	5.71E-11	2.08E-7
13	E	9.47E-08	5.71E-11	5.71E-11	2.08E-7
14	E	9.47E-08	5.71E-11	5.71E-11	2.08E-7
15	E	9.47E-08	5.71E-11	5.71E-11	2.08E-7
16	F	1.38E-08	5.71E-11	5.71E-11	8.99E-6
17	F	1.38E-08	5.71E-11	5.71E-11	8.99E-6
18	F	1.38E-08	5.71E-11	5.71E-11	8.99E-6
19	G	4.57E-09	4.57E-09	4.57E-09	8.99E-6
20	G	4.57E-09	4.57E-09	4.57E-09	8.99E-6
21	G	4.57E-09	4.57E-09	4.57E-09	8.99E-6
22	G	4.57E-09	4.57E-09	4.57E-09	8.99E-6

¹ Equal to default recharge, no source applied.

² Percolation rates used in HSI GeoTrans (1999b).

³ Rates for lower and upper sideslopes were not changed in sensitivity run.

⁴ Phases defined in Table 9.

Table 6. TMA Cell 1B percolation rates by stress period.

Stress Period	Phase ⁴	Percolation (Exfiltration) Rate (ft/day) ²			Percolation Rate ³ Sensitivity Run ft/day)
		Base	Lower Sideslope	Upper Sideslope	Base
1	X	2.21E-03 ¹	2.21E-03 ¹	2.21E-03 ¹	2.21E-3
2	A	1.47E-06	5.71E-11	2.21E-03	1.47E-6
3	B	1.93E-06	5.71E-11	2.34E-10	1.93E-6
4	B	1.93E-06	5.71E-11	2.34E-10	1.93E-6
5	C	8.86E-06	2.28E-10	4.57E-10	8.86E-6
6	D	7.45E-07	2.28E-10	5.71E-11	7.45E-7
7	D	7.45E-07	2.28E-10	5.71E-11	7.45E-7
8	D	7.45E-07	2.28E-10	5.71E-11	7.45E-7
9	D	7.45E-07	2.28E-10	5.71E-11	7.45E-7
10	E	9.47E-08	5.71E-11	5.71E-11	2.08E-7
11	E	9.47E-08	5.71E-11	5.71E-11	2.08E-7
12	E	9.47E-08	5.71E-11	5.71E-11	2.08E-7
13	E	9.47E-08	5.71E-11	5.71E-11	2.08E-7
14	E	9.47E-08	5.71E-11	5.71E-11	2.08E-7
15	E	9.47E-08	5.71E-11	5.71E-11	2.08E-7
16	F	1.38E-08	5.71E-11	5.71E-11	8.99E-6
17	F	1.38E-08	5.71E-11	5.71E-11	8.99E-6
18	F	1.38E-08	5.71E-11	5.71E-11	8.99E-6
19	F	1.38E-08	5.71E-11	5.71E-11	8.99E-6
20	G	4.57E-09	4.57E-09	4.57E-09	8.99E-6
21	G	4.57E-09	4.57E-09	4.57E-09	8.99E-6
22	G	4.57E-09	4.57E-09	4.57E-09	8.99E-6

¹ Equal to default recharge, no source applied.

² Percolation rates used in HSI GeoTrans (1999b).

³ Rates for lower and upper sideslopes were not changed in sensitivity run.

⁴ Phases defined in Table 9.

Table 7. TMA Cell 2 percolation rates by stress period.

Stress Period	Phase ⁴	Percolation (Exfiltration) Rate (ft/day) ²			Percolation Rate ³ Sensitivity Run ft/day)
		Base	Lower Sideslope	Upper Sideslope	Base
1	X	2.21E-03 ¹	2.21E-03 ¹	2.21E-03 ¹	2.21E-3
2	X	2.21E-03 ¹	2.21E-03 ¹	2.21E-03 ¹	2.21E-3
3	X	2.21E-03 ¹	2.21E-03 ¹	2.21E-03 ¹	2.21E-3
4	A	1.47E-06	5.71E-11	2.21E-03 ¹	1.47E-6
5	B	1.93E-06	5.71E-11	2.34E-10	1.93E-6
6	B	1.93E-06	5.71E-11	2.34E-10	1.93E-6
7	B	1.93E-06	5.71E-11	2.34E-10	1.93E-6
8	C	8.86E-06	2.28E-10	4.57E-10	8.86E-6
9	D	7.45E-07	2.28E-10	5.71E-11	7.45E7
10	D	7.45E-07	2.28E-10	5.71E-11	7.45E7
11	D	7.45E-07	2.28E-10	5.71E-11	7.45E7
12	D	7.45E-07	2.28E-10	5.71E-11	7.45E7
13	E	9.47E-08	5.71E-11	5.71E-11	2.08E-7
14	E	9.47E-08	5.71E-11	5.71E-11	2.08E-7
15	E	9.47E-08	5.71E-11	5.71E-11	2.08E-7
16	E	9.47E-08	5.71E-11	5.71E-11	2.08E-7
17	F	1.38E-08	5.71E-11	5.71E-11	8.99E-6
18	F	1.38E-08	5.71E-11	5.71E-11	8.99E-6
19	F	1.38E-08	5.71E-11	5.71E-11	8.99E-6
20	F	1.38E-08	5.71E-11	5.71E-11	8.99E-6
21	G	4.57E-09	4.57E-09	4.57E-09	8.99E-6
22	G	4.57E-09	4.57E-09	4.57E-09	8.99E-6

¹ Equal to default recharge, no source applied.

² Percolation rates used in HSI GeoTrans (1999b).

³ Rates for lower and upper sideslopes were not changed in sensitivity run.

⁴ Phases defined in Table 9.

Table 8. TMA Cell 3 percolation rates by stress period.

Stress Period	Phase ⁴	Percolation (Exfiltration) Rate (ft/day) ²			Percolation Rate ³ Sensitivity Run ft/day)
		Base	Lower Sideslope	Upper Sideslope	Base
1	X	2.21E-03 ¹	2.21E-03 ¹	2.21E-03 ¹	2.21E-3
2	X	2.21E-03 ¹	2.21E-03 ¹	2.21E-03 ¹	2.21E-3
3	X	2.21E-03 ¹	2.21E-03 ¹	2.21E-03 ¹	2.21E-3
4	X	2.21E-03 ¹	2.21E-03 ¹	2.21E-03 ¹	2.21E-3
5	X	2.21E-03 ¹	2.21E-03 ¹	2.21E-03 ¹	2.21E-3
6	X	2.21E-03 ¹	2.21E-03 ¹	2.21E-03 ¹	2.21E-3
7	A	1.47E-06	5.71E-11	2.21E-03 ¹	1.47E-6
8	B	1.93E-06	5.71E-11	2.34E-10	1.93E-6
9	B	1.93E-06	5.71E-11	2.34E-10	1.93E-6
10	B	1.93E-06	5.71E-11	2.34E-10	1.93E-6
11	C	8.86E-06	2.28E-10	4.57E-10	8.86E-6
12	D	7.45E-07	2.28E-10	5.71E-11	7.45E-7
13	D	7.45E-07	2.28E-10	5.71E-11	7.45E-7
14	E	9.47E-08	5.71E-11	5.71E-11	2.08E-7
15	E	9.47E-08	5.71E-11	5.71E-11	2.08E-7
16	E	9.47E-08	5.71E-11	5.71E-11	2.08E-7
17	E	9.47E-08	5.71E-11	5.71E-11	2.08E-7
18	F	1.38E-08	5.71E-11	5.71E-11	8.99E-6
19	F	1.38E-08	5.71E-11	5.71E-11	8.99E-6
20	F	1.38E-08	5.71E-11	5.71E-11	8.99E-6
21	F	1.38E-08	5.71E-11	5.71E-11	8.99E-6
22	G	4.57E-09	4.57E-09	4.57E-09	8.99E-6

¹ Equal to default recharge, no source applied.

² Percolation rates used in HSI GeoTrans (1999b).

³ Rates for lower and upper sideslopes were not changed in sensitivity run.

⁴ Phases defined in Table 9.

Table 9. Phases of landfill operations with distinct exfiltration rates, in Applicant’s model.

Phase	Description	Duration (years)
X	Pre-construction	0 - 22
A	First phase of operation	2 - 4
B	Second phase of operation	4 - 10
C	Consolidation	2
D	Cap in place part 1	8
E	Cap in place part 2	20
F	Cap in place part 3	104 - 114
G	Degraded flexible-membrane liner, steady-state	--

Note: From HSI GeoTrans, 2000. See Tables 5 - 8 for phases and exfiltration rates at each TMA cell.

Table 10. Simulations testing model sensitivity to dispersivity.

Run Name	α_L (ft)	α_{TH} (ft)	α_{TV} (ft)
NMC BEJT	50	5	5
disp01a	50	5	0
disp02a	50	0	5
disp03	5	5	5
disp04	5	0.5	0.5
disp05	0.5	0.5	0.5
disp06	50	0.5	0.5
disp07	50	5	0.5
NMC PWCT	25	2.5	0.5

Note: α_L = longitudinal dispersivity; α_{TH} = transverse horizontal dispersivity; α_{TV} = transverse vertical dispersivity.

Table 11. Sensitivity to vertical hydraulic conductivity and dispersivity.

Run Name	Vertical K (ft/d)	α_L (ft)	α_{TH} (ft)	α_{TV} (ft)
NMC BEJT	0.075 to 8	50	5	5
lowkv	0.0075 to 0.8	50	5	5
NMC PWCT	0.0075 to 0.8	25	2.5	0.5

Note: K = hydraulic conductivity; ft/d = feet/day; α_L = longitudinal dispersivity; α_{TH} = transverse horizontal dispersivity; α_{TV} = transverse vertical dispersivity.

Table 12. Maximum concentrations at the TMA DMZ with changes in porosity and vertical dispersivity.

Run Name	Porosity	Vertical Dispersivity (ft)	Maximum concentration at TMA DMZ	Ratio of maximum concentration at TMA DMZ
48_1	0.1	0.05	1.05E-03	3.71
49_1	0.3	0.05	2.83E-04	
50_1	0.1	0.5	6.03E-04	3.55
51_1	0.3	0.5	1.70E-04	

Table 13. Model runs to evaluate effect of pinchout zone. The hydraulic conductivity (K) values reported for the fine and coarse outwash are assigned to each cell according to the proportion of fine to coarse outwash in that cell. The high-K channel in run 29_1 was simulated by assigning the coarse outwash K-value to an area of 3 rows by 5 columns in layers 2-6. Model runs to evaluate effect of pinchout zone.

Model run	Pinchout zone interpretation	General description	Fine Outwash K (ft/day)		Coarse Outwash K (ft/day)	
			layers 1 & 7	layers 2 - 6	layers 1 & 7	layers 2 - 6
25_1	Applicant	Wider and higher K	20	6	80	6
28_1	TWG	Narrower and lower K	20	3	80	3
29_1	TWG with channel	Narrower and lower K with a high-K channel	20	3	80	3

Table 14. ECURVE results at the TMA DMZ. The maximum relative concentration occurring along the DMZ at a particular model time step, and the layer, row and column where this occurs. Bold values are maxima; shaded rows indicate times when the location of the maximum changes from west to east side of domain.

Time (years)	Run 25_1				Run 28_1				Run 29_1			
	rel. conc.	layer	row	column	rel. conc.	layer	row	column	rel. conc.	layer	row	column
2	4.27E-12	2	23	13	7.76E-13	2	23	13	4.87E-13	2	23	13
5	5.65E-07	2	23	13	1.68E-07	2	23	13	1.17E-07	2	23	13
6	2.78E-06	2	23	13	9.48E-07	2	23	13	6.94E-07	2	23	13
10	1.58E-04	4	19	16	6.68E-05	4	19	16	3.74E-05	4	19	16
15	6.12E-04	4	19	16	4.41E-04	4	20	15	3.12E-04	4	20	15
16	6.74E-04	4	19	16	5.15E-04	4	20	15	3.87E-04	4	20	15
18	7.60E-04	4	19	16	6.32E-04	4	20	15	5.15E-04	4	20	15
20	8.10E-04	4	19	16	7.12E-04	4	20	15	6.14E-04	4	20	15
22	9.30E-04	4	23	13	7.55E-04	4	20	15	6.77E-04	4	20	15
24	1.02E-03	4	23	13	8.51E-04	4	23	13	7.69E-04	4	23	13
25	1.04E-03	4	23	13	8.89E-04	4	23	13	8.09E-04	4	23	13
28	1.04E-03	4	23	13	9.48E-04	4	23	13	9.21E-04	5	23	13
30	9.83E-04	4	23	13	9.37E-04	4	23	13	9.95E-04	5	23	13
32	8.96E-04	4	23	13	9.43E-04	5	23	13	1.03E-03	5	23	13
34	8.46E-04	5	23	13	9.29E-04	5	23	13	1.01E-03	5	23	13
35	8.49E-04	5	23	13	9.15E-04	5	24	12	9.90E-04	5	23	13
38	7.90E-04	5	23	13	8.40E-04	5	24	12	8.73E-04	5	23	13
40	7.21E-04	5	23	13	7.59E-04	5	23	13	7.77E-04	5	23	13
45	5.11E-04	5	22	14	5.34E-04	5	23	13	5.96E-04	6	23	13
50	3.38E-04	5	22	14	4.79E-04	6	23	13	5.64E-04	6	22	14
55	3.26E-04	6	19	16	4.07E-04	6	22	14	4.94E-04	6	22	14
58	3.21E-04	5	44	63	3.57E-04	6	22	14	4.30E-04	6	22	14
60	3.69E-04	5	43	63	3.27E-04	5	40	64	3.84E-04	6	22	14
64	4.47E-04	5	43	63	3.69E-04	5	40	64	3.01E-04	6	22	14
65	4.62E-04	5	43	63	3.81E-04	5	40	64	2.82E-04	6	22	14
70	5.19E-04	5	43	63	4.17E-04	5	40	64	2.09E-04	6	22	14
75	5.42E-04	5	43	63	4.13E-04	5	40	64	1.72E-04	7	22	14
80	5.31E-04	5	42	63	3.90E-04	5	40	64	1.69E-04	7	22	14
83	5.20E-04	5	42	63	3.67E-04	5	40	64	1.66E-04	7	22	14
85	5.08E-04	5	42	63	3.50E-04	5	40	64	1.64E-04	7	22	14
89	4.73E-04	5	42	63	3.16E-04	5	40	64	1.59E-04	7	22	14
90	4.62E-04	5	42	63	3.07E-04	5	40	64	1.58E-04	7	22	14
95	4.02E-04	5	42	63	2.64E-04	5	40	64	1.51E-04	7	22	14
100	3.42E-04	6	42	63	2.28E-04	5	40	64	1.44E-04	7	22	14
105	2.94E-04	6	42	63	1.97E-04	5	40	64	1.37E-04	7	22	14
108	2.66E-04	6	42	63	1.82E-04	5	40	64	1.32E-04	7	22	14
110	2.49E-04	6	42	63	1.72E-04	5	40	64	1.29E-04	7	22	14
114	2.19E-04	6	42	63	1.56E-04	5	40	64	1.24E-04	7	22	14

Time (years)	Run 25_1				Run 28_1				Run 29_1			
	rel. conc.	layer	row	column	rel. conc.	layer	row	column	rel. conc.	layer	row	column
115	2.12E-04	6	42	63	1.53E-04	5	40	64	1.22E-04	7	22	14
120	1.84E-04	7	11	25	1.36E-04	5	40	64	1.15E-04	7	22	14
125	1.84E-04	7	10	26	1.23E-04	5	40	64	1.08E-04	7	22	14
130	1.84E-04	7	10	26	1.12E-04	5	40	64	1.02E-04	7	22	14
133	1.84E-04	7	10	26	1.07E-04	5	40	64	9.81E-05	7	22	14
135	1.84E-04	7	10	26	1.03E-04	5	40	64	9.57E-05	7	22	14
139	1.83E-04	7	10	26	9.74E-05	5	40	64	9.10E-05	7	22	14
140	1.83E-04	7	10	26	9.62E-05	5	40	64	8.98E-05	7	22	14
145	1.83E-04	7	10	26	9.08E-05	5	40	64	8.43E-05	7	22	14
150	1.81E-04	7	10	26	8.91E-05	6	38	64	7.91E-05	7	22	14
155	1.79E-04	7	10	26	8.80E-05	6	38	64	7.41E-05	7	22	14
158	1.80E-04	7	10	27	8.73E-05	6	38	64	7.21E-05	5	39	64
160	1.80E-04	7	10	27	8.78E-05	7	36	63	7.18E-05	5	39	64
164	1.80E-04	7	10	27	9.09E-05	7	36	63	7.12E-05	5	39	64
165	1.80E-04	7	10	27	9.17E-05	7	36	63	7.10E-05	5	39	64
170	1.79E-04	7	10	27	9.63E-05	7	36	63	6.99E-05	5	39	64
175	1.78E-04	7	10	27	1.01E-04	7	36	63	6.88E-05	5	39	64
180	1.77E-04	7	10	27	1.06E-04	7	36	63	6.76E-05	5	39	64
185	1.77E-04	7	10	27	1.10E-04	7	36	63	6.62E-05	5	39	64
190	1.75E-04	7	10	27	1.13E-04	7	36	63	6.45E-05	5	39	64
195	1.74E-04	7	10	27	1.15E-04	7	36	63	6.23E-05	5	39	64
200	1.72E-04	7	10	27	1.16E-04	7	36	63	6.00E-05	5	39	64
210	1.70E-04	7	10	27	1.17E-04	7	36	63	5.50E-05	5	39	64
220	1.66E-04	7	10	27	1.16E-04	7	36	63	4.97E-05	5	39	64
230	1.63E-04	7	10	28	1.11E-04	7	36	63	4.48E-05	5	39	64
240	1.60E-04	7	10	28	1.06E-04	7	36	63	4.02E-05	5	39	64
250	1.56E-04	7	10	28	9.97E-05	7	36	63	3.61E-05	5	39	64
258	1.52E-04	7	10	28	9.47E-05	7	36	63	3.31E-05	5	39	64
260	1.51E-04	7	10	28	9.34E-05	7	36	63	3.23E-05	5	39	64
264	1.49E-04	7	10	28	9.09E-05	7	36	63	3.09E-05	5	39	64
270	1.44E-04	7	10	28	8.71E-05	7	36	63	2.89E-05	3	40	64
280	1.40E-04	7	10	28	8.07E-05	7	36	63	2.77E-05	3	40	64
290	1.34E-04	7	10	28	7.45E-05	7	36	63	2.67E-05	3	40	64
300	1.28E-04	7	10	28	6.82E-05	7	36	63	2.59E-05	3	40	64
310	1.21E-04	7	10	28	6.21E-05	7	35	63	2.48E-05	3	40	64
320	1.15E-04	7	10	28	5.64E-05	7	35	63	2.40E-05	3	40	64
330	1.09E-04	7	10	28	5.12E-05	7	35	63	2.33E-05	3	40	64
340	1.02E-04	7	10	28	4.66E-05	7	35	63	2.25E-05	3	40	64
350	9.64E-05	7	13	36	4.27E-05	7	35	63	2.17E-05	3	40	64
358	9.57E-05	7	13	36	3.99E-05	7	35	63	2.10E-05	3	40	64
360	9.56E-05	7	13	36	3.92E-05	7	35	63	2.09E-05	3	40	64

Time (years)	Run 25_1				Run 28_1				Run 29_1			
	rel. conc.	layer	row	column	rel. conc.	layer	row	column	rel. conc.	layer	row	column
364	9.52E-05	7	13	36	3.79E-05	7	35	63	2.05E-05	3	40	64
370	9.29E-05	7	13	36	3.61E-05	7	35	63	2.00E-05	3	40	64
380	9.11E-05	7	13	36	3.32E-05	7	35	63	1.92E-05	3	40	64
390	8.91E-05	7	13	36	3.06E-05	7	35	63	1.84E-05	3	40	64
400	8.67E-05	7	13	36	3.02E-05	5	40	64	1.76E-05	3	40	64
425	8.05E-05	7	13	36	2.99E-05	5	40	64	1.56E-05	3	40	64
450	7.32E-05	7	13	36	2.96E-05	5	40	64	1.34E-05	3	40	64
475	6.63E-05	7	13	36	2.94E-05	5	40	64	1.14E-05	3	40	64
500	5.91E-05	7	13	36	2.88E-05	5	40	64	9.61E-06	3	40	64
525	5.23E-05	7	13	36	2.79E-05	5	40	64	7.94E-06	3	40	64
550	4.60E-05	7	13	36	2.66E-05	5	40	64	6.37E-06	3	40	64
575	4.04E-05	7	13	36	2.47E-05	5	40	64	5.02E-06	3	40	64
600	3.52E-05	7	13	36	2.25E-05	5	40	64	3.91E-06	3	40	64
625	3.19E-05	7	14	37	2.03E-05	5	40	64	2.99E-06	3	40	64
650	2.88E-05	7	14	37	1.81E-05	5	40	64	2.26E-06	3	40	64

Note: Run 25_1 incorporates the applicant's interpretation of the pinchout zone; run 28_1 is the WDNR interpretation (narrower) of the pinch out zone; Run 29_1 is the WDNR interpretation with a hypothetical high-K channel.

Table 15. Exfiltration rates for TMA and RP, from Benson and Grefe (2002).

Landfill HELP- A ^a						
Period	In in/yr:			In mm/yr:		
	Base	Lower Side	Upper Side	Base	Lower Side	Upper Side
Operations Stage 1	4.18E-02	1.98E-06	--	1.06E+00	5.03E-05	--
Operations Stage 2 & Consolidation	3.97E-02	2.26E-06	3.88E-06	1.01E+00	5.75E-05	9.85E-05
Post Closure 0-40yrs	1.40E-03	1.88E-07	1.32E-07	3.54E-02	4.79E-06	3.34E-06
Post Closure 41-65yrs	1.05E-04	1.05E-07	0.00E+00	2.66E-03	2.66E-06	0.00E+00
Post Closure 66-90yrs	6.64E-05	1.78E-08	0.00E+00	1.69E-03	4.51E-07	0.00E+00
Post Closure 91-115yrs	4.49E-06	0.00E+00	0.00E+00	1.14E-04	0.00E+00	0.00E+00
Post Closure 116-140yrs (no LCS)	1.22E-01	0	0	3.10E+00	0	0
Post Closure 141-240yrs (no FML)	1.22E-01	0	0	3.10E+00	0	0
Post Closure 241-340yrs	1.22E-01	0	0	3.10E+00	0	0
Post Closure 341+yrs	1.22E-01	0	0	3.10E+00	0	0

Landfill HELP- B ^b						
Period	In in/yr:			In mm/yr:		
	Base	Lower Side	Upper Side	Base	Lower Side	Upper Side
Operations Stage 1	4.18E-02	1.98E-06	--	1.06E+00	5.03E-05	--
Operations Stage 2 & Consolidation	3.97E-02	2.26E-06	3.88E-06	1.01E+00	5.75E-05	9.85E-05
Post Closure 0-40yrs	1.40E-03	1.88E-07	1.32E-07	3.54E-02	4.79E-06	3.34E-06
Post Closure 41-65yrs	1.05E-04	1.05E-07	0.00E+00	2.66E-03	2.66E-06	0.00E+00
Post Closure 66-90yrs	6.64E-05	1.78E-08	0.00E+00	1.69E-03	4.51E-07	0.00E+00
Post Closure 91-115yrs	4.49E-06	0.00E+00	0.00E+00	1.14E-04	0.00E+00	0.00E+00
Post Closure 116-140yrs (no LCS)	1.46E-04	0	0	3.70E-03	0	0
Post Closure 141-240yrs (no FML)	1.46E-04	0	0	3.70E-03	0	0
Post Closure 241-340yrs	1.46E-04	0	0	3.70E-03	0	0
Post Closure 341+yrs	1.46E-04	0	0	3.70E-03	0	0

Landfill HELP- C ^c						
Period	In in/yr:			In mm/yr:		
	Base	Lower Side	Upper Side	Base	Lower Side	Upper Side
Operations Stage 1	4.18E-02	1.98E-06	--	1.06E+00	5.03E-05	--
Operations Stage 2 & Consolidation	3.97E-02	2.26E-06	3.88E-06	1.01E+00	5.75E-05	9.85E-05
Post Closure 0-40yrs	1.40E-03	1.88E-07	1.32E-07	3.54E-02	4.79E-06	3.34E-06
Post Closure 41-65yrs	1.05E-04	1.05E-07	0.00E+00	2.66E-03	2.66E-06	0.00E+00
Post Closure 66-90yrs	6.64E-05	1.78E-08	0.00E+00	1.69E-03	4.51E-07	0.00E+00
Post Closure 91-115yrs	4.49E-06	0.00E+00	0.00E+00	1.14E-04	0.00E+00	0.00E+00
Post Closure 116-140yrs (no LCS)	1.22E-05	0	0	3.10E-04	0	0
Post Closure 141-240yrs (no FML)	1.22E-05	0	0	3.10E-04	0	0
Post Closure 241-340yrs	1.22E-05	0	0	3.10E-04	0	0
Post Closure 341+yrs	1.22E-05	0	0	3.10E-04	0	0

a - Post Closure 116+ based on Upper Bound Steady State Exfiltration (3.1 mm/yr)
b - Post Closure 116+ based on Designed Single Composite Steady State Exfiltration (3.7E-03 mm/yr)
c - Post Closure 116+ based on Double Composite Cover Steady State Exfiltration (3.1E-04 mm/yr)

Reclaim Pond					
Period	In in/yr:		In mm/yr:		
	D ³	Drp ⁴	D ³	Drp ⁴	
Full Operation ¹ , 0-31 yrs	1.5350E-05	4.3310E-04	3.8989E-04	1.1001E-02	
Post-Mill Closure ² , 32-50 yrs	4.7240E-06	1.2600E-04	1.1999E-04	3.2004E-03	

¹Average Pond Depth = 15 ft
²Average Pond Depth = 7.5 ft
³D - design
⁴Drp - design with reduced performance

Table 16. Maximum concentrations along the TMA DMZ over 650 and 150 years of the simulation. A ratio is presented to compare results to applicant’s BEJT simulation (t13c). Results are calculated by assuming the same unit source concentration for a hypothetical constituent for all six simulated phases and summing the results.

MT3D run ID	transverse vertical dispersivity (ft)	porosity	mine dewatering rate (gpm)	source area exfiltration	relative maximum concentration along TMA DMZ, 0 - 650 yrs	ratio to t13c	relative maximum concentration along TMA DMZ, 0 - 150 yrs	ratio to t13c 0-150 yrs
t13c1 - t13c6	5	0.1	BEJT	NMC	8.61E-04	1.00	8.61E-04	1.00
47_1 - 47_6	0.05	0.1	1250	HELPA	1.99E-02	23.08	1.34E-03	1.56
48_1 - 48_6	0.05	0.1	602	HELPA	2.30E-02	26.71	1.10E-03	1.28
53_1 - 53_6	0.05	0.1	602	HELPA	1.10E-03	1.28	1.10E-03	1.28
55_1 - 55_6	0.05	0.1	602	HELPA	1.10E-03	1.28	1.10E-03	1.28
52_1 - 52_6	0.05	0.1	285	HELPA	2.30E-02	26.78	9.71E-04	1.13
59_1 - 59_6	0.5	0.1	285	HELPA	1.77E-02	20.58	6.65E-04	0.77
50_1 - 50_6	0.5	0.1	602	HELPA	1.77E-02	20.61	6.56E-04	0.76
60_1 - 60_6	0.5	0.1	1250	HELPA	1.65E-02	19.22	6.18E-04	0.72
49_1 - 49_6	0.05	0.3	602	HELPA	1.81E-02	21.08	2.99E-04	0.35
58_1 - 58_6	0.5	0.3	1250	HELPA	1.48E-02	17.18	2.31E-04	0.27
54_1 - 54_6	0.5	0.3	602	HELPA	2.63E-04	0.31	2.03E-04	0.24
56_1 - 56_6	0.5	0.3	602	HELPA	2.63E-04	0.31	2.03E-04	0.24
51_1 - 51_6	0.5	0.3	602	HELPA	1.56E-02	18.12	2.03E-04	0.24
57_1 - 57_6	0.5	0.3	285	HELPA	1.56E-02	18.10	1.91E-04	0.22

APPENDIX 1

MODIFICATIONS TO THE MT3DMS CODE

Notes on the Modification of the MT3DMS code for the Crandon TMA Transport Model

Chunmiao Zheng & Patrick Wang
Groundwater Systems Research Ltd.

1. Background

The MT3DMS computer code (Zheng and Wang, 1999) is the basis for a predictive transport model constructed by the representatives of the mining company applying for the Crandon mine permit. The model was designed to predict contaminant transport over time from the proposed tailings landfill (called the TMA) toward a nearby creek. The USGS-Wisconsin District was asked by the Wisconsin Department of Natural Resources to review the model and make any necessary improvement. The results of the USGS review indicated that the TVD solver, which is one of the several solution options available in MT3DMS, would produce the most reliable results for the TMA model. This is because the TVD solver has the ability to eliminate mass-balance error, and suppress artificial smearing (called numerical dispersion) which tends to lower the predicted concentration values. Unfortunately, the TVD solver can have difficulty with three-dimensional model grids characterized by irregular stratigraphy, as in the case of the TMA model. As a result, the TVD solver would become unstable (blowing-up) and yield large negative concentrations for some combinations of input parameters. This project was thus initiated in response to the need of the USGS-Wisconsin District to improve the TVD solver so that it can handle reliably three-dimensional problems such as the TMA model. Such work would allow the USGS to complete its review and modifications of the TMA model.

2. Modifications of the TVD Algorithm

The improvements to the TVD algorithm are contained in the *CFACE* subroutine of the Advection Package. They include (a) more effective handling of concentration calculation adjacent to inactive model nodes; (b) correction of a coding error that could result in inaccurate concentration weighting in model grids of highly irregular grid spacing; and (c) complete restructuring of the so-called "flux limiter", which is the key numerical algorithm used by the TVD solver to suppress artificial oscillation. These improvements result in a much more robust and stable TVD solver. The TMA model, with the improved TVD solver, can simulate the transport conditions for any length of time (e.g., 150 years) without prematurely blowing up or producing large negative concentrations. The modified TVD solver also passed successfully a comprehensive suite of standard benchmark problems for MT3DMS.

3. The Positivity Preserving Scheme

The changes to the TVD solver as explained in the previous section eliminate the potential for large negative concentrations due to numerical instability associated with solution of the advection term. However, relatively small negative concentrations can still arise from solution of the dispersion term. For the TMA model, the negative concentrations resulting from dispersion can lead to as much as 3-4% percentage of total mass in the aquifer. To correct this problem, a positivity preserving (PP) algorithm is developed and incorporated into the explicit finite-difference method for solution of the dispersion term (the *DSP3SV* subroutine in the Dispersion Package). The positivity preserving scheme works as follows. First, the principal components of the dispersive flux are computed independent of the off-diagonal components (cross terms). Since the principal components do not contribute to negative concentrations, it is unnecessary to check the positivity of the resulting concentrations. Next, the off-diagonal components are computed and checked individually to determine whether any of the flux components results in negative concentration at a model cell. If so, the particular flux component is prohibited and the cell concentration is not updated. The scheme effectively eliminates negative concentrations while preserving the accuracy and mass balance of the resulting solution.

4. Comparison of Transport Solutions

The TMA transport model was run with six combinations of solution options, including

- a) Fully explicit finite-difference method with upstream weighting for the advection term (FD Explicit);
- b) Fully implicit finite-difference method with upstream weighting for the advection term (FD Implicit);
- c) Fully implicit finite-difference method with central-in-space weighting for the advection term (FD Implicit-CIS);
- d) Method of characteristics for the advection term and implicit finite-difference method for the dispersion term (MOC);
- e) TVD for the advection term and implicit finite-difference method for the dispersion term (TVD GCG);
- f) TVD for the advection term and explicit finite-difference method plus the positivity preserving scheme for the dispersion term (TVD PP).

Figure 1 shows the maximum concentrations along a DMZ boundary (TMA1200a) at selected times as calculated by the different solution options listed above. Option (c) was found to be unstable and excessively oscillatory for the TMA model and thus the result for option (c) is not shown. The TVD solutions lie between the higher MOC solution and the lower finite-difference solutions. The TVD solution with the positivity preserving scheme is nearly identical to that without the PP scheme. However, as shown in Figure 2, without the PP scheme, the total negative mass in the aquifer ranges from 1 to 3% of the total positive mass during the course of the simulation. With the PP scheme, the negative mass is reduced to around zero.

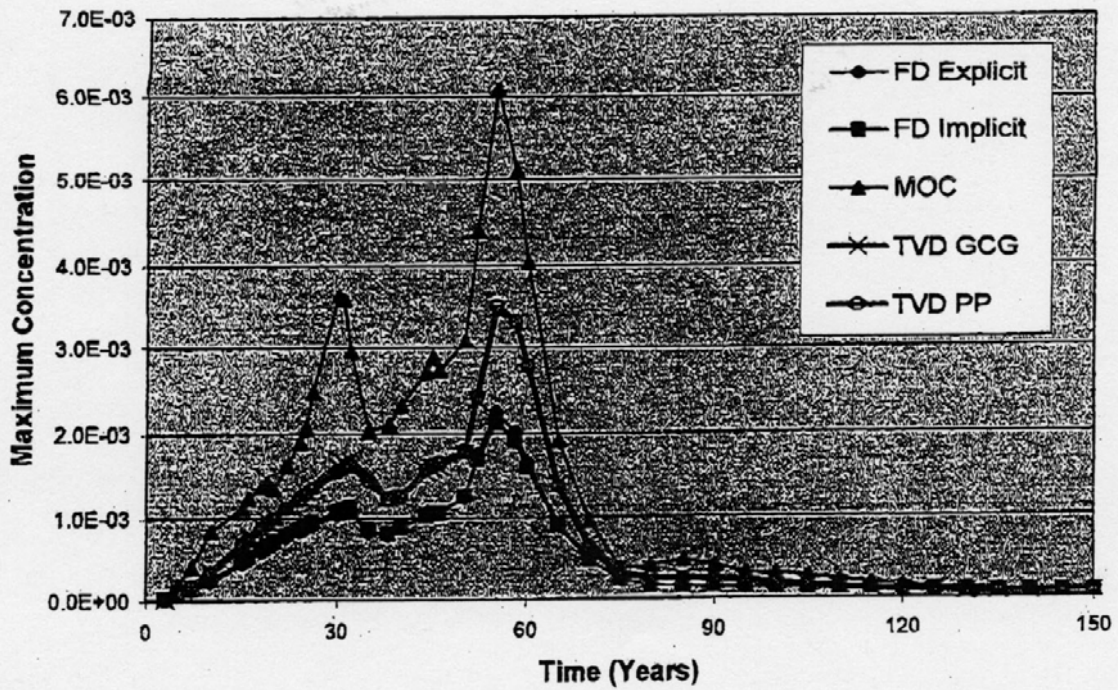


Figure 1. Comparison of maximum concentrations along a DMZ boundary (TMA1200a) calculated by the Crandon TMA model using different transport solution options.

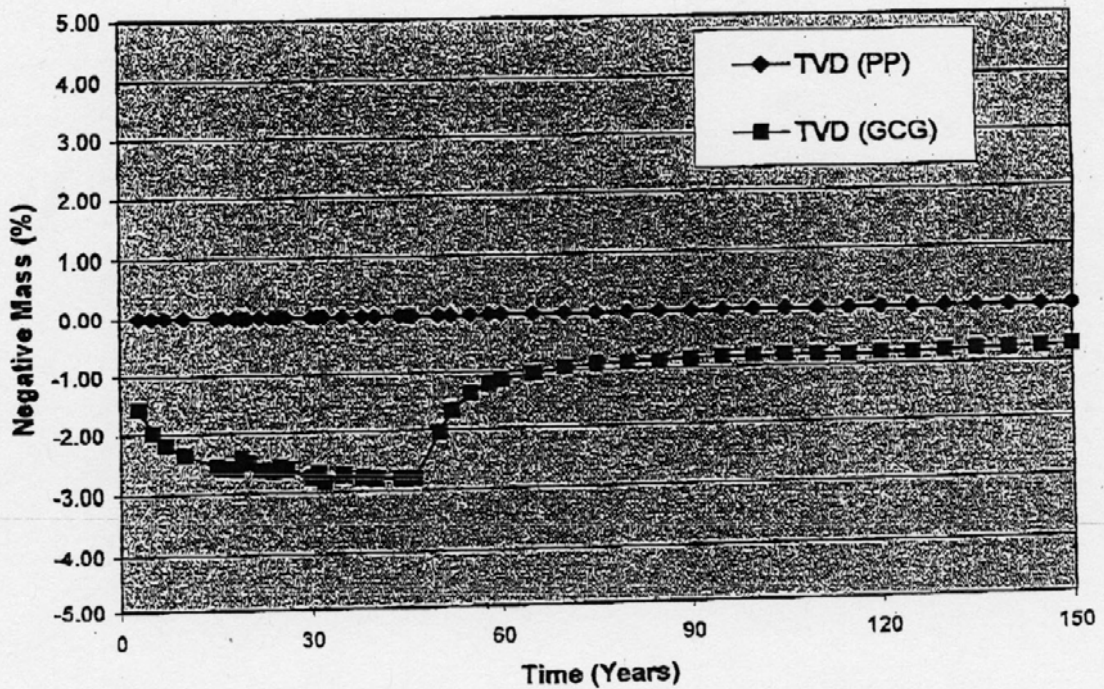


Figure 2. Effect of the positivity preserving (PP) scheme on the TVD solution.

As shown in Figure 1, the concentration values predicted by the MOC solution are considerably higher than those by the TVD solutions, which, in turn, are significantly higher than those by the finite-difference solutions. Under normal circumstances, the MOC solution and the TVD solution would be much closer as both tend to minimize the “numerical dispersion” error which artificially lowers the predicted concentration values. However, for the Crandon TMA model, the MOC solution has numerical difficulty because of the irregular model grid required to accommodate uneven stratigraphy. As a result, the MOC solution has severe mass balance discrepancy errors as shown in Figure 3. The large mass balance errors render the MOC solution unreliable.

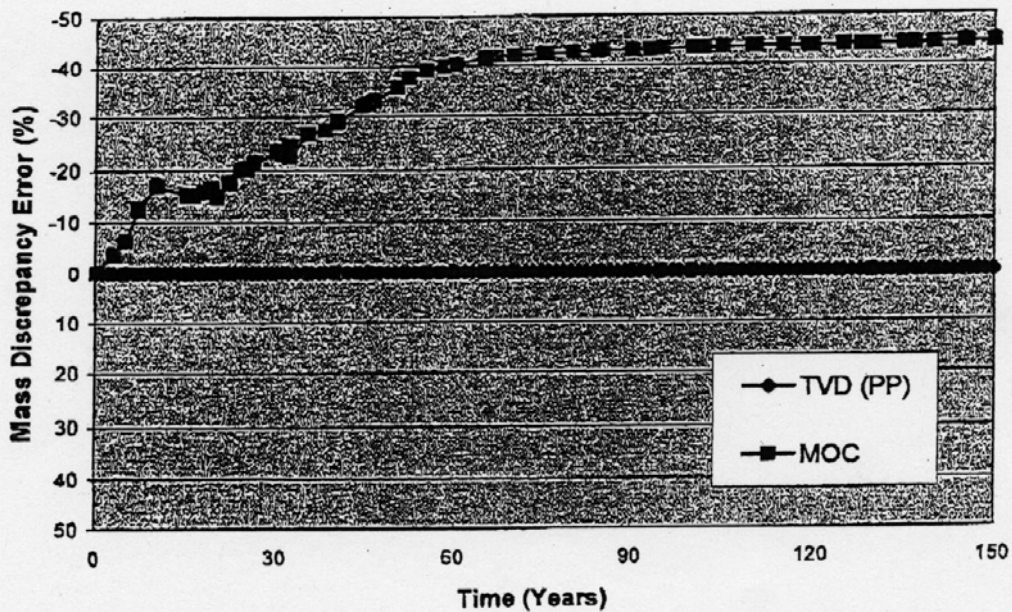
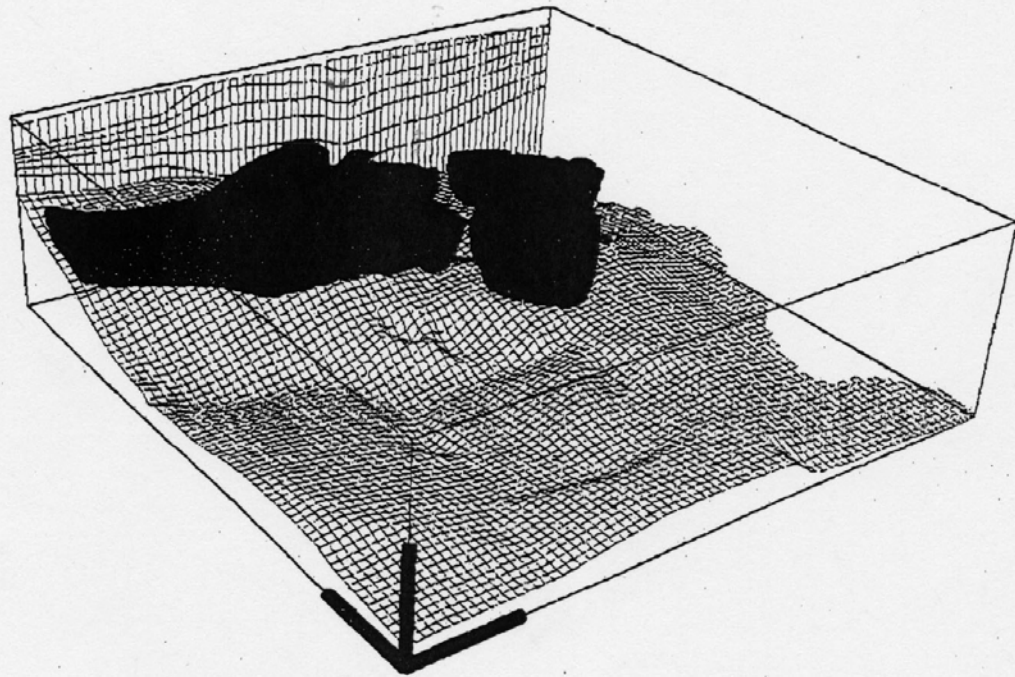


Figure 3. Comparison of mass balance discrepancy errors for the TVD and MOC solutions.

5. Description of the Modified MT3DMS Code and TMA Model Files

The CD-ROM disk accompanying this report contains a version of the MT3DMS code resulting from the development work for this project. The version is referred to as Release 3.50.C, which is identical to the most recent version – Release 3.50.B – except for the *CFACE* and *DSP3.SV* subroutines as discussed previously. Two executable programs are included, *MT3DMS.exe* compiled by the Lahey LF90 Fortran 4.0 and *MT3D_VF.exe* compiled by the Compaq Visual Fortran 6.0. In addition, the companion CD-ROM disk includes a set of input and output files for the TMA model. The model input files are set to use the TVD solver for the advection term and explicit finite-difference method plus the positivity preserving scheme for the dispersion term. Figure 4 shows a snapshot of the calculated plume above a concentration cutoff value of 10^{-4} at a total elapsed time of 30 years.

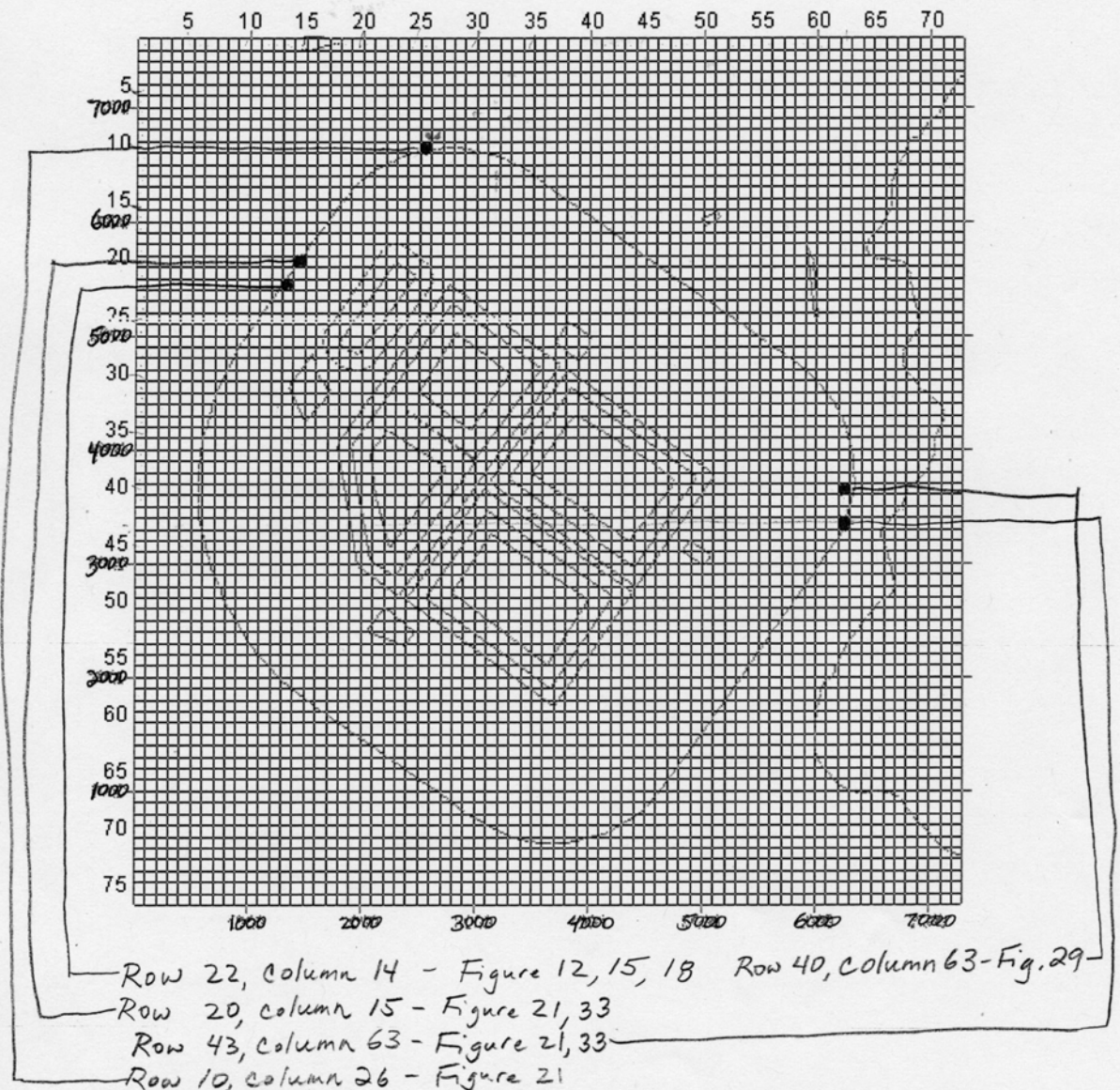


Time = 1.098e+004

Figure 4. Calculated solute plume above a concentration cutoff value of 10^{-4} at 30 years after the simulation starts. The transport solution option used is the modified TVD plus the positivity preserving scheme.

APPENDIX 2

BREAKTHROUGH CURVE LOCATIONS IN MODEL DOMAIN



Column and row numbers of model grid are as noted. Model coordinates are in feet, and cell size is 100 ft by 100ft. Locations of various breakthrough curves used in the model review are also indicated.